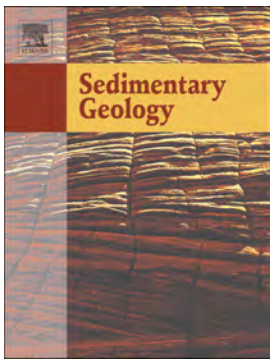

Space-time geological model of the Quaternary syntectonic fill of a foreland basin (Po basin, Northern Italy)

Chiara Zuffetti, Riccardo Bersezio

PII: S0037-0738(21)00097-X

DOI: https://doi.org/10.1016/j.sedgeo.2021.105945

Reference: SEDGEO 105945

To appear in: *Sedimentary Geology*

Received date: 8 January 2021

Revised date: 13 May 2021

Accepted date: 13 May 2021

Please cite this article as: C. Zuffetti and R. Bersezio, Space-time geological model of the Quaternary syntectonic fill of a foreland basin (Po basin, Northern Italy), *Sedimentary Geology* (2021), https://doi.org/10.1016/j.sedgeo.2021.105945

Space-time geological model of the Quaternary syntectonic fill of a foreland basin (Po basin, Northern Italy)

Chiara Zuffetti*, Riccardo Bersezio

Dipartimento di Scienze della Terra, Università degli Studi di Milano, via Mangiagalli 34, 20133 I-Milano, Italy

**Corresponding Author. Authors e-mail: Chiara Zuffetti:* chiara.zuffetti@unimi.it *(OrcID 0000-0002-7391-4829); Riccardo Bersezio:* riccardo.bersezio@unimi.it *(OrcID 0000-0002-6629-8917).*

Abstract

Quantitative models of the large and widely populated Quaternary foreland basins, which host relevant resources like groundwater, heat, fertile soils, may be computed if space-time models of the basin fills are available. The paper presents the combination of geometrical (space) and evolutionary (time) constraints to model Quaternary stratigraphy in the southern Po basin in Lombardy, disentangling the tectonic and climatic controls. Five Quaternary high-rank unconformities and seven intermediate-rank unconformities were recognised, down-traced, and correlated from surface to subsurface. Within this framework, the surface facies associations of high-, intermediate-, and low-rank stratigraphic units were compared to the litho-textural associations of their subsurface equivalents obtained from borehole logs and published geophysical images, to draw the best fitting model, which was constrained to the Quaternary geological evolution.

Discrete, long-term thrusting, wrenching, folding, and extensional collapsing stages are inferred to have shaped the Gelasian, intra-Calabrian, Early-Middle Pleistocene, Middle-Late Pleistocene and Latest Pleistocene-Holocene high-rank composite unconformities. These surfaces are cut into synsedimentary, polyphasic, buried anticlines and correspond to conformable boundaries in the adjacent depocentres. The intermediate-rank, low-angle unconformities composing the high-rank ones, bound the stratigraphic units forming the overall regressive fill of the basin. These surfaces might correspond to steady tectonic uplift/subsidence periods when deposition was mostly controlled by Pleistocene climate

changes since the Gelasian.

The hierarchic space/time structure, translated into hard geometrical constraints (a fence diagram of cross-sections) and relative chronology of the stratigraphic relationships (intersect/erode, onlap and offset) allows to compute the geological quantitative model using a potential field interpolation method. The model building phase and subsequent inspection permit to critically analyse the current interpretations on the evolution of the Po basin during the Quaternary compared with other foreland settings. The 4-D model integrates the surface-subsurface geometry with the tectono-sedimentary evolution in a multi-scale structure that may be exported for hydrogeological, geothermal and environmental modelling.

Keywords: Apennines; foreland basin; Po Plain; Quaternary; unconformity; space-time model

1. Rationale and study aims

Models of the four-dimensional architecture of densely populated Quaternary continental basins of the world are necessary to understand basin evolution and to provide tools to evaluate, manage, and protect the relevant resources they host, such as fertile soils, groundwater and heat. Quantitative stratigraphic models should be able to represent the complex multi-scale, space-time structure of the basin stratigraphy, tectonics, and geomorphology (e.g., Wheeler, 1959; Paola, 2000; Calcagno et al., 2008; Van der Meulen et al., 2013; Maljers et al., 2015; Wellmann et al., 2018; Zuffetti et al., 2020). Space-time geological models must account for both 3-D space components (the structural-stratigraphic geometries and assemblage and the palimpsest geomorphology) and the 4^{th}-D time component of the geological architecture (the past and present dynamics, involving active tectonics, depositional/erosional processes, landscape changes, groundwater/heat flow and transport processes, which also respond to environmental changes and anthropic interference). Constraining models to both surface and subsurface data might permit to approach these goals accounting for the multi-scale, local and regional hierarchic

arrangement of the sedimentary entities through space, and for the timing of the relative increments of the geological evolution (Miall, 1985, 1996; Sheets et al., 2002; Heinz and Aigner, 2003; Allen and Allen, 2013; Bond, 2015; Russell et al., 2019).

In foreland basins, where accommodation space migrates towards the foreland responding to the propagation of the active orogenic front (Ori and Friend, 1984; Allen et al., 1986; Ricci Lucchi, 1986; Doglioni, 1993; Ingersoll, 2012), climate-driven hydrological changes concur to control the stratigraphic record. Since four-dimensional modelling requires the understanding of the incremental basin evolution, the climatic signals must be disentangled from the effects of tectonics. In order to do that, interpretations of the shallow subsurface interval of the Quaternary basin fill based on traditional seismic observations are helpful (e.g., Lee and Suk, 1998; Fantoni and Franciosi, 2010; Onnis et al., 2018; Ronchi et al., 2019) but may remain inconclusive. On the other hand, surface and shallow subsurface geological datasets may offer relevant insights into the tectono-depositional evolution of Quaternary basins at different temporal and spatial scales (e.g., Van der Meulen et al., 2013; Amorosi et al., 2017 and references therein).

This work proposes an integrated approach to realise the space-time, multi-scale model of the Quaternary syntectonic stratigraphy of the wedge-top depozone of a foreland basin (De Celles and Giles, 1996), based on the combination of surface data (geological maps, stratigraphic, sedimentological, petrographic, pedological, geomorphological and structural analyses) with subsurface direct data (borehole and well logs, geophysical soundings). Focus is on the Quaternary geology of the southern Po basin of Lombardy (northern Italy) (Fig. 1A, B), a key-sector of the Po-Adriatic foreland basin undergoing active tectonics during the Quaternary. In the proglacial to periglacial settings typical of this region, the effects of climate changes vs. foreland propagation of the thrust systems on the sedimentary evolution are still debated (Amorosi et al., 2008; Scardia et al., 2012; Gunderson

et al., 2014). Modelling the tectono-sedimentary architecture of this area offers the opportunity to investigate the wedge-top zone of this peculiar foreland setting in which: i) subsidence and sedimentation are controlled by the outwards propagation of the Northern Apennines fold and thrust belt since the Miocene (Pieri and Groppi, 1981; Bigi et al., 1990), while the sediment input is mostly supplied by the Cretaceous-Tertiary thrust belt of the Southern Alps (i.e. the opposite basin margin; Ori, 1993); ii) the buried and blind fronts of the two thrust belts interfere during the Quaternary in the centre of the Po Plain, where the active Apennine frontal arcs dissect the most external thrusts of the Southern Alps (Fig. 1) (Central Po Plain Structures after Fantoni et al., 2004); iii) the regional subsidence/uplift, seismological, and depositional patterns responded to different external controls, which include active thrusting, buttressing of the thrust fronts, flexural response of the foreland crust, isostatic readjustments (Arca and Beretta, 1985; Carminati et al., 2003; Scardia et al., 2006; Maesano and D'Ambrogi, 2016; Livani et al., 2016), as well as to erosion, discharge, and transport pattern changes following the Quaternary glacial cycles (Muttoni et al., 2003; Bini et al., 2004a; Fontana et al., 2014); iv) the basin hosts multi-layered, productive aquifers feeding one of the most densely populated areas of Europe, with a large potential for exploitation of low-enthalpy geothermal resources (Regione Lombardia and Eni-Agip, 2001; Barbero et al., 2020), and represents one of the widest fertile areas of Europe in spite of the major anthropic pressure.

The work proposes a new space-time model of the Quaternary stratigraphic architecture of the southern wedge-top depozone of the Po foreland basin, aiming to i) suggest a novel approach to integrate Space-Time geological constraints from outcrop and borehole data, and to convert the multi-source dataset into widely applicable rules for modellers; ii) propose a new Quaternary tectono-depositional evolution of the southern Po basin.

Figure 1

2. Study area: the southern wedge-top zone of the Po foreland basin

2.1. Regional setting

The Quaternary succession of the Po basin belongs to the widest Mio-Pliocene foreland basin of Italy shared by the converging Southalpine and Apennine thrust belts (Fig. 1). Since the Late Miocene, it evolved through successive tectonic pulses resulting in the outward migration of the Apennine arcs towards the North (Pieri and Groppi, 1981; Amadori et al., 2019 and references therein). Even if both thrust belts are still active (Devoti et al., 2011), the Quaternary subsidence pattern of the southern Po basin is mainly controlled by the activity of the northernmost, buried and blind Apennines structures, for which on-going thrusting (Burrato et al., 2003; Toscani et al., 2006, 2014; Boccaletti et al., 2011; Maesano et al., 2015) and extension (Bertotti et al., 1997; Argnani et al., 2003; Zuffetti and Bersezio, 2020) have been proposed.

The 3-D stratigraphic framework of the Po basin has been investigated at multiple space-time scales by different methodologies, including interpretation of seismic lines (Fig. 1C), electrical and electro-magnetic surveys (e.g., Bersezio et al., 2007; Mele et al., 2018; Amadori et al., 2019), core and well-log correlation (Regione Emilia-Romagna and Eni-AGIP, 1998; Regione Lombardia and Eni-Agip, 2001; Bersezio et al., 2004; Garzanti et al., 2011; De Caro et al., 2020), geological and geomorphological mapping (Castiglioni et al., 1999; Bersezio et al., 2010; Francani et al., 2016; Zuffetti et al., 2018a), and geoarchaeological surveys (Cremaschi, 1987; Cremaschi and Nicosia, 2012).

The Quaternary basin fill thins and wedges out towards the northern and southern basin margins, as well as towards the intra-basin culminations of the buried ramp-folds where isolated reliefs raise above the present-day average alluvial terraces (Fig. 1B) (Desio, 1965; Benedetti et al., 2003; Livio et al., 2009; Bersezio et al., 2010; Bresciani and Perotti, 2014),

delineating a complex pattern of Quaternary depocentres and structural highs. Owing to high sedimentation rates, up to 0.6-1.0 mm yr^{-1} (Bartolini et al., 1996; Mancin et al., 2009), the Quaternary stratigraphic successions may reach a thickness of more than 1 km in the main depocentres (Fig. 1D). The basin fill consists of a diachronic mega-regressive sequence of Lower-Middle Pleistocene shallow marine to fluvio-deltaic deposits, followed by Lower-Upper Pleistocene alluvial and glacio-fluvial units (Dondi et al., 1982; Regione Lombardia and Eni-Agip, 2001). Industrial seismic data show that four major angular unconformities, consequent to the major Miocene-Pleistocene Apennine tectonic stages (Latest Tortonian, intra-Messinian, intra Zanclean and Gelasian unconformities, Ghielmi et al., 2013), bound the highest-rank sequences forming the Mio-Pleistocene succession of the central Po Plain. Above the Gelasian unconformity, the Middle-Late Pleistocene unconformities identified by surface geological mapping become too close together towards the basin margins to be confidently traced in the subsurface by seismic lines and deep wells alone (Garzanti et al., 2011), and require down-tracing based on outcrop-borehole correlations (Bersezio et al., 2004, 2010, 2014; Bini et al., 2004a, 2014; Zuffetti, 2019). The subsurface Quaternary regional chronostratigraphic dataset relies on magnetostratigraphic interpretations and some biostratigraphy from sparse wells in the northern Po Plain, correlated southwards through regional seismic profiles (Scardia et al., 2006). Micropalaeontological, radiocarbon, and Optically-Stimulated Luminescence (OSL) data from surface exposures are available in the literature (review in Fontana et al., 2014; Zuffetti et al., 2018b; Zuffetti and Bersezio, 2020).

Previous work, using provenance analysis and magnetostratigraphy, links the Pleistocene advance phases of the alpine glaciers to the southward progradation of alpine-sourced glacio-fluvial systems, which reached the main depocentres in front of the Apennine arcs (Muttoni et al., 2003). In the northern Po basin, the onset of glaciations is documented by glacial amphitheatres and related glacio-fluvial and aeolian sediments (Penck and

Brückner, 1909; Bini, 1987, 1997a; Bini et al., 2004b) (Fig. 1A) and by a sudden upsection increase in grain-size, testifying to the transition from floodplain-dominated to mainly braided environments related to the outwash systems of the alpine glacio-fluvial fans (Scardia et al., 2012; Fontana et al., 2014).

2.2. Structural, stratigraphic and geomorphological setting

The study area has been selected in the region where two isolated tectonic reliefs raise above the Lombardy Po Plain (San Colombano Structure and Casalpusterlengo-Zorlesco Structure; SCS and CZS, Fig. 1B). These structures evolved because of the N-ward propagation of an emergent ramp fold belonging to the Emilia Arc, in the rear of the blind tip of the Apennine outermost thrust (Figs. 1B, 2B). Recent detailed geological mapping and morpho-structural analyses (Zuffetti et al., 2018a; Zuffetti and Bersezio, 2020) suggest that this region is a good candidate for modelling the space-time increments of tectonics and deposition under the control of Quaternary climate cycles.

The structural framework of the study area derives from N-ward thrusting, folding, and progressive uplift since the Late Miocene (Ghielmi et al., 2013). Since the Pleistocene, the San Colombano structure (SCS) (Figs. 1B, 2B) has been subjected to uplift and wrenching, driven by N-ward propagation of the San Colombano frontal thrust, a segment of the Emilia Arc, along the Pavia-Casteggio lateral ramp and the Casalpusterlengo-Zorlesco Transfer Fault (PCLR and CZTF respectively in Fig. 2B) (Benedetti et al., 2003; Zuffetti and Bersezio, 2020). The structure was dissected by repetitive faulting events up to the Latest Pleistocene. The Casalpusterlengo-Zorlesco transfer fault separates the San Colombano Structure from the Casalpusterlengo-Zorlesco WNW-ESE oriented buried structures (CZS in Figs. 1B, 2B) (compare to Bigi et al., 1990), which correspond to the mentioned morphological reliefs (Desio, 1965; Cremaschi, 1987). Middle-Late Pleistocene folding and

uplift, dextral wrenching and late extensional collapse were suggested at these sites by Bersezio et al. (2010) and Zuffetti and Bersezio (2020).

The San Colombano hill exposes the folded Upper Miocene marine sediments (Sant'Agata Fossili marls, Fig. 2A), cut by the Gelasian unconformity and covered by Lower Pleistocene, shallow-water transgressive sediments (San Colombano Formation, Fig. 2). During the Early *pro parte*-Middle Pleistocene, the Gelasian Unconformity was folded and eroded with the development of the Middle-Late Pleistocene angular unconformity (Zuffetti et al., 2018a and references therein). OSL data constrain the oldest alluvial and glacio-fluvial sediments above this unconformity to post MIS5e to MIS4 interval (Cascina Parina 1 Synthem, CPS1) (Fig. 2A; Table 1) (Zuffetti et al., 2018a). The subsequent Cascina Parina 2 Synthem is preserved only within relicts of palaeo-valleys on the San Colombano hill and correlates to Upper Pleistocene glacio-fluvial units in the surrounding plain and on the Casalpusterlengo relief (Fig. 2B) (Zuffetti et al., 2018a), whose top boundary is constrained by radiocarbon age determinations to the initial MIS2 (Table 1). These synthems are terraced and covered by the Last Glacial Maximum (LGM) glacio-fluvial Invernino Synthem (INS), whose age is constrained to the MIS2 by radiocarbon age determinations (Table 1). A mildly weathered loess covers Cascina Parina 1 and 2 and Invernino synthems at the hilltops (L2, Fig. 2A). Widespread colluvial wedges (Monteleone Synthem) (Zuffetti et al., 2018a) blanket the San Colombano hillslopes. On the surrounding plain, Invernino and Cascina Parina 1 synthems are crosscut by the latest Pleistocene Paleo Sillaro Synthem (PSS) that forms a shallow, early post-glacial terrace run by abandoned, meandering river traces. The late post-glacial-to-recent entrenchment of the river network led to deposition of the Po Synthem (PoS, Fig. 2A) within the lowermost terraced valleys, crosscutting the older deposits.

Table 1

3. Materials and methods

Surface and subsurface direct data are integrated to constrain the 3-D model to the space and time geological evolution. The surface data from the several outcrops on the tectonic reliefs (San Colombano, Casalpusterlengo, Zorlesco) (Fig. 2) and the scattered, very shallow exposures (1-6 m below the ground surface) on the terraced plain, permitted to down-trace stratigraphic boundaries and tectonic structures for surface-borehole correlations (Fig. 3). Exposures also provided the sedimentological, petrographic, stratigraphic and structural 2- and 3-D analogues for comparisons with the array of litho-textural associations drawn by 1-D borehole log descriptions. The quantitative model was computed by the potential-field method of interpolation (Chilès et al., 2004). The result is a space-time quantitative model that incorporates the effects of incremental tectonic activity and the climatic controls on stratigraphic evolution, being constrained to the hierarchy and relative chronology of geological entities and events (Zuffetti et al., 2020).

3.1. Surface geology dataset

The geological and geomorphological map at 1:10.000 scale of the 450 km^2 wide study area (Fig. 2) was the starting point to constrain surface-borehole correlations. The geological map was digitised following the Unconformity-Bounded Stratigraphic Units (UBSU) classification proposed by Zuffetti et al. (2018a). To simplify the figures, the equivalence between surface units and their subsurface counterparts has been illustrated by adding the suffix "-sse" (subsurface equivalent) to the denomination of the buried units.

Figure 2

Sedimentological and facies analysis of more than 120 exposures, described in vertical logs and/or lateral profiles, was carried out taking notes from Miall's (1996) classification of alluvial facies (Table 2). Palaeocurrent distribution was obtained by measuring planar and through cross-bedding, ripple cross lamination, gravel clasts imbrication and channel-margin

orientations. Correlation among high-resolution stratigraphic logs was drawn in the field during mapping, yielding the record of facies variability throughout the sedimentary units and of the nature and continuity of their bounding surfaces. The petrographic composition of gravel and sand samples was analysed directly in the field and on thin sections, to characterise the petrographic signature of the mapped stratigraphic units (Fig. 4), to constrain palaeo-provenance interpretations, and support subsurface correlations.

3.2. Subsurface stratigraphy dataset and surface-borehole correlations

The study is based on 527 subsurface log data (Figs. 2A, 3): 257 water wells (max. investigation depths: 210 m below ground surface, b.g.s., eight analysed in this study), 206 boreholes with core recovery (max. investigation depths: 204 m b.g.s.; 39 analysed in this study), 15 hydrocarbon wells; 46 geophysical soundings (max. investigation depths: 300 m b.g.s.; eight acquired in this study). Stratigraphic logs were normalised and classified following a specifically built litho-textural alphabetic Code (Bersezio et al., 2004; Zuffetti et al., 2020) (Table 2). Existing data were derived from the Database of Lombardy Region, Sacco (1912), Ministero dei Lavori Pubblici and Ufficio Idrografico del Po (1924, 1933), Desio and Villa (1960), MiSE et al. (2009), local public authorities, private companies and consultants. Vertical electrical soundings (VES, Fig. 2A) from Mele et al. (2013, 2018, 2019) were considered; older data from Alfano and Mancuso (1996) were re-interpreted taking notes from Mele et al. (2018). Ten N-S cross-sections, parallel to the regional trend of the stratigraphic bodies and orthogonal to the regional tectonic structures, and five W-E cross-sections oriented to depict the sedimentary variations between the tectonic sectors of the area (SCS and CZS, Fig. 2B), were drawn on polyline traces which join the data points and preserve the real separation among subsurface data.

Table 2

The study of the 1-D borehole stratigraphy was based on the litho-textural and compositional description of the disturbed samples, and on a more complete facies characterisation on cores of rocks and cohesive sediments. The surface-borehole stratigraphic correlation procedure relied on the identification of unconformable surfaces and on their ranking (Miall, 1996; Allen and Allen, 2013), following the criteria and principles listed in Table 2. Identification of buried soil profiles, colour and organic content of fine-grained sediments, and palaeontological content, were considered as complementary attributes to support correlations with surface stratigraphy. Compositional analysis of gravel-sized clasts (Fig. 4) on the available subsurface samples and data from literature supported provenance interpretation and comparisons with surface sediments. Age constraints on the Quaternary stratigraphic units were derived from the ^{14}C and OSL age determinations listed in Table 1. These data have been compared to the magnetostratigraphy of the nearest *Regione Lombardia* borehole logs (Muttoni et al., 2003; Scardia et al., 2006, 2012).

Iterative refinements of the correlation framework were operated after checking the internal consistency of the correlation procedure, non-contradiction between the datasets, likelihood and simplicity of the results compared to the outcropping units. The inspection of the maps and stratigraphic cross-sections (Fig. 3) allowed to interpret the Quaternary geological history of the study area. In the subsurface, the hierarchically ranked surfaces were interpreted as: i) unconformable boundaries either after erosional truncations, and/or depositional discordances (onlap); ii) conformable and paraconformable boundaries resulting from continuous vertical superposition of stratigraphic units with no evidence of erosional truncation or angularity; iii) downlap and toplap geometries, interpretable as progradation patterns. The tectonic structures were first recognised and mapped at the surface in the San Colombano structure (Zuffetti et al., 2018a; Zuffetti and Bersezio, 2020) and Casalpusterlengo-Zorlesco structure (Fig. 2) (Bersezio et al., 2010) then they were traced to

their forecasted subsurface location considering: i) the coherent offsets of the correlation surfaces exceeding the thickness of the Intermediate-Rank Stratigraphic Units (i.e. tens of metres), ii) the local geometrical anomalies occurring at the forecasted sites at the mentioned scale length, iii) the lateral terminations and the associated thickness, and litho-textural changes of the stratigraphic units, iv) the comparisons with the local geophysical images (Mele et al., 2018 and references therein) and the available structural schemes derived from regional seismic interpretations (Pieri and Groppi, 1981; Bigi et al., 1990).

3.3. 3-D geological modelling

Maps, cross-sections (Fig. 3), relative chronology, and age determinations provided the input constraints to quantitative geological modelling. The 3-D model was processed by 3DGeoModeller® software (Chilès et al., 2004, Calcagno et al., 2008). This software was selected because it allows to integrate surface and subsurface datasets (geological maps and cross-sections, borehole and geophysical logs) and permits to explore different solutions for the tectono-stratigraphic geometries and relations between the sedimentary bodies. Input data as contact points, located on the geological boundaries, and structural vector data (dip-azimuths), were drawn from maps and extracted from cross-sections following the methodology proposed by Zuffetti et al. (2020). GeoModeller describes the 3-D geological space through a continuous potential-field scalar function, where geological boundaries are reference isopotential surfaces and structural dips define gradients of the scalar function. The interpolation of the scalar field is based on universal co-kriging between contact data point and structural vector data at any point of the model domain (Lajaunie et al., 1997). GeoModeller employs a rule-based modelling to control the stratigraphic relationships - onlapping or erosional - and the fault chronology within the fault network. The chronological ordering of the geological units, gathered in interacting series throughout a stratigraphic pile

and after fixing the reference isosurface (top or bottom boundary), governs the time-ordering of Series within the numerical computation. Defining an onlap or erode relationship for each series drives its modelling behaviour with respect to the chronologically older ones (Calcagno et al., 2008). New modelling routines are proposed here to fit the classical procedure with the tectono-sedimentary setting of the case study, and will be presented in Section 5. The modelled geological entities (fault surfaces, stratigraphic boundaries and volumes) are implicitly defined by the value of the scalar field. The latter can be visualised in 1-D along a borehole, in 2-D on a map or section and as 3-D surface shapes and volumes, whose resolution can be chosen accordingly with the user's needs and is independent from the former model computation. The consistency of the results was verified by 3-D visual inspection, to check with geologically coherent geometries and crosscut relationships relatively to the interpreted geological evolution.

Figure 3

4. Surface and subsurface geological architecture and evolution: constraints to the quantitative model

The hierarchic stratigraphic scheme of the Quaternary southern Po basin fill resulting from this study is presented in Fig. 3. It comprises five High-Rank Stratigraphic units (HRS from 0 to 4) bounded by high-rank unconformities of regional extent, that are the Gelasian Unconformity, intra-Calabrian unconformity (U1), Early-Middle Pleistocene unconformity (U2), Middle-Late Pleistocene unconformity (U3) and latest Pleistocene-Holocene unconformity (U4). Within them, intermediate-rank stratigraphic surfaces bound 11 Intermediate-Rank Stratigraphic units (IRS, Fig. 3). In outcrops these surfaces correspond to the mapped terrace scarps (Figs. 2A, 3). The lowermost hierarchic order allowing surface-subsurface comparisons/correlations is represented by the low-rank surfaces bounding the individual genetic units, which are represented by bedsets and facies associations in the field

and by 1-D litho-textural stacking patterns in boreholes. Most of them were drawn above the Middle-Late Pleistocene unconformity, where the largest number of surface data was available.

In the following sections, the essential features of the surface and subsurface stratigraphic units and boundaries are presented. According to a specific request by the Editor we addressed most of the descriptive geological data to the supplementary material. The dataset is summarized in Table 3 and in the main text, to support the interpretations and the set-up of the model.

The pre-Quaternary substrate of the model comprises the Mio-Pliocene marine succession largely described in the literature (Ghielmi et al., 2013; Amadori et al., 2018 and references therein) (Fig. 1C, D). Within the substrate, the intra-Zanclean Unconformity (ZU) and the Pliocene sediments are missing on the San Colombano hill (Zuffetti et al., 2018a). Dip attitudes measured in boreholes adjacent to the hill (MiSE et al., 2009) testify that the intra-Zanclean Unconformity was truncated by the Gelasian Unconformity (GU, Fig. 3) after folding.

Figure 4

Table 3A

4.1. Gelasian Unconformity (GU) – Early Pleistocene High-Rank Stratigraphic Unit 0 (HRS0)

The Gelasian angular unconformity bounds at the base the Early Pleistocene (Calabrian) High-Rank Stratigraphic Unit 0, formed by the outcropping shallow marine sediments of the San Colombano Formation (SCF, Fig. 2A) and subsurface equivalents (SCF-sse, Fig. 3). The Gelasian Unconformity is buried at the Casalpusterlengo-Zorlesco hills (Fig. 3). The San Colombano Formation is locally missing at the San Colombano hill due to erosion below the Middle-Late Pleistocene Unconformity U3 (Zuffetti et al., 2018a). The thickness of the High-

Rank Stratigraphic Unit 0 ranges between 5 and at least 90 m, with the minimum values on the crests of the San Colombano and Casalpusterlengo-Zorlesco structures (5 m and 50 m, respectively). A Calabrian age is attributed to the High-Rank Stratigraphic Unit 0 based on foraminiferal assemblages of lithozones SCFb and SCFc (Fig. 6A), owing to the presence of several species typical of the *Globigerina cariacoensis* zone (Cita et al., 2012 and references therein) like *Neogloboquadrina pachiderma*, *Globigerina cariacoensis* and to the absence of *Truncorotalia truncatulinoides excelsa* (Fig. 3; Table 3A). The well-known "northern guests" *Hyalinea baltica* and *Arctica islandica* appear in samples from the uppermost lithozone of the formation (lithozone SCFc, Fig. 6A), confirming this attribution.

In outcrops, the Gelasian Unconformity and the San Colombano Formation are gently folded by an ENE-WSW-trending anticline, which refolds the former anticline involving the Miocene formations at the San Colombano hill (Zuffetti et al., 2018a). At Casalpusterlengo-Zorlesco (Fig. 3), subsurface correlations suggest that a WNW-ESE-trending anticline folds the High-Rank Stratigraphic Unit 0, re-deforming the intra-Zanclean and the Gelasian unconformities (Ghielmi et al., 2013). At stratigraphic depths corresponding to the position of the High-Rank Stratigraphic Unit 0, Vertical electrical soundings show electrical resistivities between 2 and 50 Ωm, in keeping with the expected electrical response of the succession of fine-grained, saltwater-logged sediments covering the basal conglomerate-sandstone facies, which was found in the nearest boreholes (Mele et al., 2018).

The High-Rank Stratigraphic Unit 0 correlates to the informal subsurface unit GU0 of Bersezio et al. (2010) and its features compare to the conductive electrostratigraphic Group 4 of Mele et al. (2018). Regionally, the Unit corresponds to part of the generic marine Quaternary as it is defined in logs from the hydrocarbon wells drilled in the central Po Plain (MiSE et al., 2009). Yet, the distinction between 'Continental Quaternary', 'Marine Quaternary', 'Pliocene' proposed by the old AGIP-ENI borehole logs available to the public

refers to chronostratigraphic scales predating the present-day timescale (Cohen and Gibbard, 2019) and biostratigraphic details are not freely accessible, so the stratigraphic position and depth of the base Quaternary from this source must be critically considered. Regionally, in the southern Po basin, the High-Rank Stratigraphic Unit 0 might correspond to part of the former Gelasian-Calabrian large-scale PL4 sequence of Ghielmi et al. (2013), which has been replaced by PS1a sequence by Amadori et al. (2019) and PS1 large-scale sequence belonging to the PS Allogroup by Amadori et al. (2020). At the Alpine basin margin, it could correspond to the lowermost shelf sequence described by Scardia et al. (2012).

Figure 5

4.1.1. Stratigraphy, facies associations and interpretation

In outcrops, the San Colombano Formation comprises six facies associations (facies F1 to F6, Fig. 5) organised into three lithozones (SCFa, SCFb, SCFc) (Fig. 6A; Table 3A) that are described in the supplementary material to which the reader is addressed.

Lithozone SCFa lies above the Gelasian Unconformity. The association of F1 and F2 (Fig. 5; Table 3A) in outcrops suggests deposition of the lithozone SCFa in a gravel-sand beach/shoreface setting, where isolated patches of encrusting colonial organisms, typical of warm climates and shallow bathymetry, could develop on the raised crests of the pre-Gelasian folds at San Colombano and Casalpusterlengo-Zorlesco structures. The transition to a sandy, prograding shoreface away from these settings, is suggested by the location of the subsurface F3 litho-textural association and stacking patterns (Figs. 5, 6; Table 3A). Gravel composition suggests recycling of Alpine-derived clasts after erosion of the Oligo-Miocene clastic formations of the N-Apennine front (Vercesi and Scagni, 1984; Zuffetti et al., 2018a) and supports river input from the southern basin margin.

Lithozone SCFb lies above SCFa at the San Colombano hill (Fig. 6A; Table 3A). It comprises alternations of facies F4 and F5 (Fig. 5, 6A; Table 3A; see supplementary data for

description). Comparable litho-textural associations occur in the near subsurface above and adjacent to the subsurface lithozone equivalent to SCFa. The SCFb subsurface equivalent lithozone consists of blue and dark grey fossiliferous claystones and marlstones, which alternate with 5 to 10 m-thick sandy bedsets occasionally forming fining-upward sequences (Fig. 6C; Table 3A). F4 facies assemblage suggests a low-energy marine environment, dominated by clastic suspension settling punctuated by very fine sandy layers. F5 facies points to short-time, higher-energy siliciclastic input, recurrently mixed with displaced biota. The abundance of *Cardium* accompanied by an oligotypic benthic foraminifera association (Table 3A) suggests a brackish, coastal lagoon environment, probably associated with freshwater river discharge. This agrees with previous interpretations (Anfossi et al., 1971; Anfossi and Brambilla, 1980). Mixing of infralittoral and circalittoral foraminifera with the lagoonal taxa and with siliciclasts suggests recurrent input from high-energy events like storms and river surges from the mainland.

Lithozone SCFc covers and juxtaposes to the SCFb beds in outcrops (Fig. 6A). It consists of F6and F3 facies associations) (Figs. 5, 6A; Table 3A) that correlates with dam-thick, grey fossiliferous clays in the subsurface, with 5-10 m-thick sandy layers at the top (SCFc-subsurface equivalent lithozone) (Fig. 6C). The F6 mudstones with abundant planktonic foraminifera were likely deposited by settling and low-energy currents in an offshore setting, passing upwards to a lower shoreface environment with low flow-laminated fine-grained sands (F3). The common occurrence of cold-water taxa reflects the onset of environmental cooling.

4.1.2. Stratigraphic interpretation of the Early Pleistocene High-Rank Stratigraphic Unit 0.

The association of the SCF surface and subsurface lithozones suggests that after folding and uplift, the Gelasian Unconformity cut the older units down to the Miocene formations at the

crests of the San Colombano and Casalpusterlengo-Zorlesco folds during transgression. Since then, from the uplifted settings coastal sediments (beach then coastal brackish lagoon) of SCFb lithozone covered the shoreface deposits of SCFa lithozone and subsurface equivalents. Based on the palaeontological association, this first transgressive-regressive cycle developed under Calabrian warm climate conditions, before the occurrence of the "northern guests". Their appearance suggests the onset of environmental cooling that started since the transition to the successive lithozone SCSc. This latter documents a transgressive-regressive trend by the spreading of offshore muds covered by lower shoreface sands since the first occurrence of *Hyalinea balthica* and *Arctica islandica* but predating the first occurrence of *Truncorotalia truncatulinoides excelsa.* Even if the misfit calibration of the first occurrence of the "northern guests" to magnetostratigraphy and geochronology is still debated in the Po basin (Gunderson et al., 2014; Crippa et al., 2018; Maestrelli et al., 2018), in two sections some tens of kilometres E of the study area they are shown to occur since the lower part of the *G. cariacoensis* zone (Crippa et al., 2019). The comparison with our data suggests that the Calabrian High-Rank stratigraphic unit 0 developed during the lower part of the *G. cariacoensis* zone, and likely ended around the onset of the so-called "Early-Middle Pleistocene transition" that is currently matched to MIS36 (Cohen and Gibbard, 2019 and references therein).

Figure 6

4.2. Intra-Calabrian Unconformity (U1) – Calabrian High-Rank Stratigraphic Unit 1 (HRS1)

The intra-Calabrian U1 unconformity and High-Rank stratigraphic unit 1 are not exposed at the San Colombano and Casalpusterlengo–Zorlesco anticline culminations due to truncation by the U2 (Early-Middle Pleistocene) and U3 (Middle-Late Pleistocene) unconformities

(Figs. 3, 7). The high-rank Intra-Calabrian Unconformity (U1) marks the base of the High-Rank Stratigraphic Unit 1 with an increase in sandy sediments above the fossiliferous marly clays of the High-Rank Stratigraphic Unit 0 (Fig. 6B). Borehole correlations suggest an antiformal geometry for this surface above the mentioned ramp anticlines (Figs. 2B, 3). The sharp contacts of coarse- above fine-grained sediments delineate the intermediate-rank surfaces S1.1, S1.2, S1.3, bounding the Intermediate-Rank Stratigraphic Units 1.1, 1.2, 1.3 (IRS1.1, IRS1.2, IRS1.3, respectively) (Figs. 3, 7), which consist of alternating sandy (gravelly)-clayey decametric-thick sequences. Even if no apparent angular relationships could be interpreted among them, thickness changes between 0 and at least 150 m denote a wedge shape of the entire High-Rank Stratigraphic Unit 1 and of its component intermediate-rank units (Figs. 3, 7). The High-Rank Stratigraphic Unit 1 markedly thins towards the crest of the Casalpusterlengo-Zorlesco fold as well as towards the crest of the San Colombano structure, where it is missing because of subsequent erosion (Figs. 3, 7). The Calabrian age was assigned by the stratigraphic position that postdates the first occurrence of the "northern guests" *H. balthica* and *A. islandica* observed within the San Colombano Formation (High-Rank Stratigraphic Unit 0) and predates the Middle Pleistocene microfaunal associations, in agreement with micropalaeontological data from boreholes (Bini et al., 2016) (Tables 2, 3A).

4.2.1. Stratigraphy, facies associations and interpretation

The High-Rank Stratigraphic Unit 1 encompasses the litho-textural subsurface associations F4, F7, F8 (Figs. 4, 5; Table 3A), forming three Intermediate-Rank Stratigraphic Units (Figs. 3, 7; Table 3A; see supplementary data for the description).

The lowermost Intermediate-Rank Stratigraphic Unit 1.1 consists of stacked F8 and F7 litho-textural associations organised into fining-upwards or stationary stacking patterns (Figs. 5, 7; Table 3A). The Intermediate-Rank Stratigraphic Units 1.2 and 1.3, above S1.2

and S1.3 respectively, are formed by gravelly sands and coarse sand intervals passing to mud-fine sand layers, building 10 to 30 m-thick fining-upward sequences (F8 subsurface litho-textural association) (Fig. 7C; Table 3A). These units are replaced by laterally continuous, up to 20 m-thick intervals of grey to black clays and silty clays with wood fragments (F7 litho-textural association) but without marine fossils, that are here interpreted as flood-plain/swamp sediments (Table 3A).

4.2.2. Stratigraphic interpretation of the Calabrian High-Rank Stratigraphic Unit 1

The High-Rank Stratigraphic Unit 1 is formed by three clastic, intermediate-rank units with fining-upwards trends, topped by decametric-thick, mud-clay intervals, at places organic-rich, that are interpreted as regressive-transgressive sequences. From the lowermost to the uppermost intermediate-rank unit, grain-size increases upwards and marine microfossils disappear from the fine-grained intervals. The Intermediate-Rank Stratigraphic Unit 1.1 is interpreted as the result of delta plain-delta front progradation over U1 and subsequent transgression to a brackish lagoon/delta plain environment also according to the benthic foraminifera assemblage (Murray, 2006; see supplementary material). Alluvial to delta-plain environments, with meandering systems replaced by widespread floodplains and swamps, are suggested from the features of the Intermediate-Rank Stratigraphic Units 1.2 and 1.3 (Miall, 1996; Reading, 1996). The decametric-thick, regionally traceable very fine-grained and organic-rich layers at the top of the Intermediate-Rank Stratigraphic Units 1.1, 1.2, 1.3 (Figs. 3, 7) represent the transgressive periods, the last predating the regional regression recorded at U2 (see Section 4.3). For these reasons we interpret the High-Rank Stratigraphic Unit 1 as an overall Calabrian regressive sequence, punctuated by three minor regressive-transgressive units. Regionally, the High-Rank Stratigraphic Unit 1 regressive cycle might correspond to the Early Pleistocene progradation of the Po basin trunk river (palaeo-Po or palaeo-Dora

rivers and deltas fed by the Western Alps) (Garzanti et al., 2011) and its tributaries fed from the Western Southern Alps, as suggested by the dominance of metamorphic and volcanic lithoclasts with serpentinites over the sedimentary rock fragments in the gravel fraction of borehole samples in the study area (Figs. 4, 7D; Table 3A). The stratigraphic position compares the High-Rank Stratigraphic Unit 1 to part of the Marine Quaternary of Di Dio et al. (2005), as well as to part of Qm1 of ISPRA (2015) and part of PS2s of Amadori et al. (2019, 2020) that were interpreted in the subsurface of the Po basin to the E (i.e. seawards) of the study area.

Figure 7

4.3. Early-Middle Pleistocene Unconformity (U2) – Calabrian (?) – Middle Pleistocene High-Rank Stratigraphic Unit 2 (HRS2)

The buried Early-Middle Pleistocene angular Unconformity U2 bounds at the base the High-Rank Stratigraphic Unit 2, a sand and gravel subsurface unit truncated by the Middle-Late Pleistocene unconformity U3. U2 is constrained by the widely traceable, abrupt contact between the fine-grained transgressive unit that tops the Calabrian High-Rank Stratigraphic Unit 1 and the overlying gravel/sand bedsets (Fig. 7; Table 3A). Below U2, High-Rank Stratigraphic unit 1 is eroded on the limbs and crest of the San Colombano and Casalpusterlengo-Zorlesco folds. According to the best fitting solution of subsurface correlations, angular unconformity U2 dips away from the hinge of these km-scale gentle folds, drawing their limbs (Figs. 3, 7A).

Three intermediate-rank, low-angle unconformities (S2.1, S2.2, S2.3) (Fig. 3), have been traced within the High-Rank Stratigraphic Unit 2 into abrupt litho-textural contrasts. These surfaces bound the Intermediate-Rank Stratigraphic Units 2.1, 2.2, 2.3 (IRS2.1, IRS2.2, IRS2.3 in ascending stratigraphic order) (Fig. 3) that are stacked into an overall coarsening-upwards trend. All of them progressively wedge out and lap onto U2 towards the

culminations of the San Colombano and Casalpusterlengo-Zorlesco folds, assuming a wedge-shape external geometry (Fig. 7B). At these sites, the low-angle S2.1, S2.2 and S2.3 intermediate-rank unconformities merge to originate the progressive, high-rank angular unconformity U2 (Figs. 3, 7C).

The High-Rank Stratigraphic Unit 2 is missing below U3 in the San Colombano and Casalpusterlengo hills and in the southernmost study area, while its thickness ranges between 40 m at the Zorlesco hump and some 120 m N-ward, and between Zorlesco and San Colombano (cross-section 3W) (Fig. 3). The stratigraphic position and crosscut relationships with the Calabrian and Late Pleistocene units suggest a late Calabrian (?)–Middle Pleistocene time span for the development of High-Rank Stratigraphic Unit 2. Pollen spectra from samples collected at a borehole located some kilometres to the NE of the study area (Rigato, 2007) (Tables 2, 3A) documented temperate cold climate conditions in the dam-thick fine-grained layers with peat on top of the gravel sand fining-upwards sequences corresponding to the Intermediate-Rank Stratigraphic Units 2.2 and 2.3. For both units, an Early Pleistocene age can be excluded due to the absence of *Tsuga* pollens (conifer that is plentiful during the Early Pleistocene) (Moore et al., 1991). Moreover, the rare occurrence of *Carya* and *Pterocarya* permits to exclude attribution to the upper part of the Middle Pleistocene that is barren of these pollens (Moore et al., 1991). The deposits of the High-Rank Stratigraphic Unit 2 are associated with electrical resistivity values ranging between 130-170 Ωm, which are calibrated in boreholes to freshwater logged, coarse-grained clastic sediments in the specific setting of the study area (Mele et al., 2018, 2019).

4.3.1. Stratigraphy, facies associations and interpretation

The Intermediate-Rank Stratigraphic Unit 2.1 is composed of gravelly sands to medium sand layers and of sand-silt alternations, organised into 10 to 15 m-thick fining-upwards sequences

of F8 and F7 litho-textural associations (Figs. 4, 5, 6B, 7; Table 3A; see the supplementary material for the complete description). The overlying Intermediate-Rank Stratigraphic Unit 2.2 shows a quite comparable external shape, litho-textural association and stacking pattern, onlapping and wedging out at progressively increasing elevation onto the limbs of the mentioned anticlines (Fig. 7B; Table 3A; supplementary material).

The proportion of coarse-grained sediments increases within the Intermediate-Rank Stratigraphic Unit 2.3 (sandy gravels alternating with gravel-sand layers; F10 litho-textural association) (Table 3A; supplementary material) which starts abruptly above the intermediate-rank unconformity S2.3.

4.3.2. Stratigraphic Interpretation of the Calabrian (?)–Middle Pleistocene High-Rank Stratigraphic Unit 2

The sediments of the High-Rank Stratigraphic Unit 2 display typical features of alluvial depositional settings (absence of marine fossils, stationary to fining-upward trends of the lowermost rank genetic units, high ratio between coarse and fine-grained sediments). The geometry of sedimentary bodies and litho-texture assemblages of the Intermediate-Rank Stratigraphic Units 2.1 and 2.2 point to superposition and interfingering of mixed-load alluvial depositional systems replaced by floodplain sequences. The composition of gravel clasts indicates a provenance from the Central Alpine nappes and Western Southalpine basement thrusts for the Intermediate-Rank Stratigraphic units 2.1 and 2.2, with more abundant feeding from the Western Southern Alps for the Middle Pleistocene Unit 2.2. More specifically, its peculiar petrographic signature suggests provenance from the Verbano area, in accordance with the sand petrography-based palaeogeographic interpretation proposed by Garzanti et al. (2011) for the coeval sediments cored in western Lombardy. Subsequently, bedload-dominated, gravelly alluvial systems prograded then retrograded all over the area

during at least two increments nested within the Middle Pleistocene Intermediate-Rank Stratigraphic Unit 2.3. These systems were fed by the metamorphic basement of the Central and Southern Alps, with very minor contributions from the Southalpine sedimentary covers. Provenance of the gravel clasts of High-Rank Stratigraphic Unit 2 from the northern metamorphic core of the Alps and from the basement thrusts of the western Southern Alps suggests glacial routing, because during non-glacial times the Po basin drainage network was mostly sheltered from the mentioned reaches, also owing to the dumping effect of the large sub-alpine lakes (Verbano and Lario, to the NW and N of the study area, Fig. 1B). These considerations, the stratigraphic position, the comparisons and correlations with the regional framework and the palaeoenvironmental interpretations (Baio et al., 2004; Bersezio et al., 2004; Bini et al., 2004a; Garzanti et al., 2011; Scardia et al., 2012), allow to consider the Calabrian (?) Intermediate-Rank Stratigraphic Unit 2.1 and the Middle Pleistocene Intermediate-Rank Stratigraphic Unit 2.2 as the distal equivalents of the cyclically prograding-retrograding units of the glacio-fluvial outwash of the Early-Middle Pleistocene Verbano and Lario amphitheatres, respectively the Bozzente, and Binago/Specola glacio-fluvial synthems (Da Rold, 1990; Bini, 1997a; Zuccoli, 1997; Bersezio et al., 2014; Bini et al., 2014; Francani et al., 2016) (Fig. 3). Relying on the stratigraphic position and regional down-tracing of the stratigraphic units dated to the Middle Pleistocene, we propose the equivalence between Intermediate-Rank Stratigraphic Unit 2.3 and the Middle Pleistocene lowermost glacio-fluvial synthems of the Besnate Supersynthem, which correlate with the Besnate glacial amphitheatre at the Alpine margin (Bini, 1987, 1997b; Da Rold, 1990; Bersezio et al., 2014; Bini et al., 2014; Francani et al., 2016). In the subsurface, the age and stratigraphic position allow to compare the High-Rank Stratigraphic unit 2 as a whole with the upper part of the Calabrian PS2s sequence of Amadori et al. (2019) plus the lower part of the Middle Pleistocene PS3s of the same authors, overlapping PS3a of Amadori et al. (2020)

and with PLCa-b units of ISPRA (2015) in the central Po basin.

The low-angle unconformities at the base of the three Intermediate-Rank Stratigraphic Units, coarsening of the sand bodies and correlative thinning of the fine-grained intervals in between them, onlap and wedging-out above the limbs of the San Colombano and Casalpusterlengo–Zorlesco folds where the High-Rank Unconformity U2 bends upwards (Fig. 7A, C), indicate progressive development of unconformities and syntectonic deposition (Schumm et al., 2002; Kirby and Whipple, 2012) during folding and uplift. Therefore, High-Rank Unconformity U2 is interpreted as a progressive, composite angular unconformity (Anadòn et al., 1986), probably of the limb rotation type (Rafini and Mercier, 2002), that developed by composition, deformation and erosion of different segments of the intermediate-rank unconformities. The marked offset by several tens of metres of Pleistocene stratigraphy (Fig.3), abrupt thickness and geometry changes of High-Rank Stratigraphic Unit 2, its component Intermediate-Rank Stratigraphic Units and the lowest-rank cycles within them, that could be drawn in the subsurface between the San Colombano and Casalpusterlengo–Zorlesco structures (cross-section 3W, Fig. 3), are interpreted as the expression of the Casalpusterlengo-Zorlesco fault (Bigi et al., 1990; Zuffetti and Bersezio, 2020) that represents the tectonic disjunction between the two mentioned thrust-folds. To the W of this disjunction, that likely acted as a lateral ramp, the San Colombano structure was uplifted by about 100 m with respect to the Casalpusterlengo–Zorlesco structure to the E. Synsedimentary activity along this structure corroborates the tendence of westward thickening of the sedimentary bodies immediately to the E of the fault (Figs. 3, 7E) by the growth of accommodation space in its footwall. The absence of the High-Rank Stratigraphic Unit 2 along the most raised sectors of the San Colombano and Casalpusterlengo–Zorlesco structures (Figs. 3, 7E, F) might be due to non-deposition on the crests and onlaps above the limbs of the two folds, followed by erosion.

As a whole, the High-Rank Stratigraphic unit 2 represents the first Quaternary large-scale continental regressive trend associated with Calabrian-Middle Pleistocene folding and uplift along the San Colombano and Casalpusterlengo-Zorlesco structures in the rear of the northern tip of the Emilia arc and to concurrent advance-retreat cycles of the alpine glaciers from the NW and N (Verbano and Lario amphitheatres; Fig. 1B). The high-rank angular unconformity U2, that is one of the prominent stratigraphic boundaries detectable in the subsurface of this sector of the Po basin, developed in response to late Calabrian–Middle Pleistocene thrust-folding and uplift. The intermediate-rank unconformities S2.2-3 and the intervening stratigraphic units are more likely associated with the Calabrian-Middle Pleistocene glacial cycles. The pattern of tectonic subsidence controlled the development of the depocentres and contributed with differential compaction to determine thickness changes away from the hinges of the San Colombano and Casalpusterlengo-Zorlesco positive structures.

4.4. Middle-Late Pleistocene Unconformity (U3) – High-Rank Stratigraphic Unit 3 (HRS3)

The Middle-Late Pleistocene high-rank, composite angular Unconformity U3 has been recognised in the San Colombano hill outcrops (Zuffetti et al., 2018a). It erodes the folded stratigraphy down to the Langhian marine substratum (Fig. 2A) and bounds at the base the High-Rank Stratigraphic Unit 3 that has been traced in the subsurface from the San Colombano and Casalpusterlengo-Zorlesco outcrops. High-Rank Stratigraphic unit 3 is a sand-gravel succession cut on top by the Latest Pleistocene-Holocene High-Rank unconformity U4 and by the present-day topographic surface. A Middle (?)-Late Pleistocene age was assigned to the High-Rank Stratigraphic Unit 3 based on radiocarbon and OSL age determinations on both surface and subsurface samples and on the crosscut relationships with

the underlying units (Figs. 2A, 8; Table 2). The exposed High-Rank Stratigraphic Unit 3 comprises four synthems, Cascina Parina 1 Synthem, Cascina Parina 2 Synthem, Invernino Synthem, Paleo Sillaro Synthem, bounded by intermediate-rank unconformities (Figs. 2A, 3) (Zuffetti et al., 2018a) which were down-traced to the subsurface into four intermediate-rank equivalent units. The thickness of the Unit ranges between 5 and 80 m, with the minimum values on the crests of San Colombano and Casalpusterlengo-Zorlesco structures (Fig. 3). The low-rank lithosomes show gentle concave-up shapes and abrupt thickness changes approaching the reliefs (Figs. 3, 8). The electrostratigraphy of the High-Rank Stratigraphic Unit 3 displays electrical resistivity higher than 150 Ωm, typical of the freshwater-logged, coarse-grained clastic sediments of the Po basin (Mele et al., 2018). The high-rank unconformity U3 gets gently folded and offset by wrench and extensional faults at the San Colombano hill, together with the overlying High-Rank Stratigraphic Unit 3 (Fig. 8A, D).

Figure 8

4.4.1. S3.1 - Cascina Parina 1 Synthem (CPS1)

The intermediate-rank erosional boundary S3.1 bounds at the base the lowermost synthem of the High-Rank Stratigraphic Unit 3, namely the Cascina Parina 1 Synthem (Zuffetti et al., 2018a). This sand-gravel unit crops out at the San Colombano and Casalpusterlengo-Zorlesco structures. OSL age determinations attribute the upper part of the synthem to the Late Pleistocene, between ca. 107 and 67 ka (Fig. 8A, B; Table 1). In the most complete successions, the age of the base of Cascina Parina 1 Synthem is constrained only by its superposition above the Middle Pleistocene Intermediate-Rank Stratigraphic unit IRS3 (Fig. 7); as a consequence, a Middle Pleistocene age for the base of the Cascina Parina 1 Synthem cannot be excluded. Its thickness ranges between about 5 and 40 m, with the minimum corresponding to the uplifted and truncated successions on top of the San Colombano hill (Fig. 8A). Where preserved, the top of the Synthem corresponds to a m-thick, rubified

hydromorphic palaeosol (Zuffetti et al., 2018b) (soil profile 'a', Fig. 8A, B), otherwise it is truncated by S3.2 (Figs. 3, 8A, B). A m-thick loess unit covers the palaeosol (L1, log F; Fig. 8A). The NW flank of the San Colombano hill exposes the thickest succession of Cascina Parina 1 Synthem, which thins from here to the SE (Fig. 8A). The synthem is formed by two lithozones characterised by two facies associations, F7-F8 and F9-F7 (CPS1a, b lithozones respectively) (Figs. 4, 5, 8, 9; Table 3B; see the supplementary material for the description).

The F7 facies association of lithozone CPS1a is interpreted as deriving from floodplain deposition of overbank fines, locally interbedded with crevasse splay deposits (O'Brien and Wells, 1986; Miall, 1996; Bridge, 2003; Ambrosi et al., 2008; Milli et al., 2016). It is replaced up-section by the F8 facies association that documents the development of channel-bar systems, with sandy bedforms, lateral accretion macroforms, large and minor channel fills (Cant, 1982; Miall, 1985; Blum, 1993; Bridge, 1993; Best et al., 2003; Ashworth et al., 2011; Horn et al., 2012) (Fig. 9A, B, C; Table 3B). Petrographic composition and palaeocurrent trends suggest that these mixed-load, meandering alluvial systems were fed from a western alpine source and by recycling of gravel and sand from the underlying units, considering the high-percentage of weathered clasts mixed with the un-weathered ones (Fig. 9B) (Zuffetti, 2019). The transition to lithozone CPS1b suggests the change from a meandering river alluvial setting to a sandy, bedload-dominated river distribution system, fed from the NW. Change in river style and palaeocurrents (Fig. 8A), abundance of water escape structures at specific stratigraphic positions within lithozone CPS1b observed approaching the San Colombano Structure (Fig. 9D) suggest syndepositional seismicity, following the criteria proposed by Obermeier (1996) and McCalpin (2009). Also the lateral replacement between lithozones CPS1a and CPS1b in the subsurface, and the recurrent amalgamation of sand bed-sets towards the Casalpusterlengo-Zorlesco structure (Fig. 8B), suggest syn-tectonic deposition of the Cascina Parina 1 Synthem (Schumm et al., 2002; Hickson et al., 2005),

plausibly due to an uplift stage of the tectonic reliefs (Fig. 8F). Syndepositional uplift is suggested also by the slight deformation of the High-Rank Unconformity U3 at the base of the Cascina Parina 1 Synthem. Onlap trends of the sandy lithosomes of the lower Cascina Parina 1 Synthem (Fig. 8D), stationary stacking and thickening of sand deposits approaching to the San Colombano and Casalpusterlengo-Zorlesco structures (Fig. 8F) and the thickening of the interposed mud horizons towards the North, suggest that a relative depocentre formed to the N of, and in between the uplifting structures during deposition of Cascina Parina 1 Synthem.

Figure 9

Table 3B

4.4.2. S3.2 – Cascina Parina 2 Synthem (CPS2)

The intermediate-rank, low angle unconformity S3.2 truncates the Cascina Parina 1 Synthem and bounds the overlying intermediate-rank Cascina Parina 2 Synthem (Fig. 8). In the subsurface, unconformity S3.2 gently dips N-ward and joins the intermediate-rank unconformity S3.1 concurring to build the high-rank Middle-Late Pleistocene unconformity U3 (cross-section 9N, Fig. 8D). The Cascina Parina 2 Synthem is only locally observed in outcrops (Figs. 2A, 8A, B). It is a sand-gravel unit, more gravel-rich than the Cascina Parina 1 Synthem both in the subsurface and in outcrops. The top of the synthem either preserves a m-thick palaeosol (Zuffetti et al., 2018b) (soil profile 'b' in Fig. 8A) or is truncated by the intermediate-rank unconformity S3.3. The red topsoil observed in outcrops compares with the red-yellowish colours described in boreholes at the top of the subsurface equivalent of the Cascina Parina 2 Synthem (section 2N, Fig. 8D). The exposed Cascina Parina 2 Synthem is covered by 1 m-thick sandy silt, defined as L2 loess at the San Colombano and Casalpusterlengo-Zorlesco hills (Fig. 8A, B) (Cremaschi, 1987; Zuffetti et al., 2018b).

Cascina Parina 2 Synthem is constrained between ca 67 Ky BP, that is the youngest

age of the preserved top of the Cascina Parina 1 Synthem (Fig. 8B) and the ca 27 ky cal BC age of the mud interval at the top of the synthem (Fig. 8D; Table 1). Hence L2 loess can be safely considered an LGM loess, as it was already suggested by Cremaschi (1987).

Three lithozones have been recognised within Cascina Parina 2 Synthem, by the composition of the F7, F9, F10 and F11 facies and litho-textural associations (CPS2a, b, c lithozones; Figs. 4, 5, 8, 9; Table 3B; see supplementary material for the complete description).

The lithotextural and facies associations of CPS2b and CPS2c lithozones testify for heteropic alluvial depositional systems (Table 3B) (Miall, 1977), mostly fed from the Alpine basements and routed by glacio-fluvial systems. Their development predated the LGM loess L2, hence plausibly encompassing part of the Late Pleistocene-MIS4. In the subsurface of the western study area, the occurrence of thick mud intervals separating the sandy/gravelly fining upward sequences of CPS2c lithozone documents the establishment of an alluvial plain setting with floodplains and river channel/bar systems (Bridge, 2003) (Fig. 8G). Unbundling of gravel/sand bed-sets within thick flood plain mud horizons indicates that aggradation of flood plain fine-grained sediments could overcome sand/gravel deposition, suggesting a subsiding setting. These western systems prograded SE-wards, eroding their alluvial terraces into the slightly deformed Cascina Parina 1 Synthem, along S3.2 intermediate-rank unconformity (Fig. 8D). To the East, the amalgamated sand-gravel units, poor of mud caps (CPS2b lithozone) (Fig. 8D), resulted from bedload deposition in braided river systems. At the same time, on the uplifting San Colombano hill, a wide erosion surface (S3.2) was cut and a palaeo-valley was incised and filled (CPS2a) then disactivated and abandoned before the deposition of the LGM L2 loess (Fig. 8G) in agreement with pedostratigraphic and morphological interpretations of Zuffetti et al. (2018b), Zuffetti and Bersezio (2020).

4.4.3. S3.3 - Invernino Synthem (INS)

The intermediate-rank, low-angle erosion surface S3.3 bounds at the base the sand and gravel units of the Invernino Synthem (INS) (Figs. 2A, 3, 8). This unconformity could be traced in the subsurface to bound at the base the subsurface equivalent synthem of the Invernino Synthem (Fig. 8D). S3.3 is a sub-planar surface with steep upward bends; it roots into the Middle–Late Pleistocene unconformity U3 at the San Colombano hill, where it contributes to uncover the marine substratum (Figs. 3, 8C). Within the study area, the age of Invernino Synthem is constrained to the latest Pleistocene by the ca 27 ky cal BC radiocarbon age below its base, close to the top of the underlaying Cascina Parina 2 Synthem, the 21.435-22.205 cal BC radiocarbon age in the core of its succession (Fig. 8D) and the youngest ages obtained from outcrop samples (Fig. 2; Table 1). Borehole log correlations permitted also to strengthen these data with literature radiocarbon ages collected by the same subsurface units in adjacent areas (Table 2). The top of the Invernino Synthem is locally cut by intermediate-rank unconformity S3.4 in the alluvial plain adjacent the San Colombano and Casalpusterlengo-Zorlesco structures, and is covered by 1 m-thick loess (L2) on the hills flanks (Fig. 8B, C). Thickness of the Invernino Synthem ranges between 0 and 20 m in the study area because of wedging-out and missing on top of the San Colombano and Casalpusterlengo–Zorlesco structures (Fig. 3, 8D).

The Invernino Synthem comprises both sand-gravel and very fine-grained facies associations (F7, F8, F10, F12, F13) (Figs. 5, 9F, G, 10A, B; Table 3B), forming four lithozones (INSa, b, c, d lithozones; see the supplementary material for the complete description).

The sedimentary features of lithozones INSa, b, c, account for alluvial deposition sourced from the Southern Alps, as it is documented by the dominance of sedimentary and volcanic rock fragments over the metamorphic basement-derived clasts (Fig. 4). Channel-

point bar, levee and floodplain facies associations of lithozone INSa (Fig. 10) suggest mixed-load, meandering fluvial style (Leopold and Wolman, 1957; Schumm, 1981; Cant, 1982; Galloway and Hobday, 1996; Bridge, 2003). Lithozone INSb is typical of floodplain environment with oxbow lakes and shallow and semi-permanent lacustrine ponds (Lozek, 1964; Einsele, 1992; Freytet and Verrecchia, 2002). The "eastern" lithozone INSc records bedload deposition in unstable water courses with braided channels (Rust and Gibling, 1990; Miall, 1996; Moreton et al., 2002; Bridge, 2003; Bersezio et al., 2004; Smith and Rogers, 2009; Gardner and Ashmore, 2011). In the western study area, lithozone INSa records the progradation of sand-dominated rivers, mainly spreading from the western Southern Alps and the Verbano glacial amphitheatre (Fig. 1B), as it is documented by the relatively high proportions of the typical pink rhyolites (Fig. 4). Age determinations that correlate the Invernino Synthem with the LGM time-span, and regional correlations (Bersezio et al., 2004; Bini et al., 2004a) suggest to consider these systems as the distal reaches of the glacio-fluvial outwash of the Verbano glacier, lateral equivalent of the synthems forming the Laghi Supersynthem (Bini et al., 2014; Franceschini et al., 2016). The general fining-upward trend that culminates with the deposition of the floodplain facies association of lithozone INSb (Fig. 10B), might suggest backstepping of the depositional systems during one retreat phase of the LGM Verbano glacier (Bini, 1987; Bini et al., 2004b). The features of the heteropic "eastern" INSc lithozone suggests progradation of braided glacio-fluvial systems, from a closer and eastern source, like the Lario Amphitheatre (Fig. 1B), as it is suggested by the absence of the typical pink volcanic clasts. At the LGM times the San Colombano hill was already raising above the adjacent plain and might have acted as a divide between the western and eastern glacio-fluvial systems. Perching of Invernino Synthem terraces (Fig. 8H), location of colluvial wedges (lithozone INSd), and sediment deformation structures within INSb lithozone beds at the San Colombano structure (Figs. 8C, 9G), testify that faulting occurred

during and after deposition of the Invernino Synthem (Zuffetti and Bersezio, 2020).

Figure 10

4.4.4. S3.4 - Paleo Sillaro Synthem (PSS)

The S3.4 intermediate-rank unconformity is the low relief terrace scarp bounding the abandoned valleys of meandering river systems, cut into the older units of High-Rank Stratigraphic Unit 3 and preserved at the present-day topography (Figs. 3, 10A). The sediments of these abandoned river systems form the Paleo Sillaro Synthem (Zuffetti et al., 2018a), a 5 to 15 m-thick sand unit, that is cut by the deeply entrenched post-glacial-Holocene to recent river valleys (High-Rank Unconformity U4) (Figs. 2A, 3). A thin, weak topsoil is preserved at places on top of Paleo Sillaro Synthem. The age of this unit is constrained to the latest Pleistocene, by the crosscut relationship with the most recent sediments of the Invernino Synthem (OSL age determinations between 18.740–16280 y BP) (Table 1) and the radiocarbon age of the oldest sediments belonging to the High-Rank Stratigraphic Unit 4, above unconformity U4 (11.440-12.997 cal BC) (cross-section 2N, Fig. 8D; Table 1). The Paleo Sillaro Synthem comprises F8-F7 facies associations (Figs. 5, 10C; Table 3B; supplementary material). North of the San Colombano hill (Fig. 2A) the abandoned river traces, that are revealed by field and remote geomorphological mapping, are elongated NNW-SSE, and palaeocurrent consistently indicate SSW to SE-directed flows (Table 3B). S of the same hill, the abandoned river traces are comparable in width and average direction to the Holocene Po-river meanders, whose terrace scarps crosscut the Paleo Sillaro Synthem abandoned traces.

The geometry and distribution of the Paleo Sillaro Synthem sedimentary bodies and their preserved surface morphologies suggest deposition by different meandering palaeo-rivers, with the development of point bar-channel-abandonment sequences (Fig. 8I). Gravel composition of the northern river bodies of Paleo Sillaro Synthem testifies to provenance

from the Southern Alps foothills; the westward enrichment in volcanic clasts is consistent with the recycling of the exposed porphyrite-rich Invernino Synthem of the western study area (Fig. 4), as well as with the course of a NW-sourced palaeo-river from the Verbano amphitheatre area (Fig. 1B), in keeping with the petrography of the stratigraphic units that correlate with Paleo Sillaro and Invernino synthems North of the study area (Bersezio et al. 2004, 2010). No river diversions or river-style changes occur throughout the development of these river traces that are mildly encased within the average surface of the Pleistocene plain (Bersezio, 1986; Castiglioni and Pellegrini, 2001). These features suggest that Paleo Sillaro Synthem developed in a period of tectonic stability and low uplift rate during retreat of the LGM Verbano and Lario glaciers.

4.4.5. Stratigraphic interpretation of the Middle-Late Pleistocene High-Rank Stratigraphic Unit 3

The Middle-Late Pleistocene High-Rank Stratigraphic Unit 3 was deposited under control of ramp folding, uplift, wrenching and late extension of the San Colombano and Casalpusterlengo–Zorlesco structures, in the rear of the outermost front of the Emilia Arc, as it has been described in the former sections, also according to Zuffetti and Bersezio (2020). As a result, the high-rank unconformity U3 developed as a progressive angular unconformity (Rafini and Mercier, 2002 and references therein), that was onlapped by the Cascina Parina 1, Cascina Parina 2 and Invernino synthems during the growth of the San Colombano and Casalpusterlengo-Zorlesco anticlines. Syndepositional uplift and gentle folding are indicated by the progressive bending of composite unconformity U3 and overlying synthems, by the mutual erosion and onlap terminations among the progressively younger units and by their facies changes approaching the limbs of the folds. Field and subsurface stratigraphic and structural reconstructions document (Fig. 8): i) the ongoing separation between the San

Colombano and Casalpusterlengo-Zorlesco structures, the former upraised by several tens of metres above the latter in association with right-hand offset along the Casalpusterlengo-Zorlesco transfer fault zone (Figs. 2A, 3); ii) the development of Late Pleistocene depocentres on the northern frontal side of the two structures and in between them, in correspondence of the mentioned fault zone (Fig. 2B); iii) the late extensional dissection of the positive relief of San Colombano, owing to wrenching and collapse that displaced the Latest Pleistocene (LGM) alluvial terraces of the Invernino Synthem. Under this tectonic control, four clastic intermediate-rank sequences (Fig. 3; Table 3B) show upwards transitions from meandering alluvial floodplain systems to braided depositional systems. In the frame of the Late Pleistocene climate cyclicity and controlled by the southernmost maximum extension of the glacial amphitheatres during their advances (Penck and Brückner, 1909; Shackleton, 1987; Bini et al., 2004b), the architecture, provenance and age determinations of the Late Pleistocene intermediate-rank units Cascina Parina 2 Synthem, Invernino Synthem and Paleo Sillaro Synthem suggest correlation with the advance and retreat cycles of the Late Pleistocene alpine Verbano (W) and Lario (E) glacial amphitheatres (Fig. 1B). Specifically, the Cascina Parina 2 Synthem, likely corresponding in age to MIS4, correlates with the uppermost synthems of the Besnate Supersinthem, and the Invernino Synthem, tightly constrained to the LGM, correlates with the Laghi Supersinthem (Bini et al., 2014; Francani et al., 2016). However, the formerly described structural and depositional features of these units testify tectonic activity of the San Colombano, Casalpusterlengo-Zorlesco structure during the same time span. The OSL data collected in the upper part of the Cascina Parina 1 Synthem (the lowermost Intermediate-Rank Stratigraphic Unit within the High-Rank Stratigraphic Unit 3), constrain the observed transition from meandering river to sandy bedload river facies associations to the MIS5–MIS 4 transition. The lowermost sequences forming Cascina Parina 1 Synthem are only presumably attributable to the Middle

Pleistocene, so that the plausible correlation with the Middle Pleistocene glaciofluvial synthems of the Besnate Supersinthem remains somewhat uncertain. The meandering palaeo-rivers sourced from the Southern Alps that formed the uppermost unit of High-Rank Stratigraphic Unit 3, the late glacial Paleo Sillaro Synthem, developed during the last retreat of the LGM glacial sources from their former southernmost reaches in a phase of regional tectonic stability, as it is documented by the absence of any evidence of morphostructural control on their courses across the buried structures.

Chronostratigraphic comparisons suggest that the High-Rank Stratigraphic Unit 3 might correspond as a whole to either the upper part of PS3s sequence of Amadori et al. (2019) or to the upper part of the PS3b sequence of Amadori et al., (2020).

4.5. Latest Pleistocene-Holocene Unconformity (U4) – High-Rank Stratigraphic Unit 4 (HRS4)

The unconformity U4 is a composite erosional surface which forms the scarps and the base of the lowermost alluvial terraces entrenched within the average morphological surface of the Po Plain (Plain Main Level, Castiglioni and Pellegrini, 2001), bounding at the base the sand and gravels of High-Rank Stratigraphic Unit 4, that includes the deposits of the present-day river network. We denominate Po Synthem this succession (Figs. 2A, 3) according to the stratigraphic definition and ranking introduced by the recent sheets of the Italian Geological Map at 1:50.000 for the post-glacial units at the alpine margin of the Po basin (Bini et al., 2014; Francani et al., 2016) and consequently adopted also by Zuffetti et al. (2018a) for the geological map of the study area. A high-rank is assigned to unconformity U4, because it crosscuts all the previous units and surfaces, fitting the criteria adopted to draw the hierarchy classification, independently from the time span encompassed by the unconformity itself and the sediments it delimits (Fig. 3). By means of U4, the High-Rank Stratigraphic Unit 4 may

cover any of the former stratigraphic units, from which its high rank is deduced. Its short time span is irrelevant for ranking, also because the it is still under formation.

The age of the base of the High-Rank Stratigraphic Unit 4 is constrained by the crosscut relationship with the Paleo Sillaro Synthem and by the radiocarbon age determination of 11440-12997 cal BC close to the lower boundary (Table 1). Archaeological findings and radiocarbon data on the Adda, Lambro and Po sand bodies document the Holocene to recent age of the overlying sediments (Pellegrini et al., 2003; Baio et al., 2004; Bersezio et al., 2010) (Fig. 1B; Table 2, Table 3; see supplementary metarial for the description).

The Po Synthem records the entrenchment of the river network from N to S, towards the southern basin margin, that occurred after the final retreat of the LGM glaciers and the abandonment of the river network forming the late glacial Paleo Sillaro Synthem. Confined river systems, affected by continuous changes of river style and deposition patterns along their course, developed within a valley network that deepens towards the basin axis, chasing after the entrenchment of the Po trunk river. The abandonment of the former river courses, the systematic diversion of all the U4-related valleys, that bend from SSE- to ESE-ward trends N of the study area in correspondence of the buried tips of the outermost Emilia arcs, and the changes in river style occurring across the same structural belt (Bersezio, 1986; Castiglioni and Pellegrini, 2001; Burrato et al., 2003; Zuffetti and Bersezio, 2020) (Fig. 1B), suggest that tectonics contributes to control the development of unconformity U4 and of the Po Synthem. In a very short span of post-glacial time, mostly corresponding to the Holocene, under tectonic control and during the relative sea-level rise of the Adriatic base-level (Correggiari et al., 1996; Amorosi et al., 2017 and references therein), erosional deepening of the U4 terrace occurred progressively towards the southern reaches of the Po basin, also thanks to enhancement of post-glacial river discharge and erosion and to dumping of bedload

into the post-glacial alpine lakes.

5. The space-time geological model of the southern Po basin

The hierarchic spatial relationships between the stratigraphic surfaces and facies assemblages, drawn by the correlation fence diagram (Fig. 3), allow to link the interpreted architecture to a time sequence of tectono-depositional high-rank stages and intermediate/low-rank increments/sub-increments of evolution. The 4-D model has been computed accordingly and is shown here starting from the constraints composing its structure (Fig. 11): i) the space structure, comprising the 3-D geometry of the hierarchic stratigraphic units; ii) the implicit time structure, defining the relative ordering and relationships among the stratigraphic and structural elements and their link to chronostratigraphy. The computed model is then inspected to evaluate its simplicity and likelihood compared to the space-time constraints and to discuss its uncertainties.

5.1. Space structure: the tectono-stratigraphic geometries

The 3-D model shows the present-day volume of the sedimentary bodies drawing the potential isosurfaces (Figs. 2A, 11; Section 3) corresponding to the low-rank depositional sub-increments. Relying on the hierarchic stratigraphic approach (Fig. 3), the space structure of the model reproduces the tectono-depositional geometries, like the features of the basin depocentres and intra-basin/marginal structural highs that originated at each evolutionary stage (Fig. 11):

- a nearly E-W-trending, submarine antiformal palaeo-high (San Colombano Structure; Fig. 2B) that was uplifted some km N of the southern basin margin during the Gelasian and was onlapped by a transgressive-regressive sequence (Fig. 6D) above the Gelasian Unconformity;

- a NW-SE-trending high which formed during intra-Calabrian thrust-folding at the San Colombano Structure, paired to a S-ward dipping depocentre to the N. The Calabrian High-Rank Stratigraphic unit 1 onlapped the palaeo-topography at the intra-Calabrian Unconformity U1 (Fig. 7D);
- two intra-basin highs (at San Colombano and Casalpusterlengo-Zorlesco structures) were separated since the Late Calabrian-Middle Pleistocene by a NW-SE-trending lateral ramp acting as a transfer fault zone (Casalpusterlengo-Zorlesco Transfer Fault) (Fig. 7E, F). Local depocentres accommodated the Calabrian-Middle Pleistocene High-Rank Stratigraphic unit 2 to the N and in-between the San Colombano and Casalpusterlengo-Zorlesco structures. The progressive, incremental, low-angle onlap terminations of its intermediate-rank units resulted in the Early-Middle Pleistocene high-rank Unconformity U2;
- the Middle-Late Pleistocene asynchronous evolution of the San Colombano and Casalpusterlengo-Zorlesco structural reliefs determined the location of alluvial terraces above and around them (Fig. 8F-I). During the Late Pleistocene spreading of the Cascina Parina 2 Synthem, the western San Colombano hill and part of the Zorlesco hill were already raised above the adjacent alluvial terraces (Fig. 8G). During the LGM, the latest uplift and extensional collapse of the San Colombano structure controlled the formation of the LGM terraces (intermediate-rank Invernino Synthem), while the Casalpusterlengo-Zorlesco structure was subsiding (Fig. 8H).

A high-rank geometry was produced at each high-rank stage of folding and faulting, from the composition of intermediate-and low-rank erosion-deposition stages. Hence, the geological boundaries to be modelled are:

- stratigraphic surfaces of erosion and deposition: Gelasian angular Unconformity, intra-

Calabrian angular Unconformity U1, composed by intermediate-rank unconformities S1.1-to-3; Early-Middle Pleistocene progressive unconformity U2, composed by intermediate-rank unconformities S2.1-to-3; Middle-Late Pleistocene progressive unconformity U3, composed by the intermediate-rank unconformities S3.1-to-4; Latest Pleistocene-Holocene unconformity U4, composed by the segments of S4.1 (Fig. 3);

- stratigraphic surfaces of aggradation: base of the Late Pleistocene loess units L1 and L2; base of the INSb and INSd lithozones of the Late Pleistocene (LGM) Invernino Synthem (Fig. 8A-D);
- morphological surfaces of stabilisation marked by (palaeo-) soils ('a, b, c'; Fig. 8A-D) (Zuffetti et al., 2018c);
- tectonic surfaces of normal faulting/transfer faulting, crossing the stratigraphy at high angles (fault system of the San Colombano hill and Casalpusterlengo-Zorlesco Transfer Fault; Figs. 3, 8).

Figure 11

Table 4

The nature of the geological boundaries and their crosscut relationships represent the spatial constraints to setup the model. Since no explicit hierarchic relationship is predisposed in the currently available software procedure, we implemented a new routine based on 3DGeomodeller®. The vertical ordering of the geological units (stratigraphic pile), the set of reference surfaces (top/bottom) and the nature of the interpolation for each surface (erode/onlap) were conceptualised into two "Hierarchic Rules" valid to represent complex stratigraphic architectures at each scale (Zuffetti, 2019). Hierarchic rule 1 aims at modelling high-rank and intermediate-rank architectures. The ad hoc built input stratigraphic pile responds to the assumptions listed in Table 4. Hierarchic rule 2 aims at modelling intermediate-rank and low-rank geometries, introducing further refinement of the 3-D model.

This rule allows to visualise the internal geometries, coherent with the incremental geo-history and does not apply to the high-rank boundaries (Table 4). The reference top surface used to run the interpolation of intermediate/low-rank features encompasses many physically-traceable surfaces: i) the present-day topography is a good proxy for the top boundary of the exposed Late Pleistocene (LGM) Invernino Synthem and Paleo Sillaro Synthem; ii) the morphological surfaces marked by palaeosols ('a' and 'b'; Fig. 8A-D) represent the palaeo-top boundaries of older, buried or partly truncated units (Late Pleistocene Cascina Parina 1 and Cascina Parina 2 synthems). Each morphological surface has a chronostratigraphic meaning, representing a good proxy for the GeoModeller isopotential surfaces, in keeping with Mallet (2004), Guillen et al. (2008), Caumon (2010).

5.2. Time structure: the incremental geological evolution

The tectono-depositional evolution of the southern Po basin is the implicit time component of the geological model. It has been described and interpreted in Section 4. The sequence of the Quaternary tectono-sedimentary high-rank stages and the nested increments of lower hierarchy that constrained the computation of the quantitative model is summarised as follows (Fig. 11).

- *Stage 0: Early Pleistocene thrusting and N-ward propagation of the San Colombano-Casalpusterlengo–Zorlesco structures – Gelasian Unconformity GU.*

  The Gelasian stage of N-ward thrusting along the frontal Emilia arc of the Apennines caused uplift increments at the San Colombano-Casalpusterlengo-Zorlesco structures (Fig. 11) and folding of the pre-Gelasian marine stratigraphy along two *en enchelon*, WNW-ESE-striking anticlines (Pieri and Groppi, 1981; Zuffetti et al., 2018a). The pre-Gelasian unconformities known in the Po Plain subsurface (Fig. 1C, D) (Amadori et al., 2019, 2020 and references therein) got truncated at the San Colombano fold crest by the

composite Gelasian Unconformity at the base of the Calabrian High-Rank Stratigraphic Unit 0 (HRS0, Figs. 3, 11). Two intermediate-rank depositional increments, nested within HRS0 (San Colombano Formation lithozones a-b and the subsequent lithozone c; Table 3A), represent two shallow water transgressive-regressive cycles that developed within the Calabrian *G. cariacoensis* zone, the former predating the occurrence of the "northern guests", the latter predating the occurrence of *T.truncatulinoides excelsa*.

- *Stage 1: Calabrian thrusting and continentalisation – Intra-Calabrian Unconformity U1*

  The intra-Calabrian stage of Apennine thrusting folded the Gelasian Unconformity and the overlying High-Rank Stratigraphic Unit 0 shaping a NW-SE-trending palaeo-high in the southern study area (Figs. 7D, 11). The Calabrian high-rank, sandy regressive sequence HRS1 onlapped this palaeo-topography marked by the high-rank angular unconformity U1. Three depositional increments bounded by intermediate-rank erosional surfaces (S1.1-2-3) recorded S- and SE-ward progradation of Alpine-sourced meandering river systems followed by short-term transgressions of shallow marine (Intermediate-Rank Stratigraphic Unit 1.1) to floodplain settings (Intermediate-Rank Stratigraphic Units 1.2 and 1.3). The parallelism between the intermediate-rank surfaces suggests tectonic stability or steadiness during the deposition of the High-Rank Stratigraphic Unit 1.

- *Stage 2: Calabrian (?)-Middle Pleistocene thrusting, wrenching, and progradation of glacio-fluvial systems – Unconformity U2*

  Thrusting, wrenching, and folding along the San Colombano and Casalpusterlengo-Zorlesco structures of the Emilia arc shaped the wedge-top depocentres to the N of the raising structures and between them. A NW-SE-trending transfer fault (Casalpusterlenzo-Zorlesco Transfer Fault) drove dextral wrenching and relative uplift of San Colombano vs. Casalpusterlengo-Zorlesco structures since the end of the Calabrian

(Figs. 7E, 11). The continental High-Rank Stratigraphic unit 2 partly filled the depocentres above U2. Depositional increments corresponding to the Intermediate-Rank Stratigraphic units 2.1, 2.2, and 2.3, have been related to the progradation of coarse-grained glacio-fluvial systems, recording the Alpine glacial cycles attributed to the Calabrian (?) (Bozzente Supersynthem) and Middle Pleistocene (Specola and Binago synthems, lower part of the Besnate Supersynthem) (Bersezio et al., 2014; Bini et al., 2014; Francani et al., 2016 and references therein). The glacio-fluvial distal sediments onlapped the San Colombano and Casalpusterlengo-Zorlesco growing anticlines above the intermediate-rank unconformities S2.1-2-3 (Fig. 3). The tectonic depocentres were progressively filled during uplift of the two folds. These features and the low angularity of the intermediate-rank unconformities suggest steady uplift of the structures, rather than discrete increments of unsteady tectonics or deposition (Kim and Paola, 2007).

- *Stage 3: Middle-Late Pleistocene uplift and collapse of the intra-basin reliefs – Unconformity U3*

  Renewed thrusting, wrenching, and folding involved the San Colombano and Casalpusterlengo-Zorlesco structures at the front of the Apennine Emilia Arc (Benedetti et al., 2003; Burrato et al., 2003; Zuffetti and Bersezio, 2020) presumably since the end of Middle Pleistocene and lasted until the late LGM. The high-rank, progressive angular unconformity U3 collected the glacio-fluvial and alluvial terraces of the High-Rank Stratigraphic Unit 3 (Fig. 11). Effect of this tectonic stage was the N-ward propagation of alluvial erosion, witnessed by the development of the deep erosion surface below the Cascina Parina 1 Synthem (S3.1 intermediate-rank unconformity, segment of U3). Uplift of the San Colombano and Casalpusterlengo-Zorlesco highs lowered the stream gradients and accommodation space approaching the reliefs during the deposition of the Cascina Parina 1 Synthem (Fig. 8F), whose lower sequences predate the MIS5 age

assigned to the uppermost ones by the mentioned OSL data, and hence might correlate to a MIS6 glaciofluvial unit of the Besnate Supersynthem. MIS4 glaciation triggered the progradation of the Cascina Parina 2 Synthem whose glacio-fluvial and alluvial sediments progressively eroded and covered the gently folded Cascina Parina 1 Synthem at the intermediate-rank unconformity S3.2. The first drainage network on the raised San Colombano hill formed at this time; it was rapidly uplifted at the eastern hill where perched remnants of the erosional surface S3.2 are preserved (Fig. 8G) (Zuffetti and Bersezio, 2020). At the glacial acme of MIS4, the L1 loess aggraded on the uplifted surfaces, then pedogenesis affected the morphological surfaces which developed above different stratigraphic units during the MIS3 interglacial (Zuffetti et al., 2018b). The LGM glacio-fluvial systems of the Invernino Synthem (MIS2) fed by the Verbano and Lario amphitheatres, terraced the San Colombano structure to the W and the Casalpusterlengo-Zorlesco one to the E, respectively (Fig. 8H). Some of these river terraces were raised, then dissected during uplift and extension of the San Colombano hill (Zuffetti and Bersezio, 2020). Loess L2 aggraded on the stable sites of the reliefs. Contemporaneously, in the subsiding depocentre N of the San Colombano hill, a Southalpine-sourced, low energy fluvial and floodplain system aggraded (lithozone INSc, Fig. 8H). At the end of the LGM, a set of post-glacial, meandering tributaries of the palaeo Po River could flow SSE-wards (Fig. 8I) without any tectonic interference on their courses, documenting a period of tectonic quiescence (Paleo Sillaro Synthem).

- *Stage 4: Latest Pleistocene to Holocene uplift and river entrenchment – Unconformity U4*

  The latest Quaternary stage of activity of the northern Apennine Emilia arc (Zanchi et al., 2019), together with the Holocene climatic-hydrologic turnover, caused the S-wards regional entrenchment and the systematic SE-ward bending of the Alpine tributaries of

the Po River at the unconformity U4 (Figs. 3, 11). Local drainage anomalies and diversions at the San Colombano and Casalpusterlengo-Zorlesco structures fit with late Quaternary faulting (Zuffetti and Bersezio, 2020). Comparable regional geomorphic evidences are discussed by Burrato et al. (2003), Michetti et al. (2012) in other sectors of the Po Plain, on both the Apennine and Alpine sides.

Figure 12

5.3. Inspection of the model

The space-time geological model (Figs. 11, 12) describes the effects of syndepositional thrusting, folding, and faulting at the San Colombano and Casalpusterlengo-Zorlesco structures. It reproduces the most complete and almost horizontal Quaternary stratigraphic successions in the depocentres N of the Apennine Emilia Arc and their up-warping and wedging out towards the antiformal culminations.

The high-rank visualisation shows the unconformities, framing the regressive Quaternary succession above the deformed marine units, honouring the hierarchy, the angular relationships, and the relative chronologies drawn in the fence correlation model (compare Figs. 3, 12). The model reproduces the intermediate-rank elements and geometries, respecting the sequence of Quaternary depositional increments. For instance, the model shows i) the progressive development of the Early-Middle Pleistocene high-rank unconformity U2, made by low-angle onlap and mutual erosion among the late Calabrian-Middle Pleistocene Intermediate-Rank Stratigraphic Units 2.1, 2.2, 2.3 (Figs. 11C, 12A) owing to the infilling of depocentres during steady uplift of the San Colombano and Casalpusterlengo-Zorlesco structures; ii) the composite nature of the high-rank unconformity U2, formed by the merging of the segments of the intermediate-rank bounding surfaces onlapping on the flanks of the raising structures. Seemingly, the model reproduces the composite and progressive features of the high-rank unconformity U3 (Figs. 11, 12) showing that the hierarchic space-time

approach permits to model the nature of different types of high-rank unconformable surfaces respecting their evolution as progressive unconformities composed by lower-rank segments.

In the low-rank visualisation, the unconformities always crosscut the potential isosurfaces internal to the predating stratigraphic units, and collect the related isosurfaces above them (Fig. 12A). Since the low-rank isosurfaces are interpreted as relative isochrones, these relationships reproduce the time-transgressive nature of the major stratigraphic surfaces, in accordance with the geological evolution.

The model permits to draw and investigate the late Calabrian-Middle Pleistocene activation of the Casalpusterlengo–Zorlesco transfer fault zone between the San Colombano and Casalpusterlengo-Zorlesco structures (Fig. 7): in keeping with observations, the modelled High-Rank Stratigraphic unit 2 is not reproduced on the western hangingwall of the fault zone but it appears and thickens away from it. N of the San Colombano hill (Fig. 12B); E of the transfer fault, the interpolation renders a synformal depocentre for the High-Rank Stratigraphic Unit 2, bounded at the base by the Early-Middle Pleistocene high-rank unconformity U2, in keeping with the geological constraints. These realisations permit to critically check the geological space-time constraints, eventually going back to look for new data and interpretations aiming to reduce uncertainties and to improve the fit between the input data and the model outcomes.

Removing the stratigraphic units from the 3-D model visualisations (Fig. 11C) helps to investigate the unexposed geology, also in areas where complex relationships between stratigraphy, folds, dense fault networks and very low thickness of sediments are involved, like in the San Colombano hill area (Fig. 12C). Any observed misfit between the computed model and the surface-subsurface geological constraints can thus be highlighted, promoting removal of mistakes and refinement of the constraints and/or the model.

The space resolution that we adopted to match the surface and subsurface input data,

ranging between metres along the Z-axis and tens to hundreds of metres in the X-Y plane, is adequate to correlate and reproduce the three hierarchic orders we introduced, provided that the lowermost one (the lithozone or bed-set) remains mostly confined to the field reconstruction and is barely approximated by the modelled potential iso-surfaces drawn between the intermediate-rank boundaries. Based on this relation between space resolution/accuracy and hierarchy of the stratigraphic entities, uncertainty on the model outcomes and interpretations can be evaluated by comparing the misfits between features of the same rank to the potential errors that can be accepted at this specific rank. In this case, we considered the intermediate-rank geometrical features that remain substantially unaffected by vertical errors up to 10 m as safely acceptable. As an instance, following this criterion, we evaluated one of the most uncertain model outcomes, that is the set of tectono-stratigraphic features associated with the Casalpusterlengo–Zorlesco transfer fault zone. Considering the potential vertical error of 10 m, we observed how the high- and intermediate-rank modelled geometries might change, noticing that the location of the geological surfaces could slightly change but the significant tectono-stratigraphic relationships were not substantially modified.

The resolution of the modelled geological architecture, which honours the input data and relationships, strictly depends on the reliability and resolution of the input data. The resolution of the dataset of any surface-subsurface setting increases upwards, conditioned by the number and accuracy of the available well-logs, geophysical images and surface exposures. In our approach, any new data from surface/subsurface geological-geophysical investigations will improve the reconstruction of the deep geometries; any additional constraint to the time-component, from age determinations and refinements of the relative chronologies, will strengthen the model. The adopted method and software allow to easily handle any supplementary data.

Potentially, starting from the proposed hierarchic rules, the model can be upscaled and

downscaled according to the user's aims. The model exports in 2-D maps or 3-D meshes might represent the starting point for mathematical modelling of the inherent processes throughout the basin fill, like groundwater and heat flow simulations (examples in Pantea and Cole, 2004; Ross et al., 2005; Hassen et al., 2019; Scheidler et al., 2019). Exported meshes allow to preserve the resolution of the volumes, to represent complex geological features like pinch-out geometries, inclined faults, folds, angular truncations, providing models of the geological shapes constrained by the space and time input data.

6. Discussion

The model outcomes permit to discuss the modelling approach and the tectono-depositional history of a Quaternary tectonically active sector of the Po foreland basin, which are the main aims of this research.

6.1. Modelling approach

The target of our research is the shallow subsurface of a continental foreland basin, where the models for hydrogeological, hydro-geothermal, storage, and waste applications are run (Van der Meulen et al., 2013; Maljers et al., 2015). Subsurface borehole logs, geophysical soundings and surface geology and geomorphology are the most widely used input data to these models, considering the high cost and the low availability and resolution of industrial seismic data. In the Po basin, several models have been proposed, sometimes at a very wide regional scale, in 2- or 3-D (Ghielmi et al., 2013; Turrini et al., 2014; ISPRA, 2015; Amadori et al., 2019, 2020; De Caro et al., 2020), or referring to more local settings (e.g., Bersezio et al., 2010; Bresciani and Perotti, 2014; Maestrelli et al., 2018). To reconstruct basin evolution, the interaction between climate- and tectonic-driven erosion-deposition processes is investigated by field analyses, while decompaction of the stratigraphic pile is computed to quantify tectonic subsidence/uplift through time in subsurface-oriented regional studies (Maesano and D'Ambrogi, 2016, and references therein). 3-D models provide the background for these latter

computations that need detailed chronostratigraphy. Relying on surface-subsurface correlation, this study aims to provide a 4-D, background geological model. Our approach explicitly constrains the 3-D computation to the space and time components of the geological hierarchic architecture, in order to obtain a multi-scale 4-D model (Figs. 11, 12). Nature, hierarchy, and chronology link the stratigraphic surfaces to the phases of Quaternary palaeo-landscape modifications and to the controls on their origin, so that a high-rank "stage" represents a tectono-depositional event of regional significance producing high-rank angular unconformities; intermediate-rank "increments" and low-rank "sub-increments" are the result of competing climate-tectonic controls producing low-angle intermediate- and low-rank surfaces. (Fig. 11; Table 4). This structure of the model permits to introduce new knowledge revising the input data and interpretations at any round of the critical inspection of the outcomes.

Hierarchy, relative chronology, and significance of the sedimentary surfaces and units were down-traced from surface geology to the subsurface. Exposures also provided analogues to interpret the equivalent subsurface stratigraphic entities. The threefold ranking of the hierarchic scheme depends on the capability to resolve and interpret the subsurface, which is quite lower and more uncertain than at the surface exposures.

The model describes the geological history of a sector of the southern Po basin as the time-sequence of five high-rank Quaternary tectono-sedimentary stages, which gave rise to the unconformities of the highest level of hierarchy (Fig. 3). The hierarchic approach highlights the progressive and composite nature of these stratigraphic boundaries. Their intermediate- and low-rank stratigraphic components were due to the competition between steady tectonic uplift, subsidence, including differential compaction of fine-grained sediments, and cyclical advances and retreats of the Verbano and Lario glaciers (Figs. 1B, 3).

The high-rank stratigraphic boundaries are time-transgressive surfaces rather than

chronostratigraphic (isochronous) horizons. They are the product of five Quaternary deformation, erosion, and deposition high-rank stages. According to the available chronostratigraphic resolution and excluding the Latest Pleistocene–Holocene stage that is still under evolution since the last 10 ka, the stages show durations in the order of several 10^5 years. The stages collected the transgressive-regressive cycles that evolved during the intermediate-rank increments. The comparison of high-resolution surface stratigraphy with the low-resolution subsurface reconstruction permits to compare the computational isopotential surfaces to the low-rank sub-increments (Fig. 12).

The model accounts for the different origin and significance of the stratigraphic and morphological surfaces of erosion, aggradation, and stabilisation which correspond, respectively, to the component segments of the high-rank unconformities, to the aggrading, undissected top of intermediate-rank depositional units, and to the soil profile developed at the morphological stable sites that were subtracted from the sedimentary dynamics.

6.2. Quaternary tectono-depositional history of the southern Po foreland basin

The configuration of the southern Po foreland basin in the studied sector responds to N-ward thrusting of the Emilia Arc of the Apennines, whose Quaternary activity is documented in the literature and by recent seismicity (Meletti et al., 2012; Gunderson et al., 2014; Vannoli et al., 2015; DISS Working Group, 2018). The studied sector is relatively close to both the present-day Pede-Apennine Thrust Front to the S (Maestrelli et al., 2018, and references therein), that is the morpho structural boundary between the Po plain and the Apennine mountains, and the blind leading edge of the fold and thrust belt to the N (Emilia Arc) that interfere with the opposite Southalpine thrusts in the centre of the Po plain (CPPS, Fig. 1B) (Fantoni et al., 2004; Bresciani and Perotti, 2014). The intra-basin hill corresponding to the San Colombano structure, raises above both the elevation of the average plain (Castiglioni and Pellegrini, 2001) and the low height of the subtle Casalpusterlengo-Zorlesco intra-basin relief. Our model shows

how these reliefs co-evolved with different depocentres that developed on their northern sides and between them (Fig. 3). Until the development of the Early–Middle Pleistocene high-rank, progressive angular unconformity U2 (Fig. 11), the two structures were paired and accommodation space was mostly created in front of them. Since stage 2, i.e. starting from about the Calabrian–Middle Pleistocene boundary, the San Colombano structure started to rise above and slip N-ward with respect to the Casalpusterlengo–Zorlesco structure. Since then, the separation between the structures was accommodated by dextral slip along the Casalpusterlengo-Zorlesco transfer fault zone (Figs. 7, 11, 12). The outcomes of the 4-D model fit the wedging geometries and the erosion-onlap relations across the fault zone. In fact, the accepted range of error on interpolation (±10 m) is at least one order of magnitude lower than the vertical offset across the fault (Figs. 3, 12 to compare the constraining data and the computed model). The amount of uplift of the Calabrian marine units in the western hangingwall (several tens of metres above the Middle Pleistocene glacio-fluvial units of the High-Rank Stratigraphic Unit 2 in the eastern footwall) indicate that compaction alone could not be the cause of this geometry strengthening the interpretation. The model suggests that decompaction and restoration of folding and tilting might permit to quantify the tectonic component of vertical displacement removing the effect of sediment compaction and permits to estimate subsidence, sedimentation, and slip rates on the opposite fault blocks, provided that additional constraints on age determinations and petrophysical parameters are introduced.

An out-of-sequence propagation of the San Colombano structure (Dunne and Ferrill, 1988; Morley, 1988; McClay, 1992) is suggested by: i) the buttress effect opposed to the N-ward propagation of the leading edge of the Emilia Arc (Fig. 1B; Section 2.2) by the pre-existing Southalpine frontal thrusts (Pieri and Groppi, 1981; Fantoni et al., 2004, Bresciani and Perotti, 2014; Toscani et al., 2014), ii) the relevant rising of the San Colombano structure above the Casalpusterlengo-Zorlesco structure (Fig. 2), iii) the polyphase deformation history

recorded at the San Colombano structure, and iv) the involvement of progressively younger units in fault propagation folding, on the rear and above the northern tip of the Emilia Arc. A comparable conclusion was drawn for the out-of-sequence reactivation of the buried outermost Emilia Arc some 25 km E of the San Colombano structure, that was generically attributed to the Pleistocene by Toscani et al. (2014). Out-of-sequence reactivation has been shown also for the Pede-Apennine Thrust front in the rear of the Emilia Arc, since Maestrelli et al. (2018) documented its Early–Middle Pleistocene reactivation that led also to uplift of the buried connected structures to the N and influenced deposition and geomorphic evolution since the latest Pleistocene. Differently, at the Piadena anticline, one of the outermost blind reaches of the Emilia Arc about 40 km E of the study area, Maesano and D'Ambrogi (2016) computed decreasing uplift rates (lower than sedimentation rates) from the Calabrian to the Late Pleistocene. This observation holds with our interpretation of the out-of-sequence propagation of the San Colombano ramp-anticline, that developed during Middle and Late Pleistocene times in the rear of this blind tip of the Emilia arc and quite closer to the Southalpine buttress than the Piadena frontal thrust.

The model outcomes indicate that the hierarchic approach helps to recognise the effects of tectonic and climatic controls on the stratigraphic architecture at different ranks. The five high-rank and high-angle unconformities frame five high-rank stratigraphic units responding to five discrete high-rank deformation stages (Fig. 11). Among them, the Gelasian Unconformity (GU) and the intra-Calabrian Unconformity (U1) are recognised as angular unconformities onlapped by the overlying marine to continental sequences they bound at the base. Somewhat differently, the Early-Middle Pleistocene U2 and the Middle-Late Pleistocene U3 progressive unconformities are associated with the development of sedimentary wedges formed by growth strata onlapping the truncated pre-growth units (Rafini and Mercier, 2002 and references therein). In the case of U2, the relationships between the basal unconformity

and the intermediate- and low-rank stratigraphic units within the wedge formed by High-Rank Stratigraphic unit 2 (Figs. 3, 7, 12), suggest a configuration comparable to the "rotative onlap type" described by Anadòn et al. (1986) in the Tertiary foreland basin of the Southern Pyrenees and to the "limb rotation type" of Rafini and Mercier (2002). The pattern of thickness changes and onlap terminations indicates a decreasing amount of deformation with respect to sedimentation rate through time, according to both mentioned papers. The growth strata wedge associated with the Middle-Late Pleistocene progressive unconformity U3 shows a more complicated pattern, with reciprocal erosion among the growth strata (the intermediate- and low-rank stratigraphic units forming High-Rank Stratigraphic Unit 3) and variable elevation of the onlap terminations through Late Pleistocene times (Figs. 3, 8, 12). According to Anadòn et al. (1986) and Rafini and Mercier (2002), this configuration suggests that increasing tectonic uplift could overcome sedimentation rates until the deposition of the sealing LGM Invernino Synthem, that was affected by the extensional collapse of the San Colombano hill structure.

The palimpsest of high-rank unconformities, mobile structural highs and depocentres originated as a response to the Apennine-related Quaternary tectonic stages, while sediment routing and input derived mostly from the opposite Alpine belt to the N. It was driven by the advances and retreats of the Pleistocene glacial amphitheatres from the same mountain range, that fed gravel-sand glacio-fluvial terraces as far S as the basin axis (Figs. 1, 3). On the contrary, the tectonically active southern basin margin with the Apennines remained constantly deglaciated. The stratigraphic reconstruction and the 4-D model show that the intermediate- and low-rank units forming the five high-rank Quaternary stratigraphic units are characterised by low-angularity of the intermediate-rank unconformities and mostly parallel geometry away from the uplifting structures. These features and the related facies and sediment-composition changes (Section 4 and supplementary material) indicate that, since the intra-Calabrian unconformity U1, the control on sedimentation exerted by the cyclic advances of the Verbano

and Lario glacial amphitheatres could be recognised, and associated with the steady/decreasing uplift and/or tectonic quiescence phases during which sedimentation could overcome tectonic rates at the San Colombano and Casalpusterlengo-Zorlesco structures. This is recorded by the described depositional patterns of Intermediate-Rank Stratigraphic units 2.1 (Late Calabrian) and 2.2 (Middle Pleistocene) that might correspond to the Calabrian Bozzente and Middle Pleistocene Binago-Specola glacial and glacio-fluvial synthems (Bini et al., 2004b). The same observations hold for the glacio- fluvial Middle Pleistocene Intermediate-Rank Stratigraphic Unit 2.3, the Middle-Late Pleistocene Cascina Parina 1 and the Late Pleistocene Cascina Parina 2 synthems that correlate with the Middle-Late Pleistocene synthems of the Besnate Supersynthem (Bini, 1997a, 2005), the high-rank depositional unit related to the Besnate glacial amphitheatre at the alpine margin of the basin (Fig. 3). It is apparent that the high-rank unconformity U3 does not correspond to the base of the mentioned Supersynthem (i.e. to the onset of the corresponding glacial cycles) that is more likely represented by the base of the Intermediate-Rank Stratigraphic Unit 2.3, part of the former tectonically controlled High-Rank Stratigraphic Unit 2. The origin of the high-rank unconformity U3, regionally traceable in the whole study area, has to be considered independent from the climate-driven increments of palaeogeographic reshaping that gave origin to the Middle–Late Pleistocene Besnate glacial amphithetare, instead deriving from the formerly described tectonic stage at the front of the Emilia Arc of the Apennines. The facies assemblage and crosscut relationships between the latest Pleistocene intermediate-rank units, Invernino and Paleo Sillaro synthems, relate them to the onset and waning of the LGM, corresponding to part of the Laghi Supersynthem (Bini et al., 2014) in both the Verbano and Lario amphitheatres (Fig. 3). Progradation of the glaciofluvial systems during the LGM (lithozones INSa and INSc of the Invernino Synthem) was accompanied by aggradation of the L2 loess on the stable surfaces. A marked change in fluvial style from coarse bedload-dominated to aggrading flood-plain with meandering belts

occurred during the late-glacial retreats (INSb lithozone and late glacial Paleo Sillaro Synthem). The stable surfaces, uplifted on the three isolated hills, record pedogenesis (Cremaschi, 1987; Zuffetti et al., 2018b). All of these features suggest that the LGM and post-glacial climate contributed to control unsteady deposition (Kim and Paola, 2007; Gunderson et al., 2014), competing with the ongoing uplift and collapse of the San Colombano hill (Figs. 8, 11). The intermediate-rank unconformities at the base of the glacio-fluvial units merge on the limbs of the anticlines to form the U3 high-rank progressive unconformity that separates them from the former glacio-fluvial intermediate units.

In synthesis, the integration of petrographic, sedimentological, stratigraphic hierarchic reconstruction of the High-Rank Stratigraphic Units 2 and 3 into the 4-D model helps to link the glacial and glacio-fluvial evolution of the northern side of the Po Plain (Bini, 1987; Muttoni et al., 2003; Garzanti et al., 2011; Scardia et al., 2012) to the evolution of the Northern Apennine structural front recorded in the southern sectors of the Basin, contributing to the regional-scale stratigraphic interpretation of the Middle-Late Pleistocene infill of the Po Basin.

The latest Pleistocene Holocene U4 unconformity is interpreted as a high-rank unconformity because it truncates all the former surfaces and units. Together with the overlying stratigraphic unit it is still under evolution, so that its time duration cannot yet be evaluated. It represents the erosion surface at the base of the post-glacial to recent river network, developed as a consequence of regional isostatic response to deglaciation (Carminati et al., 2003), sediment trapping within the alpine lakes, differential subsidence in correspondence of the buried structures and tectonic activity of the Emilia Arc. We suggest that the latter represents the main control in the central-southern Po plain of Lombardy considering that: i) entrenchment affects also rivers outflowing from never glaciated valleys without terminal lakes (like Serio and Brembo rivers, Fig. 1B) and excludes post-glacial

dumping of bedload, ii) the post-glacial valleys undergo systematic diversions from NNW-SSE to WNW-ESE directions whose location is tightly related to the projection on the present-day topography of the active buried tectonic structures (Fig. 1B), iii) these diversions do not affect the late-glacial abandoned traces of the Paleo Sillaro Synthem that are cut by the post-glacial valleys (Bersezio, 1986; Castiglioni and Pellegrini, 2001), documenting that a change in subsidence/uplift pattern occurred controlling the development of unconformity U4, iv) the effect of tectonic uplift can be directly observed at the San Colombano structure, with southwards displacement and entrenchment of the Po river traces documented within the latest Pleistocene Paleo Sillaro Synthem and the subsequent Po Synthem.

The 4-D model portrays the relevant space-time heterogeneity that is the peculiar feature of the studied Quaternary wedge-top setting. The different types of syntectonic progressive unconformities that developed on the uplifting limbs of fault-propagation folds compare to the growth structures observed at the margins of the Tertiary, southern foreland basin of the Pyrenees (Ebro basin, Anadòn et al., 1986). The development of progressive unconformities and growth strata often accompanies the migration of frontal folds during propagation of a frontal thrust over the foreland basin, like in the case of the Pliocene progressive unconformity at the front of the Zagros foreland belt (Hessami et al., 2001). The second peculiar tectonic feature described at the southern margin of the wedge-top Po basin is the late collapse affecting the uplifted San Colombano structure along extensional faults both parallel and oblique to the growing anticline. Syn- to late-folding extensional faults are predominantly observed as deep-water fold features, but few examples of extensional faults affecting ramp-anticlines in continental settings are known from the literature, like in the case of the Anaran anticline in the Zagros fold-thrust belt (Tavani et al., 2014). The third peculiar feature of the studied setting is the vicinity to the lithospheric heterogeneity represented by the buttressing fold-and-thrust belt of the Southern Alps (less than 20 km), that marks the

difference with the eastern sector of the Po basin progressively more distant from the alpine buttress (Toscani et al., 2014; Maesano and D'Ambrogi, 2016). Similar configurations characterise other foreland basin settings, such as the western Pyrenees where the less than 40 km wide Rioja trough develops between two facing thrust belts (Muñoz-Jiménez and Casas-Sainz, 1997) or in the Indian Himalayas where the mountain range faces an opposite-verging thrust belt with an intervening basin less than 60 km wide (Kent and Dasgupta, 2004). In the studied setting, out-of-sequence propagation of thrusting is the response to buttressing with a strong influence on the heterogeneous configuration of depocentres and erosion-sedimentation patterns, the latter described also in the above-mentioned comparable settings. Considering these features, the studied case-history provides insights on the response of accommodation and sedimentation to active tectonics in a foreland wedge top setting, that might be useful for geological modelling in other comparable settings, accounting for the origin and evolution of the observed relevant heterogeneity that impacts on applications, like seismotectonic assessment studies, hydrogeological and hydro-geothermal modelling.

7. Conclusions

This study proposes the space-time 4-D model of the southern Po foreland basin in Lombardy (Northern Italy) during the Quaternary. The model suggests the following remarks on the space-time modelling of continental architectures in active foreland basins:

- in front of the tectonically active Apennine margin, the Quaternary stratigraphic architecture of the Po basin records the high-rank control on accommodation and sedimentation/erosion patterns exerted by discrete tectonic stages, owing to polyphase and unsteady propagation of the leading edge of the blind Emilia Arc. As a result, five high-rank, angular, composite and in some cases progressive unconformities frame five Calabrian to Holocene high-rank units, forming the major Quaternary regressive cycle, from shallow marine to alluvial environments.

- The high-rank tectonic stages determined the heterogenous pattern of uplifting intra-basin reliefs and subsiding depocentres. Polyphase, unsteady deformation was responsible for abrupt thickness/facies changes and onlap terminations, permitting to interpret the decoupling of the formerly paired San Colombano and Casalpusterlengo-Zorlesco structures along a dextral lateral ramp/transfer fault, since the end of the Early Pleistocene. The role of wrenching and out-of-sequence thrusting in shaping the stratigraphy of a foreland ramp is also highlighted by the good fit obtained after computation of the quantitative model.
- The high-rank stratigraphic boundaries described in this study are composite surfaces, which originated from the superposing and interacting tectonic and depositional processes through the geologic time, at different hierarchic orders. These surfaces, which have both a stratigraphic and a chronological significance, are diachronous at the different ranks, from the basin to the local scale. Caution is requested when calibrating the subsurface geophysical images of seismic unconformities with point-like age determinations collected from sparse boreholes. The development of progressive unconformities and growth depositional wedges indicates that the Early-Middle Pleistocene and the Middle-Late Pleistocene unconformities responded to high-rank stages during which syndepositional tectonic rates could initially overcome sedimentation rates.
- During steady uplift, and/or at quiescent tectonic sites and times, intermediate- and low-rank increments of sedimentation were mostly controlled by the Pleistocene advances and retreats of the Alpine glaciers. Hence, the intermediate- and low-rank surfaces are proposed to be mostly controlled by the climatic and/or autocyclic factors, the latter owing to unsteadiness of deposition.
- The proposed space-time model integrates surface and subsurface stratigraphy, based on

down-tracing from geological maps and field geological reconstruction. The geometry of sedimentary units, the relative chronology and timing of the geological evolution were composed in a hierarchic framework. The space-time data and interpretations were converted into model constraints, that permitted to compute a quantitative model honouring the geometry of the structural-stratigraphic entities, the onlap/erode relationships between the units, the relative chronology and timing of the geological evolution. The model is hierarchic, with a threefold ranking of high-, intermediate-, and low-rank boundaries and units that derive respectively from the tectono-depositional stages, increments, and sub-increments of evolution. The model structure permits to represent the geological volume with different details, corresponding to different hierarchic orders, so it is inherently multi-scale. Model inspection permits to change the input constraints (data and interpretations) to evaluate alternatives and introduce new knowledge.

- Quantitative analysis of subsidence, sedimentation, tectonic uplift, and slip rates in view of seismotectonic applications and hydrogeological and geothermal modelling, are the expected developments for future work starting from this 4-D model. Computation and modelling of the incremental tectonic history are ongoing, hopefully taking advantage from new age determinations to strengthen the available chronological constraints.

Acknowledgments

We acknowledge the careful review by Chiara Amadori, Luigi Bruno and Livio Ronchi that we addressed to complete and strengthen the dataset and the geological description of the studied setting. The suggestions by the Editor Catherine Chagué helped us to improve and shorten the manuscript. This work was supported by funds to RB [grant-RV_ATT_COM16RBERS_M].

References

Alfano, L., Mancuso, M., 1996. Sull'applicabilità del metodo dipolo-polare continuo nelle ricerche idriche a media profondità in aree di Pianura. Acque Sotterranee 13, 61-71 (in Italian)

Allen, P.A., Allen, J., 2013. Basin Analysis: Principles and Application to Petroleum Play Assessment. John Wiley and Sons, Oxford, 632 pp.

Allen, P., Homewood, P., Williams, G., 1986. Foreland basins: an introduction. In: Allen, P.A., Homewood, P. (Eds.), Foreland Basins. IAS Special Publication 8, pp. 3–12.

Amadori, C., Garcia-Castellanos, D., Toscani, G., Sternai, P., Fantoni, R., Ghielmi, M., Di Giulio, A., 2018. Restored topography of the Po Plain-Northern Adriatic region during the Messinian base-level drop - implications for the physiography and compartmentalisation of the paleo-Mediterranean basin. Basin Research 30, 1247-1263.

Amadori, C., Toscani, G., Di Giulio, A., Maesano, F.E., D'Ambrogi, C., Ghielmi, M., Fantoni, R., 2019. From cylindrical to non-cylindrical foreland basin: Pliocene–Pleistocene evolution of the Po Plain-Northern Adriatic basin (Italy). Basin Research 31, 991–1015.

Amadori, C., Ghielmi, M., Marcin, N., Toscani, G., 2020. The evolution of a coastal wedge in response to Plio-Pleistocene climate change: The Northern Adriatic case. Marine and Petroleum Geology 122, 104675. https://doi.org/10.1016/j.marpetgeo.2020.104675.

Amorosi, A., Pavesi, M., Ricci Lucchi, M., Sarti, G., Piccin, A., 2008. Climatic signature of cyclic fluvial architecture from the Quaternary of the central Po Plain, Italy. Sedimentary Geology 209, 58–68.

Amorosi, A., Bruno, L., Campo, B., Morelli, A., Rossi, V., Scarponi, D., Hong, W., Bohacs, K.M., Drexler, T.M., 2017. Global sea-level control on local parasequence architecture from the Holocene record of the Po Plain, Italy. Marine and Petroleum Geology 87, 99–111.

Anadòn, P., Cabrera, L., Colombo, F., Marzo, M., Riba, O., 1986. Syntectonic intraformational unconformities in alluvial fan deposits, eastern Ebro Basin margins (NE Spain). In: Allen, P.A., Homewood, P. (Eds.), Foreland Basins. IAS Special Publication 8, pp. 259–271.

Anfossi, G., Brambilla, G., 1980. La fauna pleistocenica del colle di S. Colombano al Lambro (Lombardia). I - lamellibranchi. Atti dell'Istituto di Geologia dell'Università di Pavia XXIX, 49–68 (in Italian)

Anfossi, G., Desio, A., Gelati, R., Laureri, S., Petrucci, F., Venzo, S., 1971. Note Illustrative della Carta Geologica d'Italia. F.°60, Piacenza. Servizio Geologico d'Italia. Nuova Tecnica Grafica, Roma, 38 pp. (in Italian)

Arca, S., Beretta, G. Pietro, 1985. Prima sintesi geodetico-geologica sui movimenti verticali del suolo nell'Italia Settentrionale. Bollettino di Geodesia e Scienze affini 44, 125–156 (in Italian with English abstract)

Argnani, A., Barbacini, G., Bernini, M., Camurri, F., Ghielmi, M., Papani, G., Rizzini, F., Rogledi, S., Torelli, L., 2003. Gravity tectonics driven by Quaternary uplift in the Northern Apennines: Insights from the La Spezia-Reggio Emilia geo-transect. Quaternary International 101–102, 13–26.

Ashworth, P.J., Sambrook Smith, G.H., Best, J.L., Bridge, J.S., Lane, S.N., Lunt, I.A., Reesink, A.J.H., Simpson, C.J., Thomas, R.E., 2011. Evolution and sedimentology of a channel fill in the sandy braided South Saskatchewan River and its comparison to the deposits of an adjacent compound bar. Sedimentology 58, 1860–1883.

Baio, M., Bersezio, R., Bini, A., 2004. Assetto geologico della successione quaternaria nel sottosuolo tra Melegnano e Piacenza. Il Quaternario 17, 355–359 (in Italian with English abstract)

Barbero, D., Bucci, A., Forno, M.G., Lasagna, M., De Luca, D.A., 2020. Thermal model of

the Piedmont Po Plain shallow aquifer (NW Italy) with the statistical temperature distribution. Geothermics 87, 101833. https://doi.org/10.1016/j.geothermics.2020.101833.

Bartolini, C., Caputo, R., Pieri, M., 1996. Pliocene-Quaternary sedimentation in the Northern Apennine Foredeep and related denudation. Geological Magazine 133, 255–273.

Benedetti, L.C., Tapponnier, P., Gaudemer, Y., Manighetti, I., 2003. Geomorphic evidence for an emergent active thrust along the edge of the Po Plain: the Broni-Stradella fault. Journal of Geophysical Research 108, 2238. https://doi.org/10.1029/2001JB001546.

Bersezio, R., 1986. Studio fotogeologico e geofisico per la ricostruzione dell'andamento degli antichi alvei: prima ricostruzione dei paleoalvei della Pianura tra Adda e Ticino. Studi Idrogeologici Sulla Pianura Padana 2, 3.1-3.25. CLUP, Milano (in Italian)

Bersezio, R., Pavia, F., Baio, M., Bini, A., Felletti, F., Redondi, C., 2004. Aquifer architecture of the Quaternary alluvial succession of the Southern Lambro Basin (Lombardy-Italy). Italian Journal of Quaternary Sciences 17, 361–378.

Bersezio, R., Giudici, M., Mele, M., 2007. Combining sedimentological and geophysical data for high-resolution 3-D mapping of fluvial architectural elements in the Quaternary Po plain (Italy). Sedimentary Geology 202, 230–248.

Bersezio, R., Cavalli, E., Cantoni, M., 2010. Aquifer building and Apennine tectonics in a Quaternary foreland: the southernmost Lodi plain of Lombardy. Memorie descrittive della Carta Geologica d'Italia XC, 21–30.

Bersezio, R., Bini, A., Gelati, R., Ferliga, C., Rigamonti, I., Strini, A., 2014. Note Illustrative della Carta Geologica d'Italia alla scala 1:50.000. Foglio 097 – Vimercate. ISPRA, 293 pp. (in Italian with English abstract)

Bertotti, G., Capozzi, R., Picotti, V., 1997. Extension controls Quaternary tectonics, geomorphology and sedimentation of the N-Apennines foothills and adjacent Po Plain (Italy). Tectonophysics 282, 291–301.

Best, J.L., Ashworth, P.J., Bristow, C.S., Roden, J., 2003. Three-dimensional sedimentary architecture of a large, mid-channel sand braid bar, Jamuna River, Bangladesh. Journal of Sedimentary Research 73, 516–530.

Bigi, G., Cosentino, D., Parotto, M., Sartori, D., Scandone, P., 1990. Structural Model of Italy. Progetto Finalizzato Geodinamica CNR. SELCA, Firenze, 114 pp.

Bini, A., 1987. L'Apparato Glaciale Wurmiano di Como (PhD Thesis). Università degli Studi di Milano, Milan (in Italian with English abstract)

Bini, A., 1997a. Problems and methodologies in the study of the Quaternary deposits of the southern side of the Alps. Geologia Insubrica 2, 11–20.

Bini, A., 1997b. Stratigraphy, chronology and paleogeography of Quaternary deposits of the area between the Ticino and Olona rivers (Italy-Switzerland). Geologia Insubrica 2, 21–46.

Bini, A., 2005. I ghiacciai del Passato. In: Bonardi, L., Rovelli, E., Scotti, R., Toffaletti, A., Urso, M., Villa, F. (Eds.), I Ghiacciai Di Lombardia. Evoluzione e Attualità. Hoepli, Milano, pp. 11–19 (in Italian)

Bini, A., Strini, A., Violanti, D., Zuccoli, L., 2004a. Geologia di sottosuolo dell'Alta Pianura a NE di Milano. Il Quaternario 17, 343–354 (in Italian with English abstract)

Bini, A., Zuccoli, L., Bassolini, C., Da Rold, O., Corbari, D., Ferliga, C., Rossi, S., Viviani, C., 2004b. Glacial history of the southern side of the central Alps, Italy. Developments in Quaternary Sciences 2, 195–200.

Bini, A., Sciunnach, D., Bersezio, R., Scardia, G., Tomasi, F., 2014. Note illustrative della Carta Geologica d'Italia alla scala 1:50.000. Foglio 96 - Seregno. ISPRA (in Italian with English abstract)

Bini, A., Baio, M., Violanti, D., Martinetto, E., 2016. Nuovi dati da sondaggi provenienti dai dintorni di San Colombano al Lambro e dalla Pianura Padana a Est di Milano: analisi

litostratigrafica, composizionale e micropaleontologica. Geologia Insubrica 12, 163-171 (in Italian)

Blum, M.D., 1993. Genesis and architecture of incised valley fill sequences: a Late Quaternary example from the Colorado River, Gulf Coastal Plain of Texas. In: Weimer, P., Posamentier, H.W. (Eds.), Siliciclastic Sequence Stratigraphy: Recent Developments and Applications. American Association of Petroleum Geologists, Memoir 58, pp. 259–283.

Boccaletti, M., Corti, G., Martelli, L., 2011. Recent and active tectonics of the external zone of the Northern Apennines (Italy). International Journal of Earth Sciences 100, 1331–1348.

Bond, C.E., 2015. Uncertainty in structural interpretation: Lessons to be learnt. Journal of Structural Geology 74, 185–200.

Boni, A., 1967. Note illustrative della Carta Geologica d'Italia. F.°59, Pavia. Servizio Geologico d'Italia. Nuova Tecnica Grafica, Roma, 69 pp. (in Italian)

Bresciani, I., Perotti, C.R., 2014. An active deformation structure in the Po Plain (N Italy): the Romanengo anticline. Tectonics 33, 2059–2076.

Bridge, J.S., 1993. Description and interpretation of fluvial deposits: a critical perspective. Sedimentology 40, 801–810.

Bridge, J.S., 2003. Rivers and Floodplains: Forms, Processes and Sedimentary Record. Blackwell, Oxford, UK, 491 pp.

Burrato, P., Ciucci, F., Valensise, G., 2003. An inventory of river anomalies in the Po Plain, Northern Italy: evidence for active blind thrust faulting. Annales of Geophysics 46, 865–882.

Calcagno, P., Chilès, J.P., Courrioux, G., Guillen, A., 2008. Geological modelling from field data and geological knowledge Part I. Modelling method coupling 3D potential-field

interpolation and geological rules. Physics of the Earth and Planetary Interiors 171, 147–157.

Cant, D.J., 1982. Fluvial facies models and their application. In: Scholle, P. A., Spearing, D. (Eds.), Sandstone Depositional Environments. American Association of Petroleum Geologists, Memoir 31, pp. 115–137.

Carminati, E., Martinelli, G., Severi, P., 2003. Influence of glacial cycles and tectonics on natural subsidence in the Po Plain (Northern Italy): Insights from 14 C ages. Geochemistry, Geophysics, Geosystems 4, 1–14.

Castiglioni, G.B., Pellegrini, G.B., 2001. Note Illustrative della Carta Geomorfologica della Pianura Padana. Supplementi di Geografia Fisica e Dinamica Quaternaria - vol. IV. Comitato Glaciologico Italiano, Torino, 207 pp.

Castiglioni, G.B., Biancotti, A., Bondesan, M., Cortemiglia, G.C., Elmi, C., Favero, V., Gasperi, G., Marchetti, G., Orombelli, G., Pellegrini, G.B., Tellini, C., 1999. Geomorphological map of the Po Plain, Italy, at a scale of 1:250 000. Earth Surface Processes and Landforms 24, 1115–1120.

Caumon, G., 2010. Towards stochastic time-varying geological modeling. Mathematical Geosciences 42, 555–569.

Chilès, J., Guillen, A., Lees, T., 2004. Modelling the geometry of geological units and its uncertainty in 3D from structural data: the potential-field method. In: Proceedings of International Symposium on Orebody Modelling and Strategic Mine Planning. Perth, Western Australia, p. 24.

Cita, M.B., Gibbard, P.L., Head, M.J., the ICS Subcommission on Quaternary Stratigraphy, 2012. Formal ratification of the GSSP for the base of the Calabrian Stage (second stage of the Pleistocene Series, Quaternary System). Episodes 35, 388–397.

Cohen, K.M., Gibbard, P.L., 2019. Global chronostratigraphical correlation table for the last

2.7 million years, version 2019 QI-500. Quaternary International 500, 20–31.

Contini, D., 2017. Geologia di Superficie e di Sottosuolo della Successione Quaternaria a Ovest del Colle di San Colombano al Lambro (MSc Thesis). Università degli Studi di Milano, Milan (in Italian)

Correggiari, A., Roveri, M., Trincardi, F., 1996. Late Pleistocene and Holocene evolution of the North Adriatic Sea. Il Quaternario 9, 697–704.

Cremaschi, M., 1987. Paleosols and Vetusols in the Central Po Plain (Northern Italy): A Study in Quaternary Geology and Soil Development. Vol. 28, Unicopoli, Milano, 306 pp.

Cremaschi, M., Nicosia, C., 2012. Sub-boreal aggradation along the Apennine margin of the Central Po Plain: geomorphological and geoarchaeological aspects. Geomorphologie: Relief, Processus, Environnement 18, 155–174.

Crippa, G., Baucon, A., Felletti, F., Raineri, G., Scarponi, D., 2018. A multidisciplinary study of ecosystem evolution through early Pleistocene climate change from the marine Arda River section, Italy. Quaternary Research 89, 533–562.

Crippa, G., Azzarone, M., Bottini, C., Crespi, S., Felletti, F., Marini, M., Petrizzo, M.R., Scarponi, D., Raffi, S., Rai, G., 2019. Bio- and lithostratigraphy of lower Pleistocene marine successions in western Emilia (Italy) and their implications for the first occurrence of Arctica islandica in the Mediterranean Sea. Quaternary Research 92, 549–569.

Da Rold, O., 1990. L'Apparato Glaciale del Lago Maggiore, Settore Orientale (PhD Thesis). Università degli Studi di Milano, Milan (in Italian with English abstract)

Database of Lombardy Region. Banca dati geologica di sottosuolo. https://www.cartografia.servizirl.it/viewer31/index.jsp?config=config_caspita.json. (Accessed 15 February 2021).

De Caro, M., Perico, R., Crosta, G.B., Frattini, P., Volpi, G., 2020. A regional-scale conceptual and numerical groundwater flow model in fluvio-glacial sediments for the

Milan Metropolitan area (Northern Italy). Journal of Hydrology: Regional Studies 29, 100683. https://doi.org/10.1016/j.ejrh.2020.100683.

De Celles, P.G., Giles, K.A., 1996. Foreland basin systems. Basin Research 8, 105–123.

Desio, A., 1965. I rilievi isolati della Pianura Lombarda ed i movimenti tettonici del Quaternario. Rendiconti dell'Istituto Lombardo di Scienze e Lettere A, 881–894 (in Italian)

Desio, A., Villa, F., 1960. Stratigrafie di Pozzi per Acqua della Pianura Padana. 1 - Lombardia. Università di Milano, Istituto di Geologia, Milan, 379 pp. (in Italian)

Devoti, R., Esposito, A., Pietrantonio, G., Pisani, A.R., Riguzzi, F., 2011. Evidence of large scale deformation patterns from GPS data in the Italian subduction boundary. Earth and Planetary Science Letters 311, 230–241.

Di Dio, G., Piccin, A., Vercesi, P.L., 2005. Carta Geologica d'Italia alla Scala 1:50.000. Foglio 179 "Ponte dell'Olio" 1–108. ISPRA (in Italian with English abstract)

DISS Working Group, 2015. Database of Individual Seismogenic Sources (DISS), Version 3.2.0: A compilation of potential sources for earthquakes larger than M 5.5 in Italy and surrounding areas. http://diss.rm.ingv.it/diss/, Istituto Nazionale di Geofisica e Vulcanologia. https://doi.org/10.6092/INGV.IT-DISS3.2.0. (Accessed 15 February 2021).

Doglioni, C., 1993. Some remarks on the origin of foredeeps. Tectonophysics 228, 1–20.

Dondi, L., Mostardini, F., Rizzini, A., 1982. Evoluzione sedimentaria e paleogeografica nella Pianura Padana. Guida Geologica Regionale S.G.I. pp. 47–58 (in Italian)

Dunne, W.M., Ferrill, D.A., 1988. Blind thrust systems. Geology 16, 33–36.

Einsele, G., 1992. Sedimentary Basins. Springer-Verlag, Berlin, Heidelberg, 628 pp.

Fantoni, R., Franciosi, R., 2010. Tectono-sedimentary setting of the Po Plain and Adriatic foreland. Rendiconti Lincei 21, 197–209.

Fantoni, R., Bersezio, R., Forcella, F., 2004. Alpine structure and deformation chronology at

the Southern Alps-Po Plain border in Lombardy. Bollettino della Società Geologica Italiana 123, 463–476.

Fontana, A., Mozzi, P., Marchetti, M., 2014. Alluvial fans and megafans along the southern side of the Alps. Sedimentary Geology 301, 150–171.

Francani, V., Piccin, A., Credali, M., Berra, F., Battaglia, D., Gattinoni, P., Rigamonti, I., Rosselli, S., 2016. Note Illustrative della Carta Geologica d'Italia alla scala 1:50.000. Foglio 118 - Milano. ISPRA, Piacenza, 220 pp. (in Italian with English abstract)

Freytet, P., Verrecchia, E.P., 2002. Lacustrine and palustrine carbonate petrography: An overview. Journal of Paleolimnology 27, 221–237.

Galloway, W.E., Hobday, D.K., 1996. Fluvial systems. In: Galloway, W.E., Hobday, D.K. (Eds.), Terrigenous Clastic Depositional Systems. Springer Verlag, Berlin, Heidelberg. https://doi.org/https://doi.org/10.1007/978-3-642-61018-9_4

Gardner, J.T., Ashmore, P.E., 2011. Geometry and grain-size characteristics of the basal surface of a braided river deposit. Geology 39, 247–250.

Garzanti, E., Vezzoli, G., Andò, S., 2011. Paleogeographic and paleodrainage changes during Pleistocene glaciations (Po Plain, Northern Italy). Earth-Science Reviews 105, 25–48.

Ghielmi, M., Minervini, M., Nini, C., Rogledi, S., Rossi, M., 2013. Late Miocene–Middle Pleistocene sequences in the Po Plain – Northern Adriatic Sea (Italy): The stratigraphic record of modification phases affecting a complex foreland basin. Marine and Petroleum Geology 42, 50–81.

Guillen, A., Calcagno, P., Courrioux, G., Joly, A., Ledru, P., 2008. Geological modelling from field data and geological knowledge Part II. Modelling validation using gravity and magnetic data inversion. Physics of the Earth and Planetary Interiors 171, 158–169.

Gunderson, K.L., Pazzaglia, F.J., Picotti, V., Anastasio, D. a., Kodama, K.P., Rittenour, T., Frankel, K.F., Ponza, A., Berti, C., Negri, A., Sabbatini, A., 2014. Unraveling tectonic and

climatic controls on synorogenic growth strata (Northern Apennines, Italy). Bulletin of the Geological Society of America 126, 532–552.

Hassen, I., Milnes, E., Gibson, H., Bouhlila, R., 2019. Impact of groundwater flow across tectonic aquifer compartments in a Miocene sandstone aquifer: three-dimensional hydrogeological modeling of the Kasserine aquifer system in central Tunisia and northeastern Algeria. Hydrogeology Journal 27, 1345–1361.

Heinz, J., Aigner, T., 2003. Hierarchical dynamic stratigraphy in various Quaternary gravel deposits, Rhine glacier area (SW Germany): Implications for hydrostratigraphy. International Journal of Earth Sciences 92, 923–938.

Hessami, K., Koyi, H.A., Talbot, C.J., Tabasi, H., Shabanian, E., 2001. Progressive unconformities within an evolving foreland fold-thrust belt, Zagros Mountains. Journal of the Geological Society 158, 969–982.

Hickson, T.A., Sheets, B.A., Paola, C., Kelberer, M., 2005. Experimental test of tectonic controls on three-dimensional alluvial facies architecture. Journal of Sedimentary Research 75, 710–722.

Horn, J.D., Fielding, C.R., Joeckel, R.M., 2012. Revision of Platte River alluvial facies model through observations of extant channels and barforms, and subsurface alluvial valley fills. Journal of Sedimentary Research 82, 72–91.

Ingersoll, R., 2012. Tectonics of sedimentary basins with revised nomenclature. In: Busby, C., Azor, A. (Eds.), Tectonics of Sedimentary Basins: Recent Advances, First Edition. Wiley-Blackwell, Oxford, pp. 3–43.

ISPRA, 2015. Modello Geologico 3D e Geopotenziali della Pianura Padana Centrale (Progetto GeoMol). Rapporti ISPRA 234/2015. ISPRA, Rome, 104 pp. (in Italian)

Kent, W.N., Dasgupta, U., 2004. Structural evolution in response to fold and thrust belt tectonics in northern Assam. A key to hydrocarbon exploration in the Jaipur anticline area.

Marine and Petroleum Geology 21, 785–803.

Kim, W., Paola, C., 2007. Long-period cyclic sedimentation with constant tectonic forcing in an experimental relay ramp. Geology 35, 331–334.

Kirby, E., Whipple, K.X., 2012. Expression of active tectonics in erosional landscapes. Journal of Structural Geology 44, 54–75.

Lajaunie, C., Courrioux, G., Manuel, L., 1997. Foliation fields and 3D cartography in geology; principles of a method based on potential interpolation. Mathematical Geology 29, 571–584.

Lee, G.H., Suk, B.C., 1998. Latest Neogene-Quaternary seismic stratigraphy of the Ulleung Basin, East Sea (Sea of Japan). Marine Geology 146, 205–224.

Leopold, L.B., Wolman, M.G., 1957. River Channel Patterns: Braided, Meandering and Straight. Geological Survey Professional Paper 282-B. United States Government Printing Office, Washington DC, 85 pp.

Livio, F., Berlusconi, A., Michetti, A.M., Sileo, G., Zerboni, A., Trombino, L., Cremaschi, M., Mueller, K., Vittori, E., Carcano, C., Rogledi, S., 2009. Active fault-related folding in the epicentral area of the December 25, 1222 (Io=IX MCS) Brescia earthquake (Northern Italy): Seismotectonic implications. Tectonophysics 476, 320–335.

Losi, E., 2007. Geologia e Geomorfologia della Pianura Lodigiana Compresa tra il Colle di San Colombano al Lambro e la Scarpata del Terrazzo del Po (MSc Thesis). Università degli Studi di Milano, Milan (in Italian)

Lowe, D.R., Lopiccolo, R.D., 1974. The characteristics and origins of dish and pillar structures. SEPM Journal of Sedimentary Petrology 44, 484–501.

Ložek, V., 1964. Quartärmollusken der Tschechoslowakei. Rozpravy Ústředního ústavu geologického 31, 1-374 (in German)

Maesano, F.E., D'Ambrogi, C., 2016. Coupling sedimentation and tectonic control:

Pleistocene evolution of the central Po Basin. Italian Journal of Geosciences 135, 394–407.

Maesano, F.E., D'Ambrogi, C., Burrato, P., Toscani, G., 2015. Slip-rates of blind thrusts in slow deforming areas: Examples from the Po Plain (Italy). Tectonophysics 643, 8–25.

Maestrelli, D., Benvenuti, M., Bonini, M., Carnicelli, S., Piccardi, L., Sani, F., 2018. The structural hinge of a chain-foreland basin: Quaternary activity of the Pede-Apennine Thrust front (Northern Italy). Tectonophysics 723, 117–135.

Maljers, D., Stafleu, J., Van Der Meulen, M.J., Dambrink, R.M., 2015. Advances in constructing regional geological voxel models, illustrated by their application in aggregate resource assessments. Geologie en Mijnbouw/Netherlands Journal of Geosciences 94, 257–270.

Mallet, J.L., 2004. Space-time mathematical framework for sedimentary geology. Mathematical Geology 36, 1–32.

Mancin, N., Di Giulio, A., Cobianchi, M., 2009. Tectonic vs. climate forcing in the Cenozoic sedimentary evolution of a foreland basin (Eastern Southalpine system, Italy). Basin Research 21, 799–823.

McCalpin, J., 2009. Paleoseismology. Academic Press Inc., San Diego, 613 pp.

McClay, K.R., 1992 (Ed.). Thrust Tectonics. Springer-Science and Business Media, B. V, London, 447 pp.

Mele, M., Bersezio, R., Giudici, M., Inzoli, S., Cavalli, E., Zaja, A., 2013. Resistivity imaging of Pleistocene alluvial aquifers in a contractional tectonic setting: A case history from the Po plain (Northern Italy). Journal of Applied Geophysics 93, 114–126.

Mele, M., Bersezio, R., Giudici, M., 2018. An electrostratigraphic cross-section across the central Po plain: bearings on subsurface geology and hydrostratigraphy. International Journal of Earth Sciences 107, 2787–2802.

Mele, M., Zuffetti, C., Aliverti Piuri, E., Bersezio, R., Giudici, M., Comunian, A., Contini, D., 2019. Geophysical imaging of a buried faulted anticline: the San Colombano hill, southern Po Plain of Lombardy (Northern Italy). In: Carmina, B., Petti, F. (Eds.), Congresso SIMP-SGI-SOGEI, Parma, p. 488.

Meletti, C., D'Amico, V., Ameri, G., Rovida, A., Stucchi, M., 2012. Seismic hazard in the Po Plain and the 2012 Emilia earthquakes. Annals of Geophysics 55, 623–629.

Miall, A.D., 1985. Architectural-element analysis: A new method of facies analysis applied to fluvial deposits. Earth-Science Reviews 22, 261–308.

Miall, A.D., 1996. The geology of fluvial deposits: sedimentary facies, basin analysis and petroleum geology. Springer-Verlag, Heidelberg, 582 pp.

Michetti, A.M., Giardina, F., Livio, F., Mueller, K., Serva, L., Sileo, G., Vittori, E., Devoti, R., Riguzzi, F., Carcano, C., Rogledi, S., Bonadeo, L., Brunamonte, F., Fioraso, G., 2012. Active compressional tectonics, quaternary capable faults, and the seismic landscape of the po plain (northern Italy). Annals of Geophysics 55, 969–1001.

Milli, S., Mancini, M., Moscatelli, M., Stigliano, F., Marini, M., Cavinato, G.P., 2016. From river to shelf, anatomy of a high-frequency depositional sequence: The Late Pleistocene to Holocene Tiber depositional sequence. Sedimentology 63, 1886-1928.

Ministero dei Lavori Pubblici, Ufficio Idrografico del Po, 1924. Geoidrologia dei Pozzi Profondi della Valle Padana. Parte II. Vol. 3. Istituto Poligrafico dello Stato, Torino (in Italian)

Ministero dei Lavori Pubblici, Ufficio Idrografico del Po, 1933. Geologia dei Pozzi Profondi della Valle Padana. Parte III, Vol. 3. Istituto Poligrafico dello Stato, Roma (in Italian)

MiSE, Società Geologica Italiana, Assomineraria (VIDEPI project), 2009. Visibility of petroleum exploration data in Italy www.videpi.com. (Accessed 15 February 2021).

Montrasio, A., Bigioggero, B., Maino, A., Cirese, E., Tacchia, D., 1990. Carta Geologica

della Lombardia - Scala 1: 250.000. Istituto Poligrafico e Zecca dello Stato, Rome (in Italian)

Moore, P.D., Webb, J.A., Collinson, M.E., 1991. Pollen Analysis. Blackwell Publishing, Oxford, 216 pp.

Moreton, D.J., Ashworth, P.J., Best, J.L., 2002. The physical scale modelling of braided alluvial architecture and estimation of subsurface permeability. Basin Research 14, 265–285.

Morley, C.., 1988. Out-of-sequence thrusts. Tectonics 7, 539–561.

Muñoz-Jiménez, A., Casas-Sainz, A.M., 1997. The Rioja Trough (N Spain): tectono-sedimentary evolution of a symmetric foreland basin. Basin Research 9, 65–85.

Murray, J.W., 2006. Ecology and Applications of Benthic Foraminifera. Cambridge University Press, Cambridge, 426 pp.

Muttoni, G., Carcano, C., Garzanti, E., Ghielmi, M., Piccin, A., Pini, R., Rogledi, S., Sciunnach, D., 2003. Onset of major Pleistocene glaciations in the Alps. Geology 31, 989–992.

O'Brien, P.E., Wells, A. T., 1986. A small, alluvial crevasse splay. Journal of Sedimentary Research 56, 876–879

Obermeier, S.F., 1996. Use of liquefaction-induced features for paleoseismic analysis — An overview of how seismic liquefaction features can be distinguished from other features and how their regional distribution and properties of source sediment can be used to infer the location and strength of Holocene paleo-earthquakes. Engineering Geology 44, 1–76.

Onnis, L., Violante, R.A., Osella, A., De La Vega, M., Tassone, A., López, E., 2018. Neogene-Quaternary seismic stratigraphy of the Llancanelo Lake Basin, Mendoza, Argentina. Andean Geology 45, 35–46.

Ori, G.G., 1993. Continental depositional system of the Quaternary of the Po Plain (northern

Italy). Sedimentary Geology 83, 1–14.

Ori, G.G., Friend, P.F., 1984. Sedimentary basins formed and carried piggyback on active thrust sheets. Geology 12, 475–478.

Pantea, B.M.P., Cole, J.C., 2004. Three-Dimensional Geologic Framework Modeling of Faulted Hydrostratigraphic Units within the Edwards Aquifer, Northern Bexar County, Texas. Scientific Investigation Report 2005-5226, 13 pp.

Panzeri, L., Zembo, I., Bersezio, R., Martini, M., 2011. Calibration of OSL data: mismatch between stratigraphy and OSL chronology of sediments from the Po Plain. Il Quaternario 24, 114–116.

Paola, C., 2000. Quantitative models of sedimentary basin filling. Sedimentology 47, 121–178.

Pellegrini, L., Boni, P., Carton, A., 2003. Hydrographic evolution in relation to neotectonics aided by data processing and assessment: some examples from the Northern Apennines (Italy). Quaternary International 101–102, 211–217.

Penck, A., Brückner, E., 1909. Die Alpen im Eiszeitalter. Tauchnitz, Leipzig, 1199 pp (in German)

Pettijohn, F.J., Potter, P., 1964. Atlas and Glossary of Primary Sedimentary Structures. Springer Science and Business Media, Berlin, 370 pp.

Pieri, M., Groppi, G., 1981. Subsurface geological structure of the Po plain, Italy. In: Consiglio Nazionale delle Ricerche (Ed.), Progetto Finalizzato Geodinamica, Vol.. 414. Rome, 13 pp.

Rafini, S., Mercier, E., 2002. Forward modelling of foreland basins progressive unconformities. Sedimentary Geology 146, 75–89.

Reading, H.G. (Ed.), 1996. Sedimentary Environments: Processes, Facies and Stratigraphy. Blackwell Publishing, London, 704 pp.

Regione Emilia-Romagna, Eni-AGIP, 1998. Riserve Idriche Sotterranee della Regione Emilia-Romagna. Di Dio, G. (Ed.). S.E.L.C.A., Firenze, 120 pp. (in Italian)

Regione Lombardia, Eni Divisione Agip, 2001. Geologia degli Acquiferi Padani della Regione Lombardia. Carcano, C., Piccin, A. (Eds.). S.EL.CA., Firenze, 131 pp. https://doi.org/10.1017/CBO9781107415324.004 (in Italian)

Ricci Lucchi, F., 1986. Oligocene to recent foreland basins of northern Apennines. In: Allen, P.A., Homewood, P. (Eds.), Foreland Basins. IAS Special Publication 8. pp. 105–139.

Rigato, V., 2007. Geologia degli Acquiferi Alluvionali della Pianura Lodigiana tra Lodi e Camairago (MSc Thesis). Università degli Studi di Milano, Milan (in Italian)

Riva, A., 1957. Gli anfiteatri morenici a Sud del Lario e le pianure diluviali tra Adda e Olona. Atti Istituto Geologico Università di Pavia 7, 5–95 (in Italian)

Ronchi, L., Fontana, A., Correggiari, A., Remia, A., 2019. Anatomy of a transgressive tidal inlet reconstructed through high-resolution seismic profiling. Geomorphology 343, 65–80.

Ross, M., Parent, M., Lefebvre, R., 2005. 3D geologic framework models for regional hydrogeology and land-use management: A case study from a Quaternary basin of southwestern Quebec, Canada. Hydrogeology Journal 13, 690–707.

Rossi, M., Minervini, M., Ghielmi, M., Rogledi, S., 2015. Messinian and Pliocene erosional surfaces in the Po Plain-Adriatic Basin: Insights from allostratigraphy and sequence stratigraphy in assessing play concepts related to accommodation and gateway turnarounds in tectonically active margins. Marine and Petroleum Geology 66, 192-216.

Rovida, A., Locati, M., Camassi, R., Lolli, B., Gasperini, P. (Eds.), 2016. CPTI15, the 2015 Version of the Parametric Catalogue of Italian Earthquakes. Istituto Nazionale di Geofisica e Vulcanologia. https://doi.org/10.6092/INGV.IT-CPTI15

Russell, Hazen A J, Kemp, E. De, Maccormack, K.E., 2019. Overview of geological survey organizations contributions on modelling approaches. In: MacCormack, K.E., Berg, R.C.,

Kessler, H., Russell, H.A.J., Thorleifson, L.H. (Eds.), 2019 Synopsis of Current Three-Dimensional Geological Mapping and Modelling in Geological Survey Organizations. Alberta Energy Regulator, Alberta Geological Survey, pp. 7–18.

Rust, B.R., Gibling, M.R., 1990. Braidplain evolution in the Pennsylvanian South Bar Formation, Sydney Basin, Nova Scotia, Canada. Journal of Sedimentary Research 60, 59–72

Sacco, F., 1912. Geoidrologia dei Pozzi Profondi della Valle Padana. Parte I, Vol. LIV-L. Istituto Poligrafico dello Stato, Torino (in Italian)

Scardia, G., Muttoni, G., Sciunnach, D., 2006. Subsurface magnetostratigraphy of Pleistocene sediments from the Po Plain (Italy): Constraints on rates of sedimentation and rock uplift. Geological Society of America Bulletin 118, 1299–1312.

Scardia, G., De Franco, R., Muttoni, G., Rogledi, S., Caielli, G., Carcano, C., Sciunnach, D., Piccin, A., 2012. Stratigraphic evidence of a Middle Pleistocene climate-driven flexural uplift in the Alps. Tectonics 31, 1–16

Scheidler, S., Anders, B., Regli, C., Belay, S., Huggenberger, P., 2019. Geothermal use of an Alpine aquifer-Davos pilot study. Grundwasser 24, 277–286.

Schumm, S.A., 1981. Evolution and response of the fluvial system, sedimentologic implications. SEPM Special Publication 31, 19–29.

Schumm, S.A., Dumont, J.F., Holbrook, J.M., 2002. Active Tectonics and Alluvial Rivers. Cambridge University Press, Cambridge, 292 pp.

Shackleton, N.J., 1987. Oxygen isotopes, ice volume and sea level. Quaternary Science Reviews 6, 183–190.

Sheets, B.A., Hickson, T.A., Paola, C., 2002. Assembling the stratigraphic record: depositional patterns and time-scales in an experimental alluvial basin. Basin Research 14, 287–301.

Smith, N.D., Rogers, J. (Eds.), 2009. Fluvial Sedimentology VI. John Wiley and Sons, Oxford, 488 pp.

Tavani, S., Snidero, M., Muñoz, J.A., 2014. Uplift-induced residual strain release and late-thrusting extension in the Anaran mountain front anticline, Zagros (Iran). Tectonophysics 636, 257–269.

Toscani, G., Seno, S., Fantoni, R., Rogledi, S., 2006. Geometry and timing of deformation inside a structural arc: the case of the western Emilian folds (Northern Apennine front, Italy). Bollettino della Società Geologica Italiana 125, 59–65.

Toscani, G., Bonini, L., Ahmad, M.I., Di Bucci, D., Di Giulio, A., Seno, S., Galuppo, C., 2014. Opposite verging chains sharing the same foreland: Kinematics and interactions through analogue models (Central Po Plain, Italy). Tectonophysics 633, 268–282.

Turrini, C., Lacombe, O., Roure, F., 2014. Present-day 3D structural model of the Po Valley basin, Northern Italy. Marine and Petroleum Geology 56, 266–289.

Van Der Meulen, M.J., Doornenbal, J.C., Gunnink, J.L., Stafleu, J., Schokker, J., Vernes, R.W., Van Geer, F.C., Van Gessel, S.F., Van Heteren, S., Van Leeuwen, R.J.W., Bakker, M.A.J., Bogaard, P.J.F., Busschers, F.S., Griffioen, J., Gruijters, S.H.L.L., Kiden, P., Schroot, B.M., Simmelink, E.J., Van Berkel, W.O., Van Der Krogt, R.A.A., Westerhoff, W.E., Van Daalen, T.M., 2013. 3D geology in a 2D country: perspectives for geological surveying in the Netherlands. Netherland Journal of Geosciences 92, 217–241.

Vannoli, P., Burrato, P., Valensise, G., 2015. The seismotectonics of the Po Plain (Northern Italy): Tectonic diversity in a blind faulting domain. Pure and Applied Geophysics 172, 1105–1142.

Vercesi, P.L., Scagni, C., 1984. Osservazioni sui depositi conglomeratici dello sperone collinare di Stradella. Rendiconti della Società Geologica Italiana 7, 23–26 (in Italian)

Wellmann, F., Caumon, G., 2018. 3-D structural geological models: Concepts, methods, and

uncertainties. Advances in Geophysics 59, 1–121.

Wheeler, H.E., 1959. Stratigraphic units in space and time. American Journal of Science 257, 692–706.

Zanchi, A., Deaddis, M., De Amicis, M., Marchetti, M., Ravazzi, C., Vezzoli, G., 2019. Holocene deformed succession of Montodine (Cremona, Italy): evidence of recent tectonic activity? In: Carmina, B., Petti, F.M., Innamorati, G., Fascio, L. (Eds.), Congresso SIMP-SGI-SOGEI. Società Geologica Italiana, Parma, p. 499.

Zuccoli, L., 1997. Geologia dell'Alta Pianura Lombarda tra i Pianalti di Castelseprio e Tradate-Appiano Gentile (PhD Thesis). Università degli Studi di Milano, Milan (in Italian)

Zuffetti, C., 2019. Characterization and Modelling of Complex Geological Architectures: The Quaternary Fill of the Po Basin at the Po Plain-Apennines Border (Lombardy, Italy) (PhD Thesis). Università degli Studi di Milano, Milano. 246 pp.

Zuffetti, C., Bersezio, R., 2020. Morphostructural evidence of Late Quaternary tectonics at the Po Plain-Northern Apennines border (Lombardy, Italy). Geomorphology 364, 107245. https://doi.org/10.1016/j.geomorph.2020.107245

Zuffetti, C., Bersezio, R., Cortini, D., Petrizzo, M.R., 2018a. Geology of the San Colombano hill, a Quaternary isolated tectonic relief in the Po Plain of Lombardy (Northern Italy). Journal of Maps 14, 199–211.

Zuffetti, C., Trombino, L., Zembo, I., Bersezio, R., 2018b. Soil evolution and origin of landscape in a late Quaternary tectonically mobile setting: the Po Plain-Northern Apennines border in Lombardy (Italy). Catena 171, 376–397.

Zuffetti, C., Bersezio, R., Trombino, L., 2018c. Significance of the morphological and stratigraphic surfaces in the Quaternary Po Plain: the San Colombano tectonic relief (Lombardy, Italy). Alpine and Mediterranean Quaternary 31, 257–260.

Zuffetti, C., Comunian, A., Bersezio, R., Renard, P., 2020. A new perspective to model subsurface stratigraphy in alluvial hydrogeological basins, introducing geological hierarchy and relative chronology. Computers & Geosciences 140, 104506. https://doi.org/10.1016/j.cageo.2020.104506

FIGURES AND TABLES

Figure 1 – A) Location map of the studied sector of the Po basin in the structural framework of Italy. B) Location map and structural framework of the study area (dashed black frame) in the Po foreland basin (northern Italy; modified after Zuffetti and Bersezio, 2020). Solid black line: trace of the regional seismic section of Panel C. CPPS: Central Po Plain Structures, CZS: Casalpusterlengo-Zorlesco Structure, CZTF: Casalpusterlengo-Zorlesco Transfer Fault, PCLR: Pavia-Casteggio Lateral Ramp. FHS: Foothill structures, SCS: San Colombano Structure. C) Seismic line-drawing crossing the Apennine Emilia thrust front, modified after Rossi (2017). It shows the timing and vergence of the Apennines thrust front crosscutting and overriding the Southern Alps belt. MU: Intra-Messinian Unconformity; ZU: Intra-Zanclean Unconformity. D) Reference stratigraphic columns across the Po basin, suggesting relevant architectural changes across the basin fill. Polygons correlating the profiles frame the Quaternary deposits. Location: numbers in panel A. *s.l.: sensu lato*. Profile 1 after Boni (1967); profile 2 after Zuffetti et al. (2018a); profile 3 after Garzanti et al. (2011); profile 4 after MiSE et al. (2009). The dashed frame contours the study area.

Size: 2 COLUMNS

Figure 2 –Surface and subsurface datasets in the study area (solid black frame) and modelled area (dashed frame). A) Geological map after 1:10.000 field surveys of the modelled area (Bersezio et al., 2010; Zuffetti et al., 2018a, 2018b; Zuffetti and Bersezio, 2020) and 1-D borehole dataset of the study area. Within the grid of cross-sections, the bold black lines indicate the traces of the cross-sections presented in Figure 3. B) Structural map of the study area, modified after Boni (1967), Bigi et al. (1990), and Zuffetti et al. (2018a). SC: San Colombano hill, Z: Zorlesco relief, C: Casalpusterlengo relief. Labels of tectonic structures as in Figure 1.

Size: 2 COLUMNS

Figure 3 – Stratigraphic architecture of the southern Po basin. Above: fence diagram of selected 2-D cross-sections (section traces in Figure 2), showing the 3-D stratigraphic relationships among the Quaternary units of the southern Po basin. Horizontal/vertical scale ratio: 1/20. Grey layers within each Intermediate-Rank stratigraphic unit represent the most laterally continuous mud intervals (clay to silty-very fine sand). SC: San Colombano hill, C: Casalpusterlengo hill, Z: Zorlesco hill. Below: chronostratigraphic scheme and hierarchy of the stratigraphic units. Chronostratigraphic correlation table after Cohen and Gibbard (2019). Glacial amphitheatres after Bini et al. (2004) and Bini (2005). MIS: Marine Isotope Stages; Boz: Bozzente Supersynthem.

Size: 2 COLUMNS

Figure 4 - Gravel composition of the Quaternary stratigraphic units. Labels of stratigraphic boundaries and units as in Figure 3. Circled alphabetic codes refer to surface samples (black text) or borehole samples (blue text) from measured logs. Spatial location of the sampled logs is drawn in the index map on top of the figure; stratigraphic position of samples in logs is drawn in Figures 6 to 8.

Size: 1 COLUMN

Figure 5 – Comparison between surface facies associations and subsurface litho-textural stacking patterns. Facies codes as in Table 2; labels of stratigraphic units as in Figure 3.

Size: 1 COLUMN

Figure 6 - The stratigraphy of the High-Rank Stratigraphic Unit 0 (HRS0). Facies codes as in

Table 2; labels of stratigraphic units as in Figure 3. A) Features of HRS0 in outcrop (San Colombano Fm., SCF) above the marine substratum (Sant'Agata Fossili Marls, SAF). GU: Gelasian Unconformity. The reference stratigraphic column of SCF, in the San Colombano hill, shows the vertical stacking of the lithozones SCFa, SCFb, SCFc. Some of the specific facies assemblages (Fig. 5; Table 3A), are shown in the photographs. Facies association F1: poorly sorted conglomerates and sandstone rich in fossil fragments and sub-rounded clasts; F2: organogenic limestone with encrusting algae; F3: detail of a cross-bedded to planar bedded sand alternated with horizontal bedded silty clays and blue clays. F4/F5: blue silty clays with cm-thick fine sand intercalations. Facies codes as in Table 2. B)-C) HRS0 in the subsurface (subsurface equivalent of the San Colombano Fm., SCF-sse). B) marker-driven correlation of the SCF-sse in the subsurface of the Casalpusterlengo hill. Grey layers above U1: laterally continuous mud intervals (clay to silty-very fine sand). C) Reference subsurface stratigraphic logs of SCF-sse, near (left-hand side) and far (right-hand side) from the SCS and CZS culminations. Encircled codes refer to sampled sites for compositional analyses (see Figure 4). D) Reconstruction of the facies distribution of lithozone SCFa. The yellow lines contour the present-day location of the San Colombano, Casalpusterlengo and Zorlesco reliefs, with no reference to the quite different Calabrian paleogeography.

Size: 2 COLUMNS

Figure 7 - Features of the High-Rank subsurface Stratigraphic Units 1 and 2 (HRS1 and HRS2). Facies codes as in Table 2; labels of stratigraphic units as in Figure 3. A) E-W cross-section N of the San Colombano and Casalpusterlengo-Zorlesco structural crests (SCS and CZS). Grey layers within the intermediate-rank units laterally continuous mud intervals (clay to silty-very fine sand). HRS1 and the basal unconformity U1 are folded at the SCS-CZS. The parallelism between the intermediate-rank units IRS1.1-2-3 and U1 suggests post-

depositional folding. B) Subsurface stratigraphy approaching to the SCS. C) Features of the subsurface stratigraphy approaching the Zorlesco hill. HRS2 and the basal unconformity U2 are gently folded in correspondence of the SCS and CZS; here the intermediate-rank units IRS2.1, IRS2.2, IRS2.3 progressively lap-out onto the folded HRS1 and marine units while progressively eroding one into the others, suggesting syn-depositional deformation. Encircled letters refer to sampled sites for compositional analyses (see Figure 4). D) Reconstruction of facies distribution during the deposition of the fine-grained layer atop of IRS1.1. White lines: traces of the cross-sections in A, B and C; E) Reconstruction of facies distribution during the deposition of IRS2.2. F) Reconstruction of facies distribution during sedimentation of the coarse-grained facies of IRS2.3. In D, E and F the NW sources of sediments are suggested by the gravel composition (see text for discussion).

Size: 2 COLUMNS

Figure 8 - Stratigraphic architecture of the High-Rank Stratigraphic Unit 3 (HRS3). Facies codes as in Table 2; labels of stratigraphic units as in Figure 3. A) Correlation panel of selected sedimentary CPS1 and CPS2 logs on the San Colombano hill. Reference horizontal top surface: top of L2 loess. Stratigraphic logs are numbered as in Figure 4. B) Reference sedimentary logs on the Casalpusterlengo hill and Zorlesco hill (modified after Cremaschi, 1987). C) Features of the exposed INS across the northern, faulted flank of the San Colombano hill. D) Stratigraphic architecture of HRS3 along selected N-S trending cross-sections in the study area (cross-sections location in panel F). Grey to black layers within the intermediate-rank units: mud intervals (sandy silt to clay lithotextures; F7). E) Subsurface features of HRS3 along an E-W cross-section N of the tectonic reliefs. F) Facies distribution during sedimentation of CPS1 (Late Pleistocene). White traces: location of cross-sections of Panels A, C, D and E. G) Facies distribution during sedimentation of CPS2 (Late Pleistocene

- MIS4). H) Facies distribution at the end of the deposition of INS (LGM-MIS 2). I) Facies distribution and paleogeography during the evolution of PSS (Latest Pleistocene, waning LGM).

Size: FULL PAGE (landscape orientation)

Figure 9 – Facies of the Late Pleistocene CPS1 and INS (encoding as in Table 2), part of the High-Rank Stratigraphic Unit 3. A) Trough and planar cross-stratified sand facies in lithozone CPS1a. B) Gravel-sand scour cutting the trough-cross stratified bedset of a sand bar with inclined boundaries. The basal gravel lag contains large mud-clasts (CPS1a; log H, Fig. 8A). C) Detail of facies assemblage of CPS1a (log H, Fig. 8A), showing cross-stratified medium to coarse sands, with sigmoidal dunes. D) Water escape structures in F9 facies association of CPS1b (log H, Fig. 8A) with convolute laminae, laminasets and beds, and flame structures in between undeformed beds. E) Optical polarizing microscope image of coarse sands from CPS1b, F9 facies (log F, Fig. 8A): feldspatic sublitharenite with felsitic volcanites. Ochre colours characterise the pedogenic clay coatings related to the weathering profile. Left-hand side of the thin section: plane polarized light; right-hand side of the thin section: cross-polarized light. F) Optical polarizing microscope image of sands from INS (log M, Fig. 8C): lithic arkose with feldspars, quartz, volcanic rock fragments. Detail of a cm-sized erosional scour of medium sand above silty fine sand. Left-hand side: plane polarized light; right-hand side: cross-polarized light. G) Liquefaction structure of muddy sand injection into laminated sandy deposits of INS (outcrop M, Fig. 8C). Metre for scale.

Size: 1.5 COLUMNS

Figure 10 – Facies of the Latest Pleistocene synthems deposits, part of the High-Rank Stratigraphic Unit 3. A) INS (Last Glacial Maximum) is terraced by the PSS (late to post-glacial) along the erosional surface S3.4. INS (lithozone INSa): slightly weathered gravelly

sands with m- to decametric-sized trough cross-stratification on inclined bed-sets; PSS: co-sets of trough and planar cross-stratified sands and gravelly sands organised into dm-thick stationary to fining-upward sequences on inclined bed-sets (F8 facies association). B) Villanterio Unit (lithozone INSb): very fine burrowed and laminated silty sand and massive clayey sandy silt with continental mollusc association (F7) in association with planar cross-laminated sand with fine gravel (F13). C) Detail of dm-thick co-sets of trough and planar cross-stratified gravelly sands on inclined bed-sets of the PSS (F13). Facies codes as in Table 2; labels of stratigraphic units as in Figure 3.

Size: 1.5 COLUMNS

Figure 11 – Components of the space-time model of the southern Po basin. Column A: the interpreted Quaternary geological evolution of the southern Po basin fill. The main tectono-depositional stages originated the composite high-rank unconformities. The intermediate-rank increments built the intermediate-rank surfaces. Column B: the hierarchic stratigraphic architecture. The green lines represent the segments composing the present-day landscape. Column C: the present-day 3D geometry of the sedimentary bodies, represented by removing the units from the top at each evolutionary increment. F: fault.

Size: 1.5 COLUMNS

Figure 12 – Inspection of the space-time model of the southern Po basin. The model area is framed in Figure 2. A) Views of the 3-D high-rank (HRS0, HRS1), intermediate-rank (IRS2.2 to top) and low-rank (slices a, b) architecture. The two slices (a, b) cut in the model show that the dip and shape of the potential isolines honour the low angle onlaps and mutual erosional relationships among the stratigraphic units, coherently with the interpreted geological evolution. Slice a): intermediate-rank units within HRS3; slice b): intermediate-

rank units within HRS2. Labels of stratigraphic units as in Figure 3. M-P: Mio-Pliocene marine substratum. B) Excerpt of the 3-D model (along the black trace across the model block of panel A), showing the architecture of the high-rank geological boundaries. Notice the absence of U2 unconformity just W of the CZTF and its synformal geometry to the East. C) Inspection of the 3-D geological model by removing the HRS4 above the unconformity U4. Dashed lines: stratigraphic surfaces cut at U4. Model voxel dimension: 50x50x8 m. F: normal fault; CZTF: Casalpusterlengo-Zorlesco Transfer Fault; SC: San Colombano hill; C: Casalpusterlengo hill; Z: Zorlesco hill.

Size: 2 COLUMNS

Table 1. Age constraints to the stratigraphic units defined in this work, directly sampled in the study area or in closely adjacent sectors. Location in the index map of Figures 2, 4. B.g.s: below ground surface; a.s.l: above the mean sea level; *p.p.: pro parte*. OSL: optically stimulated luminescence; 14C: radiocarbon; P: pollen analysis; M: micropaleontological analysis.

Unit	**Depth** (m b.g.s)	**Elevation** (m a.s.l)	**Age**	**Method**	**Location** (Figs. 2, 4)	**Reference**
PoS	1	64	390-560 cal BC	14C	K	Losi, 2007
PoS	17	43	11440-12997 cal BC	14C	E2	Bersezio et al., 2010
VIL	3	70.3	21435-22205 cal BC	14C	B	Zuffetti et al., 2018b
INS	1.5	67.5	18740 ± 2000 y BP	OSL	E1	Panzeri et al., 2011
INS	1.8	67.2	16280 ± 2000 y BP	OSL	E1	Panzeri et al., 2011
INS	5	80.5	20785 ± 19909 cal BC	14C	North of the study area	Bersezio et al., 2004
INS	9	76.5	22035 ± 300 y BP	14C	North of the study area	Bersezio et al., 2004
INS	21	63.7	23145 ± 340 y BP	14C	North of the study area	Bersezio et al., 2004

INS	5.4	65.2	24620 ± 160 y BP	14C	J	Bersezio et al., 2004
top CPS2	32	41.3	26884-27648 cal BC	14C	B	Zuffetti et al., 2018b
top CPS2	14.5	59	28295-28679 cal BC	14C	R	Bersezio et al., 2004
top CPS1	4	64	66900 ± 6000 y BP	OSL	W	Panzeri et al., 2011
CPS1	6	70.7	88890 ± 8800 y BP	OSL	F	Panzeri et al., 2011
CPS1	5	63	107370 ± 1300 y BP	OSL	W	Panzeri et al., 2011
IRS2.3	19.5	28.5	> 44000 y BP	14C	Z	Baio et al., 2004
IRS2.3	88	-8.5	Middle Pleistocene	P	North of the study area	Rigato, 2007
HRS1	156	-85	Quaternary *p.p*	M	A	Bini et al., 2016
SCF	0	120	Calabrian	M	L	Zuffetti et al., 2018a
SCF	0	135	Calabrian	M	N	Zuffetti et al., 2018a
SCF	14	44	Quaternary *p.p*	M	T	Bini et al., 2016
SCF	29	29	Quaternary *p.p*	M	T	Bini et al., 2016
SCF	102	-36	Lower-Middle Pleistocene	M	U	Bini et al., 2016

Size: 2 COLUMNS

Table 2. Above: sediment classification and facies codes used in this work (modified after Bersezio et al., 2004). Below: criteria adopted for outcrop-borehole correlations.

1-D stratigraphic data analysis		
	Facies code	**Example of application**
Sedimentary texture (all observations)	Cong: conglomerate; Ar: arenite G: gravel, S: sand, L:silt and very fine sand, A: clay T: peat, P: pedogenic concretions (carbonate) GS: sandy gravel, SG: gravelly sand, SL: silty sand, LS: sandy silt	SG: gravelly Sand, sand > 50%, gravel < 50%
		SAL: clayey-silty Sand, sand > clay > silt
	LAS: clayey-sandy silt	vfSfG: very fine gravelly Sand, very fine

	G/S: interbedding of gravel and sand	sand > 50%, fine gravel < 50%
Additional textural codes	vf: very fine f: fine m: medium c: coarse vc: very coarse	vfSfG: very fine gravelly Sand, very fine sand > 50%, fine gravel < 50% mSAL: clayey-silty medium Sand, medium sand > clay > silt
Sedimentary structure (outcrops, excavations, pits and cohesive sediments/rock cores from boreholes)	m: massive, c: clast-supported g: normal grading; i: inverse grading h: horizontal parallel lamination l: low-angle lamination (< 15°) and very thin lamination p: planar cross-lamination r: small scale (ripple) trough cross-lamination t: trough cross-lamination	vfSfG-t: very fine gravelly Sand with trough cross-lamination, very fine sand > 50%, fine gravel < 50% mSAL-l: clayey-silty medium Sand with planar, low-angle lamination, medium sand > clay > silt
Outcrop-borehole correlations		
Criteria	**Principles**	**Applications**
Lithostratigraphic	Lithological analogy; stratigraphic position; marker beds.	Identification, comparison and correlation of: litho-textural analogies between adjacent boreholes. Additional markers (colour of sediments, fossils, petrographic content).
Depositional	Abrupt textural contrast (coarse over fine contacts) = sudden change in depositional processes.	Picking of different rank unconformable boundaries vs. conformable ones. Fining, coarsening, thinning, thickening and stationary stacking patterns recognized above the different rank boundaries are compared and used to frame the ordered litho-textural variations through space (horizontally) and time (vertically).
Hierarchic	Individual sediment packages with specific stacking patterns mark the genetic units, bounded by corresponding-rank surfaces. High-rank surfaces cannot be crossed by low-rank ones. The stratigraphic boundaries and units must assume and preserve a consistent	The hierarchic grouping of genetic units originates the ordered ranking of the stratigraphic units, which are bounded by equivalent-rank surfaces (either conformable or unconformable). The cross-cut relations among hierarchic stratigraphic boundaries represent a cross-correlation tool to validate or discard a correlation line (2-D cross-sections) or surface (3-D model).

	hierarchic order through space.	
Geometrical	Dip of boundaries follows the regional dip of the stratigraphic units and is constrained to surface attitude of beds and to prolongation/projection of the exposed tectonic structures.	Stratigraphic boundaries are traced considering the NW-SE trending base level of the Po basin; their regional gradient is locally and/or interrupted in correspondence of folds/faults near the tectonic reliefs and at the most subsiding depocentres.
Genetic	Genetic meaning and rank attributed to the stratigraphic units rely on the knowledge of the geological/structural framework of the area.	Horizontal facies variations within high-rank units are interpreted as the result of the dynamics of differently sourced depositional systems (regressive marine to glacio-fluvial and alluvial), controlled by Quaternary climate changes and incremental tectonics.
Chronological	The relative chronologies established from surface data constrain the relationships between subsurface equivalent units in keeping with age determinations.	Chronological ordering of tectono-sedimentary events interpreted in the subsurface cannot contradict the surface relative chronology, until surface reconstruction is refused. Relative chronology is accepted only in agreement with age determinations from surface/borehole samples.

Size: 2 COLUMNS

Table 3. Sedimentary features of the Quaternary depositional units of the southern Po basin. A) Features of the High Rank stratigraphic units HRS0, HRS1, HRS2; B) Features of the High-Rank stratigraphic units HRS3, HRS4. Facies codes as in Table 2. Facies and litho-textural associations as in Figure 5. Surface features from outcrops: white table line fill; subsurface features from boreholes: grey table line fill. For simplicity, the subsurface litho-textural associations are labelled as "F", like the surface facies associations, addressing this distinction to the mentioned black/grey colour code. Composition of gravel-sized rock fragments: I-igneous; M-metamorphic; P-porphyrite; S-sedimentary. Suggested provenance areas: (A)-Central Alps nappes and subordinate Southern Alps basement; (SA)-Southern

Alps and subordinate Central Alps (-L: Lario amphitheatre sector, -V: Verbano amphitheatre sector); (W-SA)-western Southern Alps; (AP)-Apennines (for quantitative gravel composition: see Figure 4).

(A)

Stratigraphic unit						**Interpretation**		
High-rank	Intermediate-rank	*Lithozone*	**Facies/ lithotextural association**	**Description**	**Fossils and age constraints**	Process/Environment	Depositional system	**Figure**
HRS2			F7	ALS, A, LS, LA, P	Sandy gravels to sands organized into two, 10-to-30 m thick fining-upward sequences, capped by 5 m thick grey to dark grey clays. I + M >> S (A)	Pinus sylvestris/mugo, Pinus Haploxylon, Picea, Abies, rare Carya, sporadic Pterocarya, Cyperaceae, Thalictrum, Sparganium emersum, S.erectum type, Typha latifolia, Nymphaea, Nuphar, Myriophyllum verticillatum type (Rigato, 2007)	Overbank fines on floodplain	Distal braided, sand-dominated alluvial/ glaciofluvial systems	Fig. 7A, C, F
	IRS2.3		F10	SG, GS-S, cS		-	Gravel-sand bedform; channel fill		
			F7	AL, LS, LAS, ALS, A, P	Gravelly sands and medium sands forming a fining-upward sequence of	*Pinus sylvestris/mugo*, Betula, Sorbus, *Alnus glutinosa type*, very rare Carya,	Overbank fines on floodplain	Meandering alluvial with flood plain	Fig. 7A, C, E

				10 to 15 m of thickness, capped by 10 to 15 m of green to dark grey silty clays with peat layers. S + P > I + M (SA)	xerofite (Artemisia, Chenopodiaceae, Hippophaë)		s, distal correlative to glacio-fluvial systems.	
	IRS2.2	F8	GS-mS-LA		-	Sand bar; channel fill		
		F7	AL, LS, LAS, ALS, A, P	Gravelly sands to silty clays forming a fining-upward, 10 to 15 m-thick sequence, capped by grey silty clay, 5 to 15 m thick. East: I + M = S (A) and (W SA); West: I + M > S (A)		Overbank fines on floodplain		
	IRS2.1	F8	GS-mS-LA		-	Channel fill; sand bar; point bar		
	U2 - Early-Middle Pleistocene unconformity							
	IRS1.3	As in IRS1.2			-	As in IRS1.2	Meandering river systems in delta plain with flood plains and swamps	Fig. 7A, C
	IRS1.2	F7	AL, P, LfS, A	Green to dark grey clays to sandy clays. Common wood fragments	-	Overbank fines on floodplain; swamp		
		F8	SG-cS-fS-L, AL	Fining-upwards sequences, 10 to 30 m thick. I + M > S (A +/- AP?)	-	Channel fills and sand bars		
HRS1	**IRS1.1**	F4	AL, P, LfS, A	Grey to dark clays and clayey silt interbedded with fine-grained sands. Common wood fragments	*Ammonia tepida, Haynesina depressula, Cribroelphidium decipiens,* common mollusks (gastropods	Marine suspentional settling, low-energy flow currents	Lower delta front with brackish waters	Fig. 6B; Fig. 7A, D

					and shallow marine fossils	and bivalves), rare ostracods. On top, reworked foraminifera of Miocene age (Bini et al., 2016)			
			F 8	SG-cS-fS-L, AL, AG, P	Fining-upwards to stationary, gravelly to fine sand sequences, 30 m thick. I + M > S (A +/- AP?)		Channel-bar systems	Delta plain	
U1 - Intra-Calabrian unconformity									
			F 3	fS-l, vfSL-r, fS-r, fS-t, vfSL-h, LvfS-l	Cm-thick layers of fine-grained laminated sandstone with cross and horizontal bedding, fossil fragments	As in SCFb, with frequent cold-water species (Anfossi and Brambilla, 1980; Zuffetti, 2019)	Low flow current deposits; storm sand layers		
HRS0	**SCF SCF-sse**	*SCF c*	F 6	AL-l, Al-m, ALfS-l	Blue claystone and marly claystone interbedded with fine-grained sandstone/siltstone	Abundant *Globigerinoides elongatus, Orbulina universa, Orbulina suturalis, Globigerina falconensis, Globigerinoides ruber, Globigerina bulloides, Globigerina cariacoensis, Globorotalia aemiliana, Neogloboqu*	Offshore suspensional settling	Lower shoreface; offshore (cool waters)	Fig. 6

				adrina dutertrei, Neogloboquadrina pachyderma. Less common *Hyalinea baltica, Artica islandica,Spiroplectammina, Gyroidina, Frondicularia, Bulimina,* nodosarids (Zuffetti et al., 2018a; Anfossi and Brambilla, 1980)			
SCFb	F4	AL-h, ALS-h, fSL-l, vfSL-l	Crudely bedded to massive, blue to olive-green claystone, with intercalations of fine-grained laminated sandstone, commonly burrowed	Common to abundant *Cardium* in association with *Elphidium, Nonion, Cibicides, Ammonia, Trochammina, Hoeglundina, Bulimina, Brizalina, Textularia, Tritaxia, Rotalia, Osangularia, Oolina*, lagenidis, nodosarids. Rare *Globigerinoides elongatus, Globigerinoides ruber, Globigerina*	Suspensional settling; low-energy currents	Lagoon with brackish waters; prograding shoreface	Fig. 6
	F5	vfS-l, vfSL-r, fS-r, fS-t	Sharp-based bioclastic fine-grained sand- to siltstone beds with ripple bedding, occasionally bioturbated		Tempestites; low flow current deposits		

				bulloides , Globigerina falconensis. (Zuffetti et al., 2018a)			
		F 3	S, fGS, fSL	Fine-grained sandstone to fine gravelly sandstone, frequently organized in m-thick coarsening upward sequences		Prograding clastic shoreface	
		F 2	K-m, Cong/Ar-m	Lens-shaped massive organogenic limestone bodies with encrusting bryozoans, corals, and massive, poorly-sorted biocalcirudites/biocalcarenites	Coralline algae, bryozoans, coral and bivalve fragments (Anfossi and Brambilla, 1980)	Encrusting bryozoan and coral patches with bioclastic aprons	
	SCFa			Well-rounded, medium sorted and grain supported biocalcirudite/arenite alternating beds; massive grain supported hybrid conglomerates. Recurrent borings on gravel clasts. S + M + P + I (AP), recycled from (A), (SA)	Fragments of mollusks, brachiopods, echinoids, bryozoans, foraminifera and ostracods (Anfossi and Brambilla, 1980 with references)		Beach; shoreface (warm waters)	Fig. 6
		F 1	Cong, Cong/Ar, G-m, GS-l			High-density flows; bedload deposits	

GU - Gelasian Unconformity

(B)

Stratigraphic unit						Interpretation		
High-rank	Intermediate-rank	*Litho zone*	**Facies/lithotextural association**	**Description**	**Fossils and age constraints**	Process/Environment	Depositional system	**Figure**
HRS 4	**POS**		vfS-l, S-m, LfS/mcS-h, mcS/fG-h, Ah, LSA-l, fSL-l	Stratified sand to gravelly sand deposits forming dm-thick fining-upwards sequences, locally interbedded with laminated silt. S > M + I (SA), sometimes mixed from recycling of underlying deposits. Paleocurrents to SSW-SSE, E, NW-N	Rare fossils, recycled from SCF	Sand bar, channel fill, overbank fines, crevasse splay, minor sediment gravity-flow	Meandering alluvial system	Fig. 8D
	U4 - Latest Pleistocene-Holocene unconformity							

HRS 3	**PSS**	F8	vfSL, SfG-p, fGcS-p, S-p, S-t, fS-r	Stratified sand to gravelly sand deposits forming fining-upwards sequences, locally interbedded with laminated silt. NW abandoned river traces: P > S > M > I (SA-V) and (W-SA). NE abandoned river traces: increased S and minor P (SA-L). S abandoned river traces: paleo-Po alluvial system.	-	Lateral accretion bars, channel fills	Meandering alluvial system	Fig. 10 A, E

		F7	LAS-l, ALS-m, P	Paleocurrents to SSE and SE Mudstone with peat and fine sand; cm-thick layers with ripple cross-stratification	-	Overbank fines, levee		
INS INS-sse	*INSd*	F12	SL-l, SLfG-l, LS-l, LSA-l	Thinly bedded heterometric sediments, interbedded with loose, non-stratified heterogeneous mixtures; colluvial soils. Mixed gravel composition.	-	Colluvial wedge	Base of hillslope; terrace slope aprons	Fig. 8C
	INSc	F7	fS-l, vfSLA, vfSA	Crudely bedded to massive sandy silt. Wood fragme	-	Overbank fines on floodplain	Distal braided, sand-dominated alluvial system	Fig. 8C, D, E; Fig. 9G

			nts. Planar and trough cross-bedded gravelly sands and medium sands forming m-thick fining-upward and stationary sequences. S > P > I and M (SA). Paleocurrents to S and SE			s	
	F10	cS-p, GfmS-t, cS-p, GcS-p, fmS-t, SG-t		-	Sand and gravel bedform, channel-fill; alluvial, point bar and chute bar		
INSb	F13	f-cSL-p, StGL-p, mS-t fmS/L-h, LAS-m	Laminated to massive silty layers developed on top of sandy bedsets, containing continental molluscs, wood fragments, abundant	*Valvata piscinalis, Planorbis planorbis, Anisus spirorbis, Aplexa hypnorum, Bithynia tentaculate, Pisidium casertanum,* ostracods (Contini, 2018; Zuffetti, 2019)	Crevasse splay, oxbow lake	Fluvial floodplain	Fig. 8D; Fig. 10D
	F7	ALS-h, P, LS-h, LSA-m			Overbank fines on floodplain		

			calcareous nodules and carbonate-cemented layers. S > M and I (SA). Paleocurrents to S and SW				
INSa	F7	LAfS-m, fSL-m	Massive silt and sandy silt with cm-thick, very fine sand interbeddings	-	Levee, overbank fines on floodplain	Mixed-load meandering alluvial systems	Fig. 8D, E; Fig. 9F; Fig. 10A
	F8	mfS-l, LS-l, SLA-l, mcS-t, fS-l, cSfG-t	Dm-thick beds of sand (rare gravel) with trough cross-stratification and low-angle lamination, bounded by concave-up erosion	-	Lateral accreted bedforms, channel-fills		

			al surfaces. P and S > M > I (SA-V) and (W-SA). Paleocurrents to SE				
	CPS 2c	F7	A, AL, ALS, ASL	Green clay and silty clay layers, 5 to 20 m-thick Sandy gravels organized into decametric-thick fining-upward sequences	-	Overbank fines on floodplain	Meandering alluvial systems with floodplains; distal braided, sand-dominated systems	Fig. 8D; Fig. 8E; Fig. 8G
		F8	fGS, SG, cS, mS, S, SL, LSA		-	Sand/gravel bedform, channel-fill; alluvial, point bar and chute bar		
CPS2 CPS2-sse		F[illegible]	fS-m, SL-m, ALS	Massive mud layers of cm thickness	-	Overbank fines on floodplain	Distal braided, sand-dominated alluvial systems	Fig. 8B, D; Fig. 8E; Fig. 8G
	CPS 2b	F9	cS-l, (fG)mcS-t	Crudely stratified and amalgamaed beds of coarse- to fine-grained sand, bounded by	-	Sand bedform; channel fill; sheet, point bar and chute bar		

			low-angle erosional surfaces and, organized into m-thick stationary, rarely fining-upward sequences. I + M > S. Paleocurrents to S and SE				
	F10	GS, SG, mS, SL, S L	Gravelly sands and medium sands terminating decametric-thick stationary sequences with rare mud interbeddings. I + M > S	-	Gravel and sand bedform; channel fill; sheet bar		
CPS 2a	F11	mSG-t, mS-t, GS-m, LAS-m	At SCS: lens-shaped, graded, stratified and massiv	-	Channel fill; sediment gravity flow	Small-scale entrenched valley fill	Fig. 8A

				e deposits in fining-upwards gravelly to silty sequences. Colluvial soils. I > S > M > P (recycling from underlying units). Higly variable paleocurrents				
		F7	LfS-m, ALS-m	Laminated to massive clay-silt bedsets	-	Overbank fines on floodplain; crevasse splay		
CPS1 CPS1-sse	*CPS 1b*	F9	mcS(fG)-t, mS-t, mfS-l, mcS, mS-l	Vertically-stacked, stationary to fining-upwards sequences of cross-bedded sands with thin (cm-thick) gravel or mud	-	Sand bedform; channel fills and bars	Sandy, bedload dominated alluvial systems	Fig. 8A, B; Fig. 8F; Fig. 9E

			interbeddings. At SCS: vertically-stacked co-sets of S-t forming sigmoidal dunes; soft sediment deformation structures. M > I = P > S (SA-V). Paleocurrents to SE					
CPS 1a	F8	cfS-t, mS-t, mSfG-t, cSfG-t, mfS-t, mS-r mS-p, mS-h, fS-h, mfSL	fining-upwards sequences of cross-bedded gravelly sands to sands, bounded by concave-up erosional surfaces. Inclined boundaries	-	Sand bedform; lateral accretion units and channell-fill	Meandering alluvial systems with floodplains	Fig. 8A, B; Fig. 8F; Fig. 9A, B, C	

		between bedsets. M > I > P > S (A). Paleocurrents to NE and E at the SCS Tabular bedsets of fine-grained clayey sands, massive to poorly horizontal-laminated, interbedded with silty-clays and cm-thick massive sands. Abundant wood fragments		
F7	LS, ALS-l, fmSLA, LfS-h, fmS-m, P		-	Overbank fines of floodplain; crevasse splay

U3 - Middle-Late Pleistocene unconformity

Size: FULL PAGE (landscape orientation)

Table 4. The hierarchic constraints implemented for 3D modelling with GeoModeller®. *Italic* font type for proper GeoModeller® terms.

	Stratigraphic assumption	**Modelling solution (3DGeoModeller)**

Hierarchic rule 1	High-rank geological boundaries cross-cut each other but are never crossed by low-rank ones	Set *erosional bottom* boundary to the high-rank *series*
	Intermediate-rank boundaries cross-cut each other merging into high-rank unconformities	Invert the stacking ordering of the intermediate-rank units in the *stratigraphic pile* and set *onlap* relation of their *bottom* boundaries that will be drawn with *reverse polarity*
Hierarchic rule 2	Intermediate-rank bottom boundaries result from each evolution increment	Set *erode bottom* boundary to the intermediate-rank boundaries
	At each increment, deposition occurs above the top boundary of a unit whose geometry is determined by the previous geological increments	Set the *top* reference surface of each unit and draw in agreement with the low-rank geometries reconstructed in 2-D. *Onlap* rules allow to confine the modelled potential field within each intermediate-rank unit. Hence, a subsequent erode increment will truncate the predating geometries

Size: 2 COLUMNS

Declaration of competing interests

☒ The authors declare that they have no known competing financial interests or personal relationships that could have appeared to influence the work reported in this paper.

☐The authors declare the following financial interests/personal relationships which may be considered as potential competing interests:

HIGHLIGHTS

- 4-D hierarchical model of the Quaternary fill of the southern Po foreland basin
- Composite, high-rank, progressive unconformities bound diachronous units
- Foreland buttress induced Late Quaternary, synsedimentary out-of-sequence thrusting
- Blind and out-of-sequence thrusting controlled the highest-rank stratigraphic units
- Glacial cycles controlled the deposition of intermediate- to low-rank continental units

Figure 1

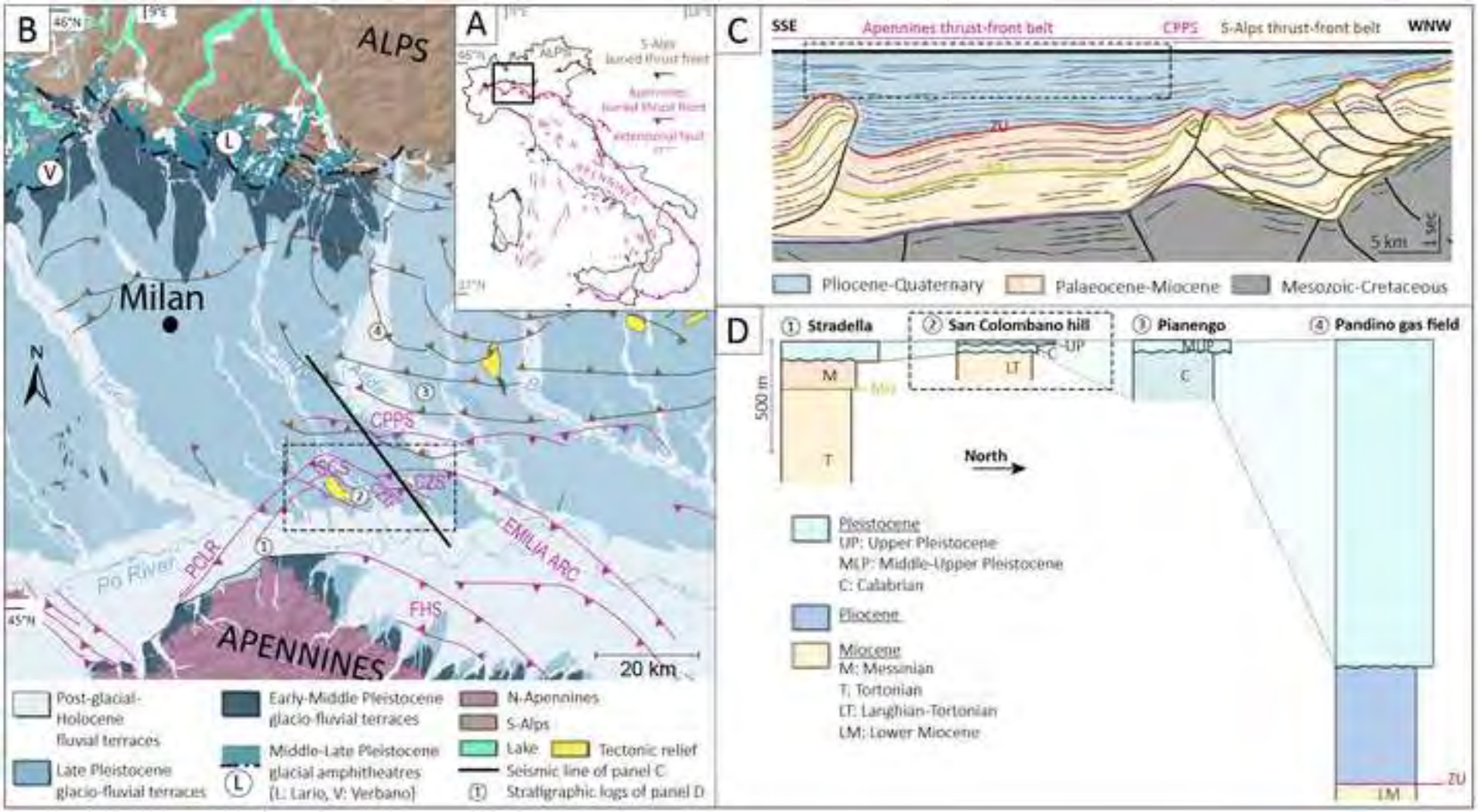

Figure 2

Click here to access/download;Figure;REV_Fig_2.jpg

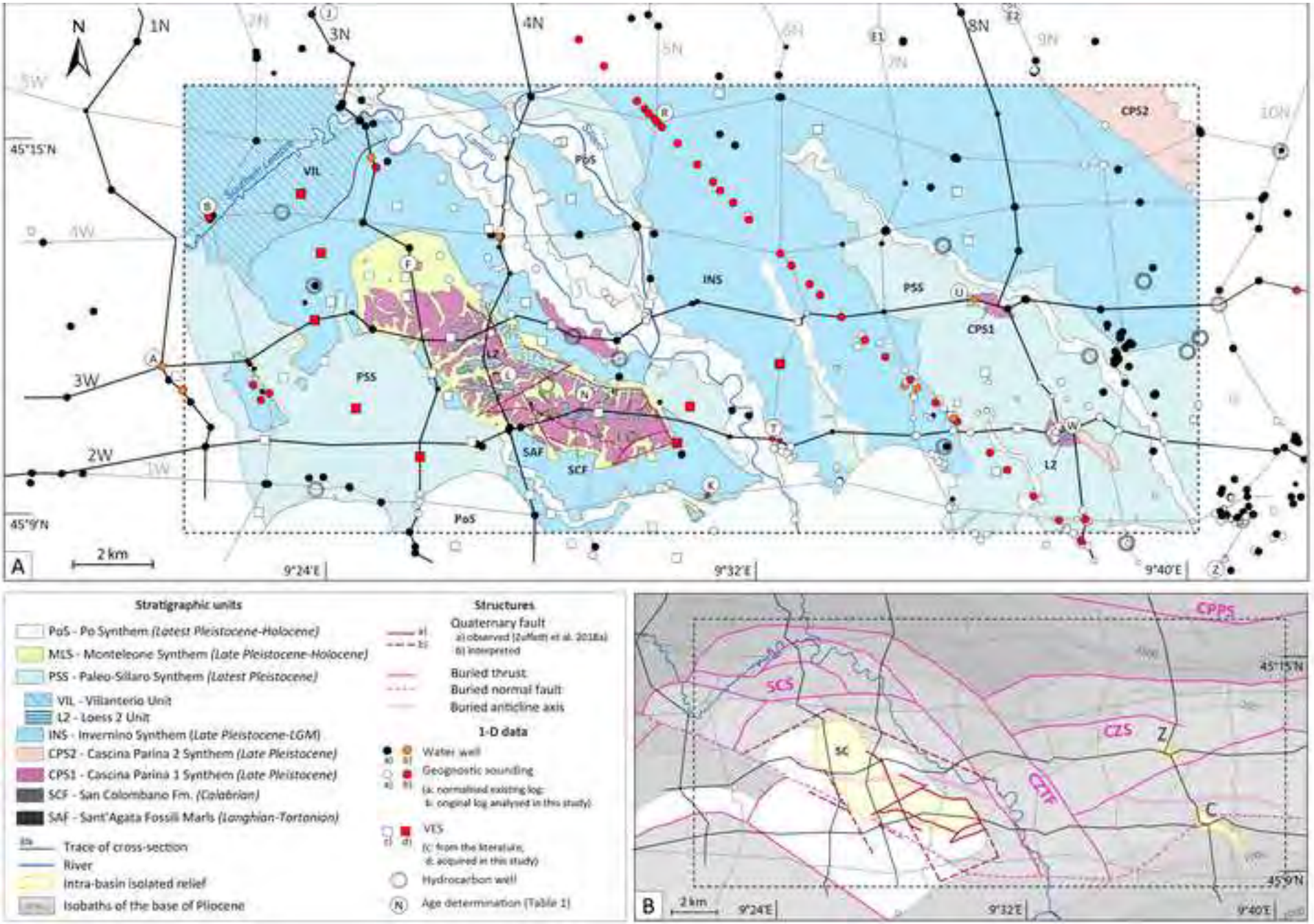

Figure 3

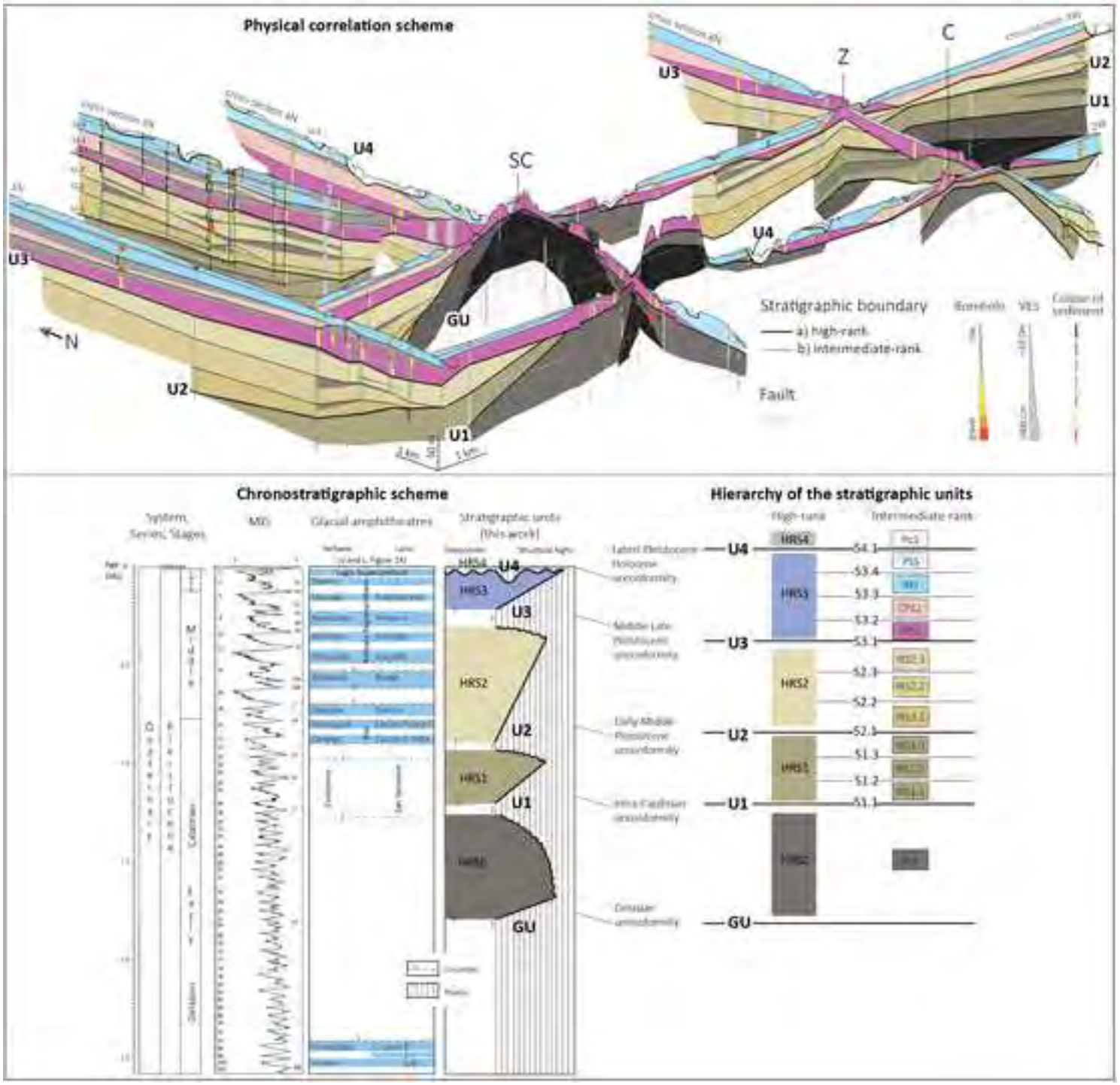

Figure 4

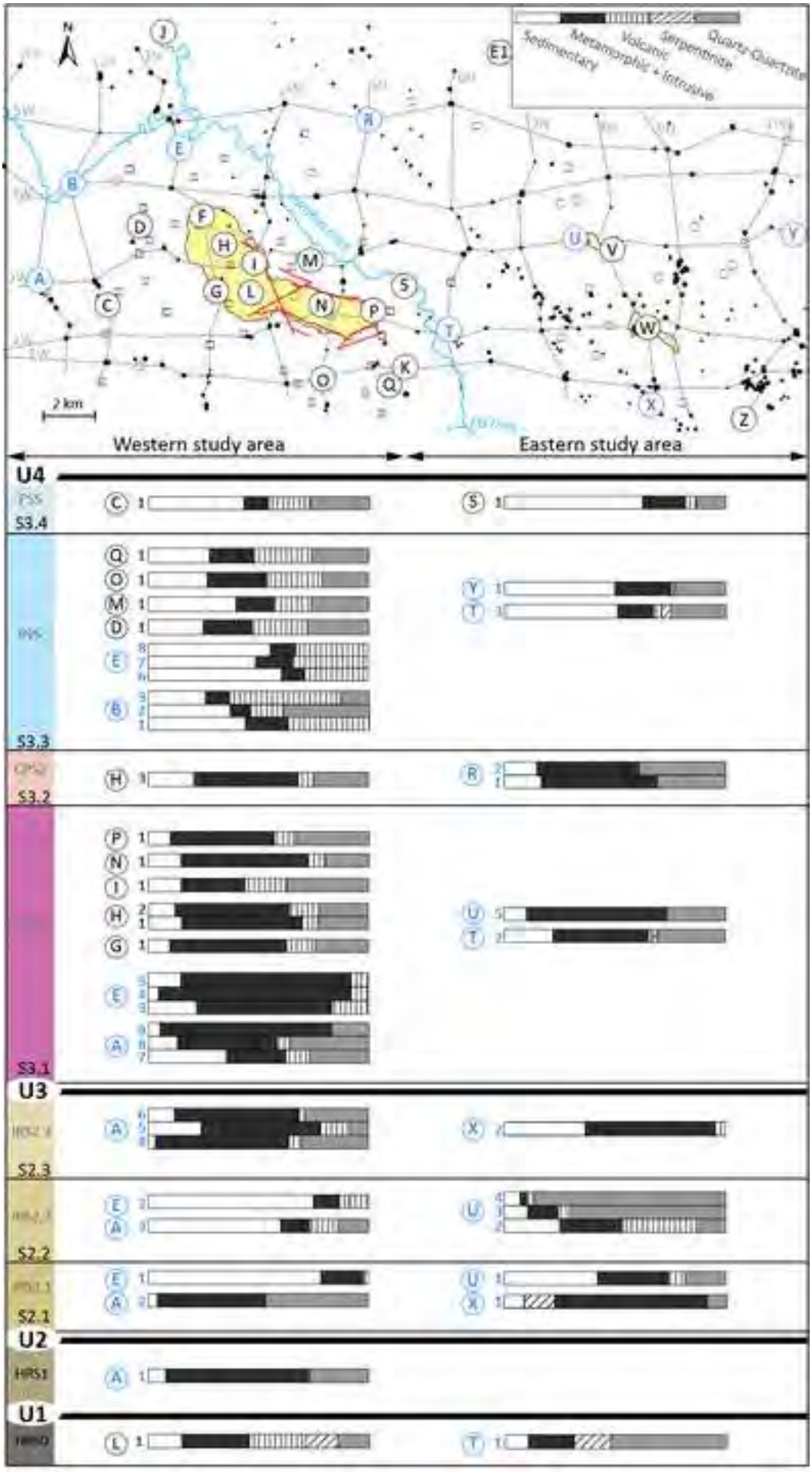

Figure 5

Click here to access/download;Figure;REV_Fig5-01.jpg

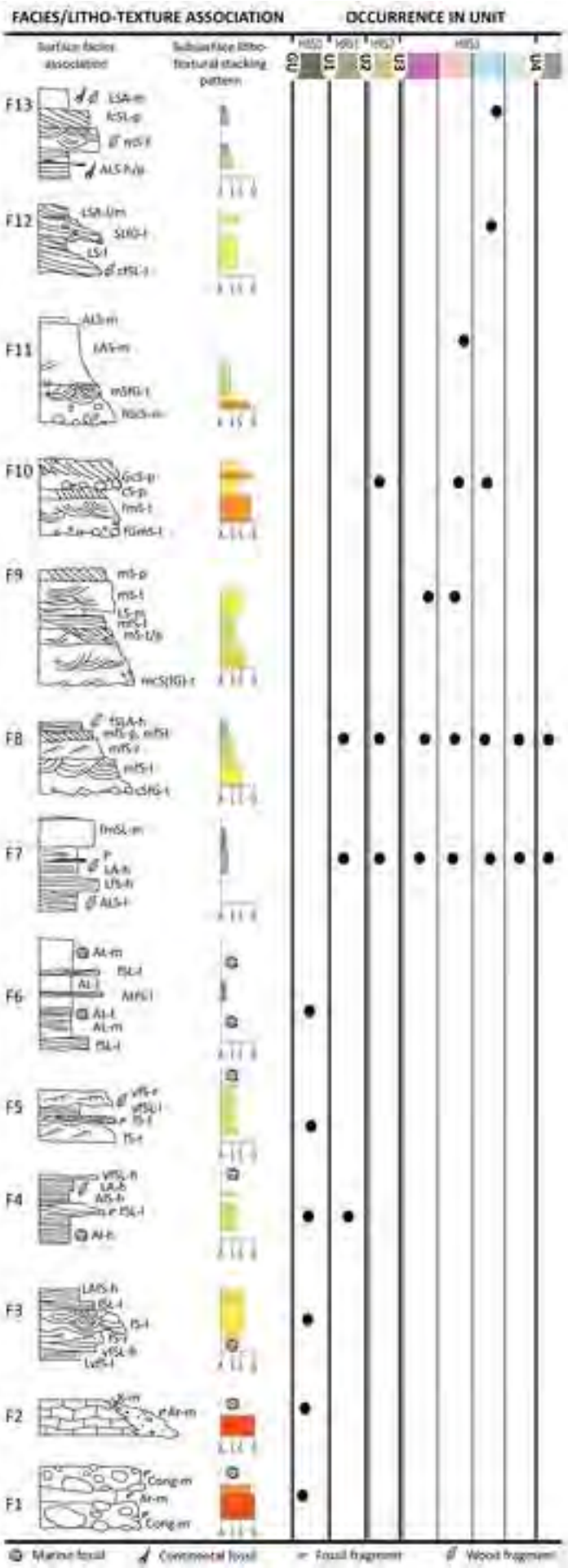

Figure 6

Click here to access/download;Figure;REV_Fig6-05.jpg

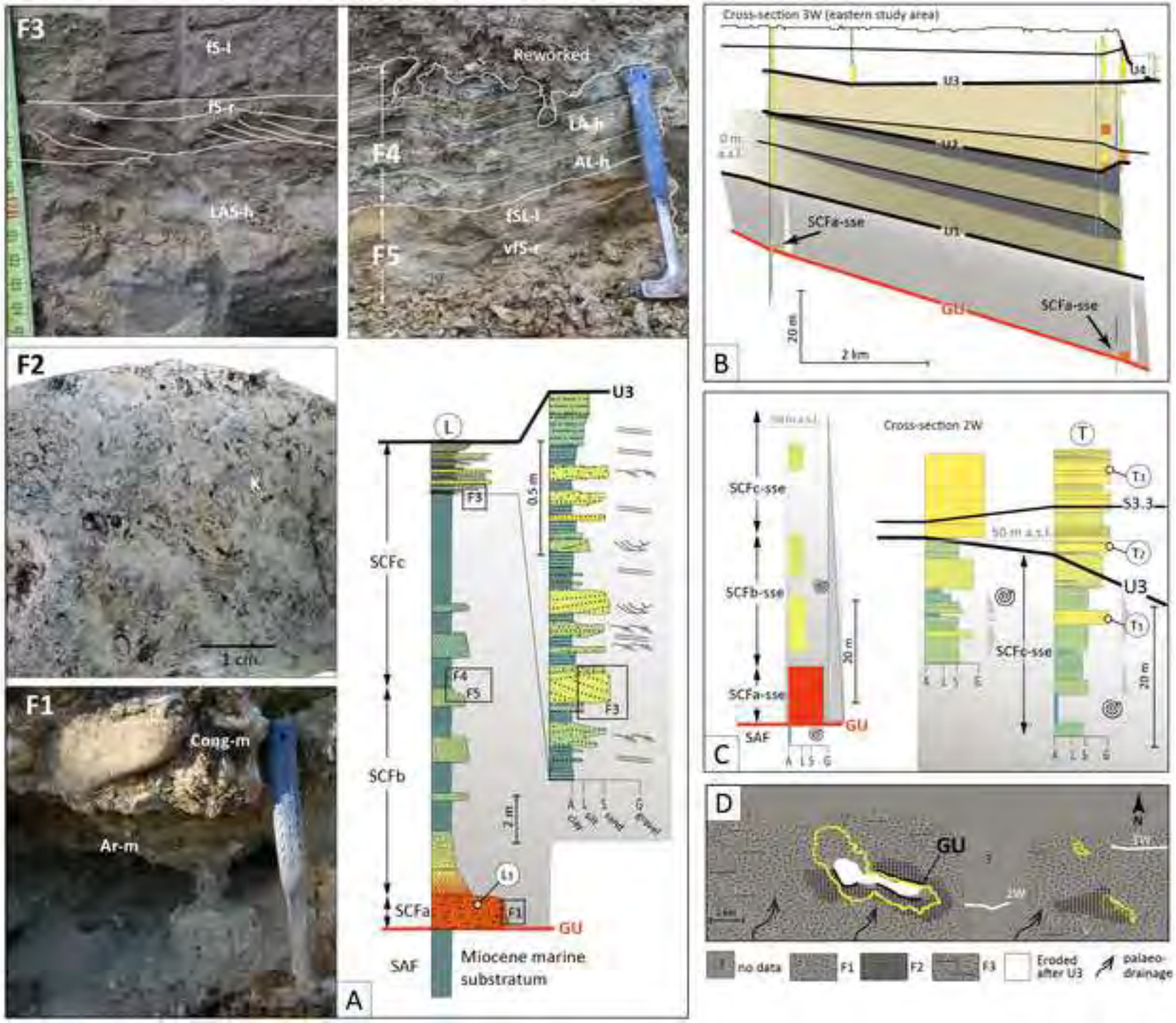

Figure 7

Click here to access/download;Figure;REV_Fig7-01.jpg

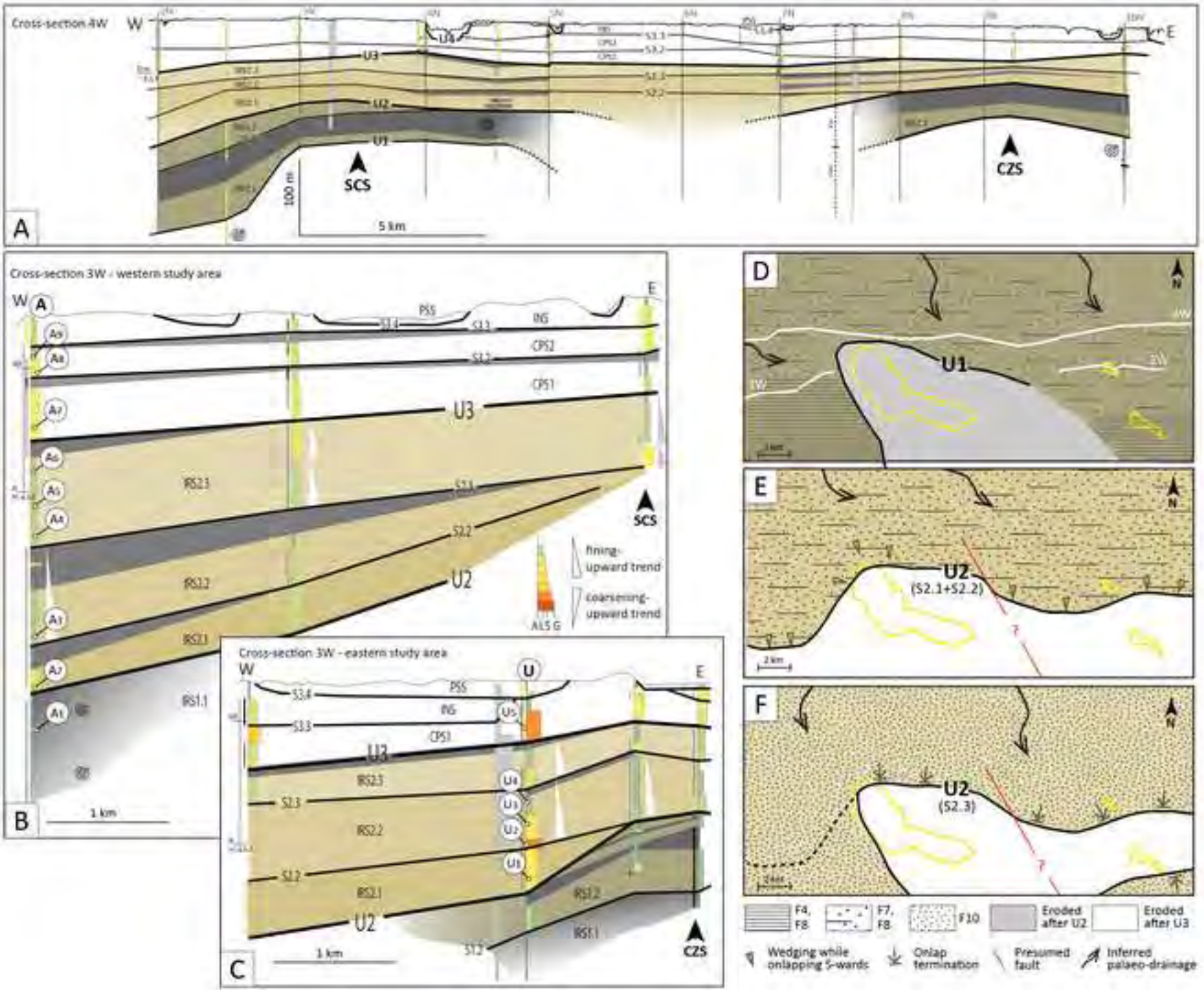

Figure 8

Click here to access/download;Figure;REV_Fig8-01.jpg

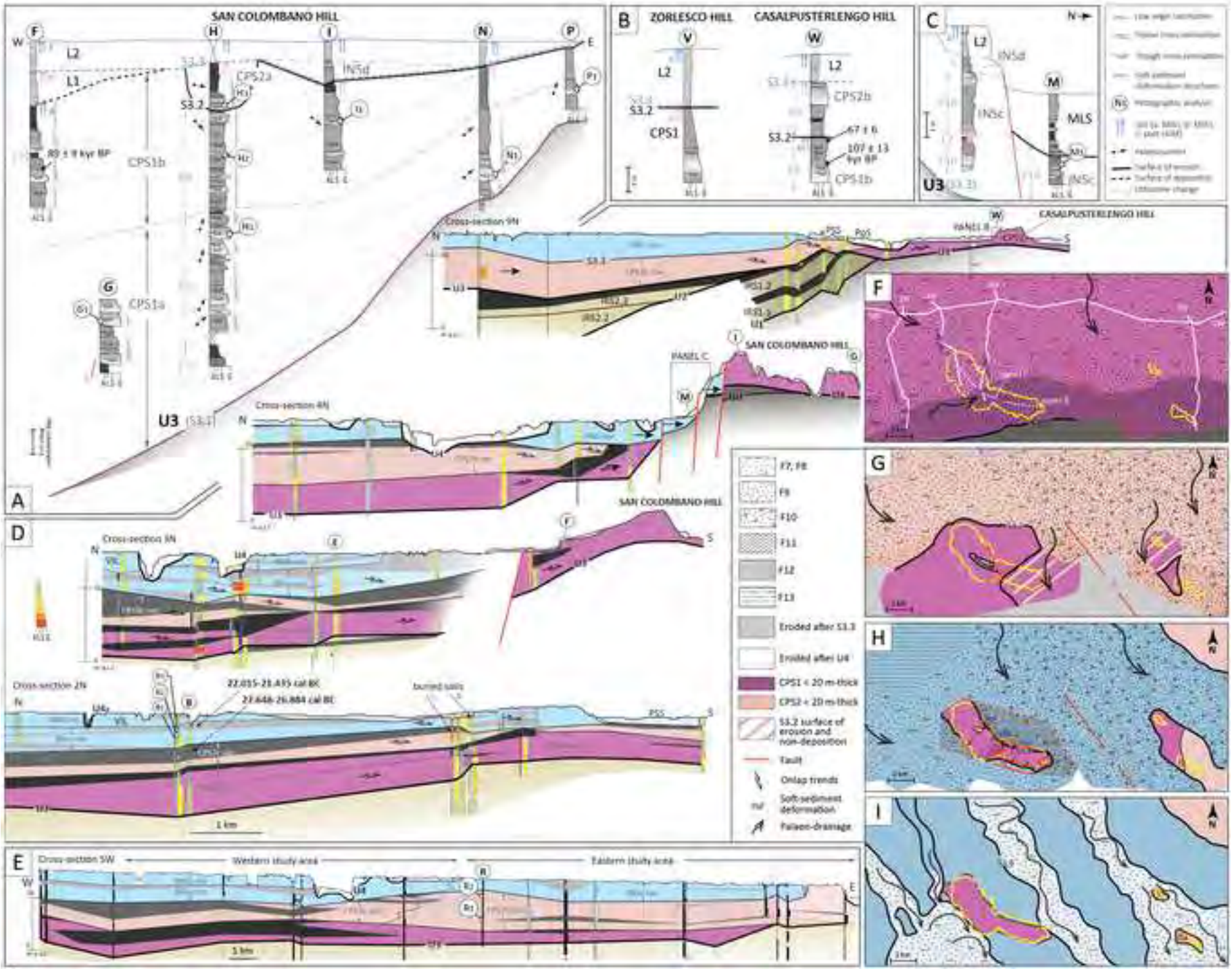

Figure 9

Click here to access/download;Figure;rev_Fig9_Rev-01.jpg

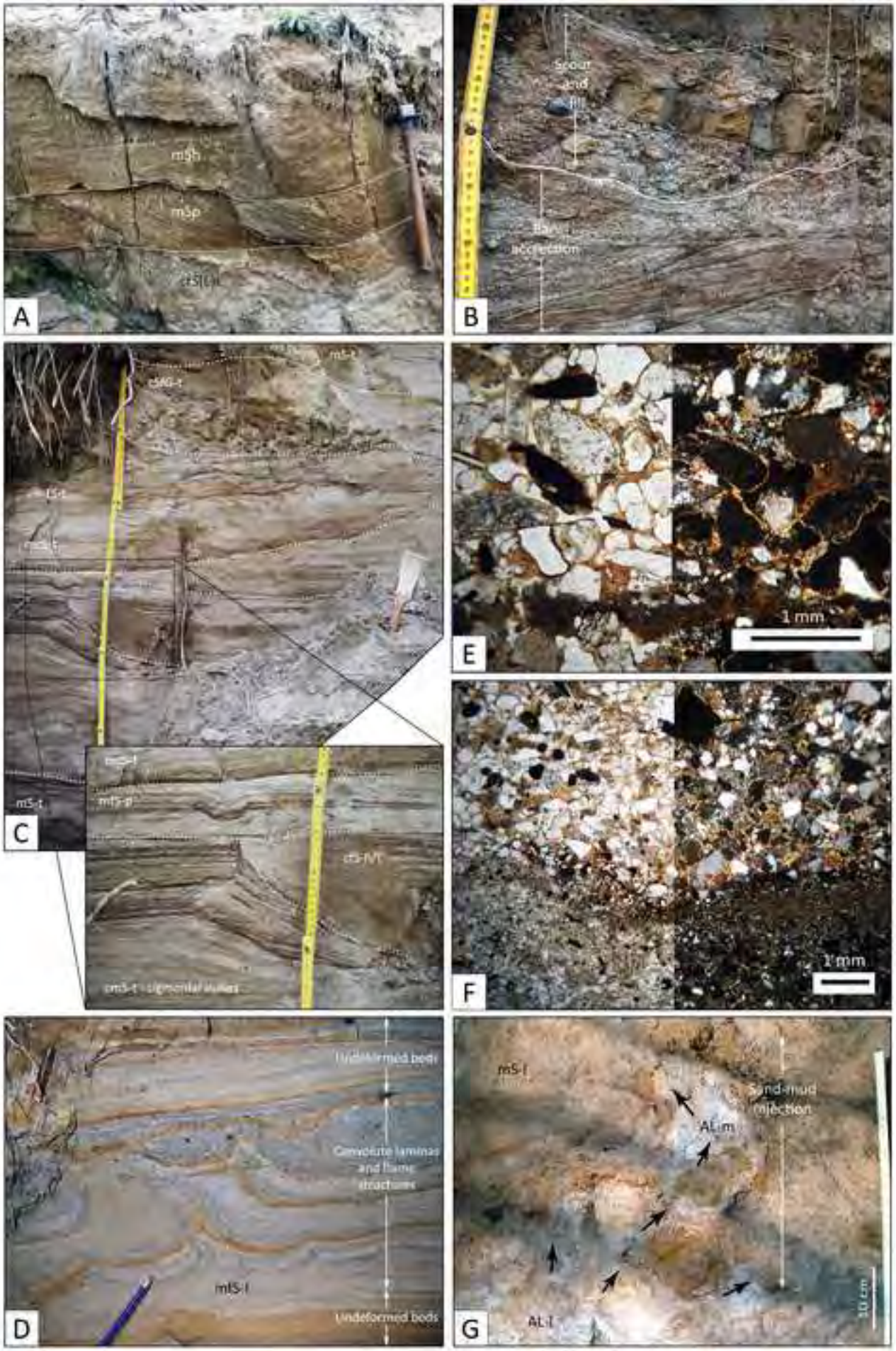

Figure 10

Click here to access/download;Figure;rev_Fig10_Rev.jpg

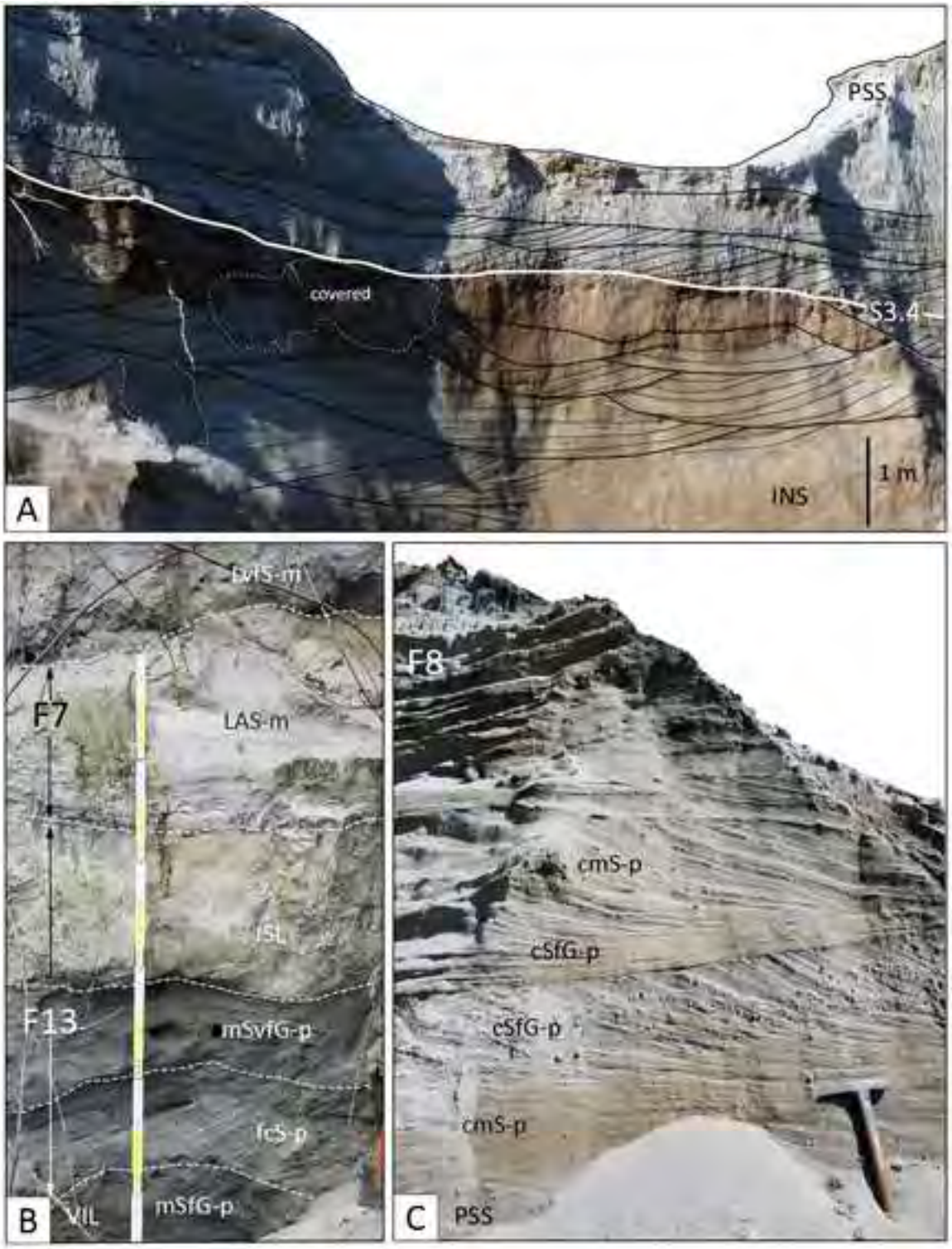

Figure 11

Click here to access/download;Figure;REV_Fig11-01.jpg

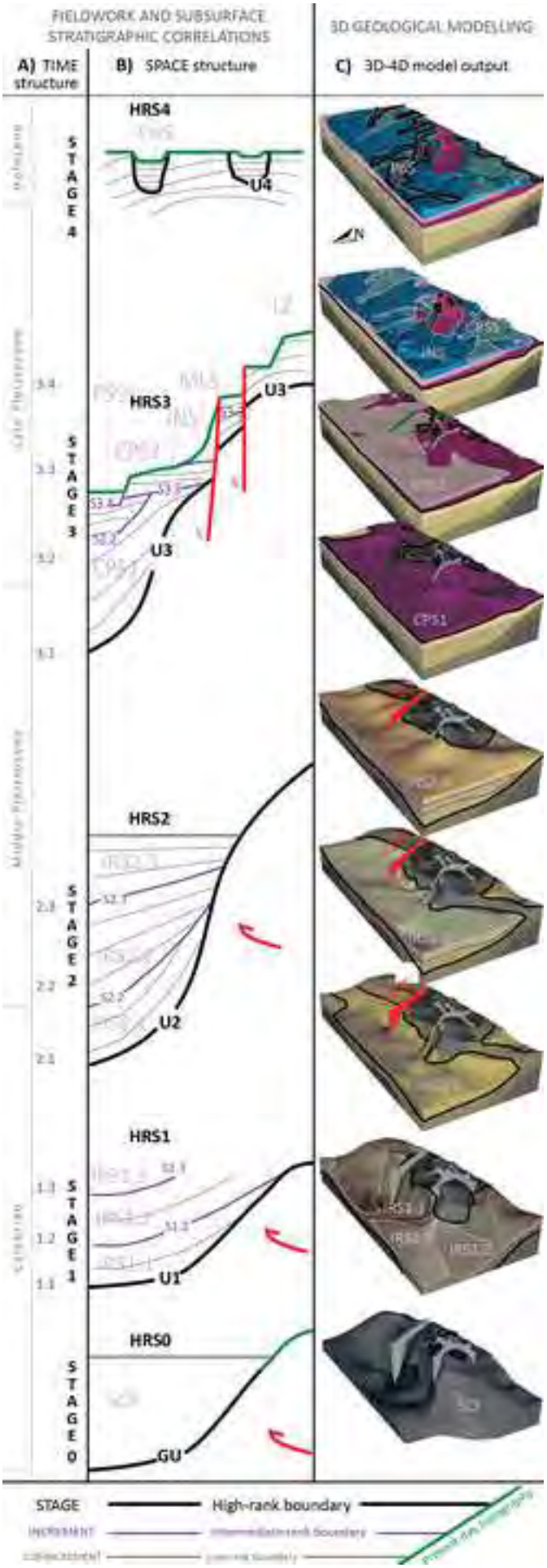

Figure 12

Click here to access/download;Figure;REV_Fig12-03.jpg

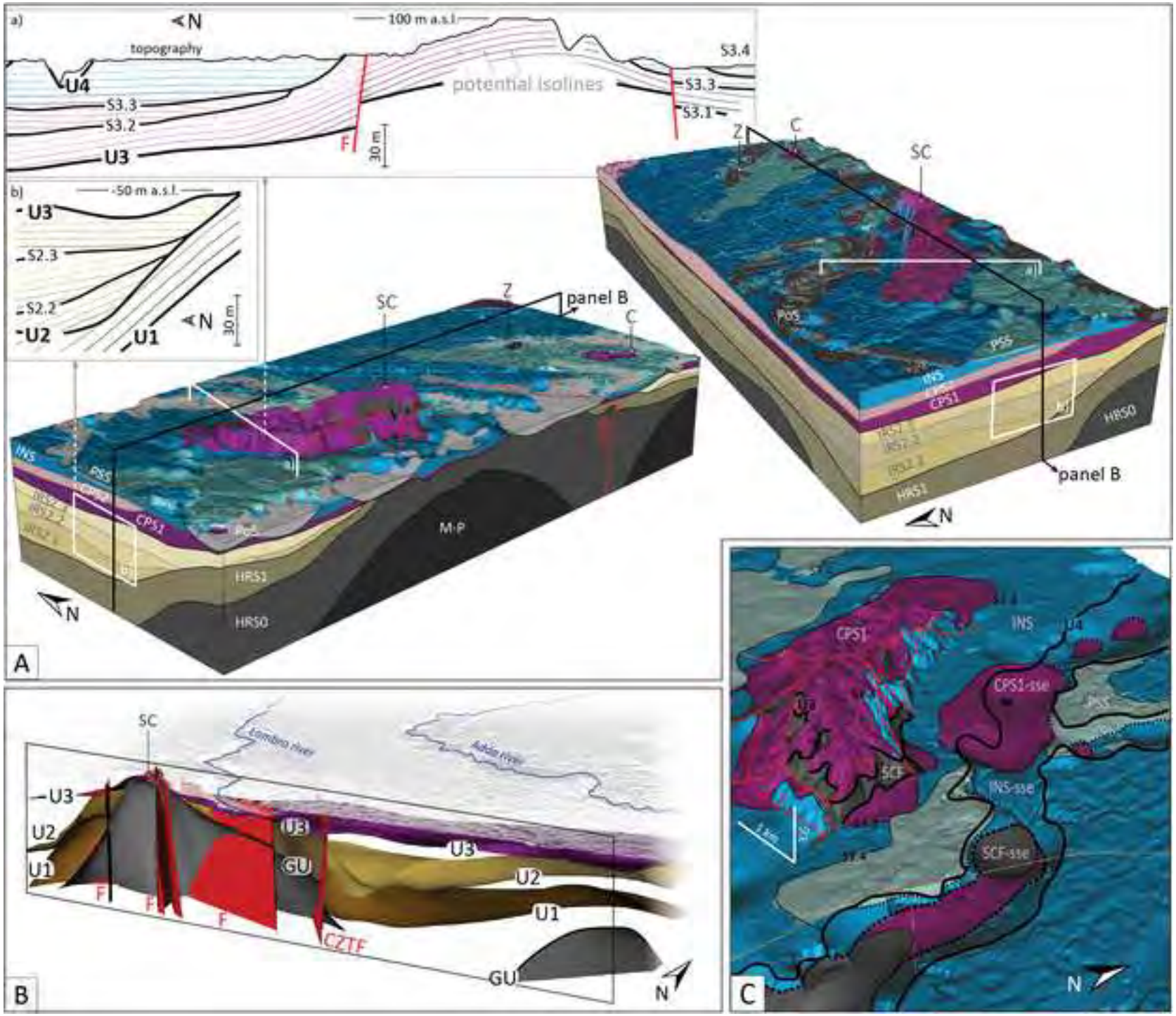

APPENDIX A - Supplementary data

Chiara Zuffetti*, Riccardo Bersezio

Dipartimento di Scienze della Terra, Università degli Studi di Milano, via Mangiagalli 34, 20133 I-Milano, Italy

**Corresponding Author. Authors e-mail: Chiara Zuffetti: chiara.zuffetti@unimi.it (OrcID 0000-0002-7391-4829); Riccardo Bersezio: riccardo.bersezio@unimi.it (OrcID 0000-0002-6629-8917).*

This supplementary material contains the sedimentological description of the five stratigraphic units that has been cut from the original main text of the paper "Space-time geological model of the Quaternary syntectonic fill of a foreland basin (Po basin, Northern Italy)" on request of the Editor. The document completes the information contained within the **Section 4 of the manuscript**. The interested Reader is addressed to this material following the citations in the main text of the paper.

4. Surface and subsurface geological architecture and evolution: constraints to the quantitative model

4.1. Gelasian Unconformity (GU) – Early Pleistocene High-Rank Stratigraphic Unit 0 (HRS0)

4.1.1. Lithozones and facies associations

In outcrops, the San Colombano Formation comprises six facies associations (facies F1 to F6; Fig. 5) organised into three lithozones (SCFa, SCFb, SCFc) (Fig. 6A; Table 3A). **Lithozone SCFa** lies above the Gelasian Unconformity, and is composed at the base of metre-thick bedded biocalcarenites and hybrid, poorly sorted conglomerates (facies F1), (Figs. 5, 6A;, Table 3A) hosting reworked Miocene fossils (Anfossi and Brambilla, 1980). Locally, these beds are replaced by lens-shaped dm- to m-thick bodies of massive organogenic limestones (framestones with encrusting bryozoans and coralline algae) associated to with massive biocalcarenites-rudites with abundant fossil fragments (facies F2) (Figs. 5, 6A; Table 3A) (Zuffetti et al., 2018a). The sharp and unconformable base of the coarse-grained layers of lithozone SCFa permits to trace the Gelasian Unconformity to the close subsurface (Fig. 6B, C) into the sharp rest of gravel, conglomerate and sandstone layers of metric to decametric thickness above mud with very fine-grained sand layers. Both thickness and grain-size of the coarse-grained layers decrease progressively away from the crests of the San Colombano and Casalpusterlengo-Zorlesco folds, where conglomerates (F1) are laterally replaced by the lithotextural subsurface association F3 (Figs. 5, 6; Table 3A). It is represented by fine-grained sandstone to fine gravelly sandstone organized organised in m-thick fining to coarsening upward sequences, less than 10 m-thick, hosting reworked Miocene fossils (Bini et al., 2016). Gravel-sized clasts of facies F1 are high-grade metamorphic rocks,

serpentinites, porphyrites, Verrucano Lombardo-like sandstones, cherty limestones and dolostones (sample 'L1' in Figs. 4, 6A) (Zuffetti, 2019). A comparable composition characterises the gravel-sized samples of facies F3 in the correlative subsurface lithozone (Bini et al., 2016).

Facies interpretation. The association of F1 and F2 in outcrops suggests deposition of Lithozone SCFa in a gravel-sand beach/shoreface setting, where isolated patches of encrusting colonial organisms, typical of warm climates and shallow bathymetry, could develop on the raised crests of the pre-Gelasian folds at San Colombano and Casalpusterlengo-Zorlesco structures. The transition to a sandy, prograding shoreface away from these settings, is suggested by the location of the subsurface F3 litho-textural association and stacking patterns (Figs. 5, 6; Table 3A). Gravel composition suggests recycling of Alpine-derived clasts after erosion of the Oligo-Miocene clastic formations of the N-Apennine front (Vercesi and Scagni, 1984; Zuffetti et al., 2018a) and supports river input from the southern basin margin.

Lithozone SCFb lies above SCFa at the San Colombano hill (Fig. 6A; Table 3A). It comprises alternations of: i) crudely bedded to massive, burrowed, blue to olive-green claystone, hosting *Cardium*, common benthic foraminifera, very rare planktonic and common wood fragments, with cm-thick, very fine sand intercalations (facies F4; Figs. 5, 6A; Table 3A). The benthic foraminifera association is a mix of the infralittoral Elphididae, Nonionidae, Rotalidae and Miliolidae, with some brackish/lagoonal species of *Elphidium* and *Ammonia* and the circalittoral Buliminidae and Brizalinidae (Table 3A); ii) cm-thick, sharp-based beds of fine-grained, cross-stratified bioclastic sandstones and stratified silty sands, locally bioturbated, organized into dm-thick fining-upward sequences (facies F5; Fig. 5; Table 3A). Comparable litho-textural associations and vertical stacking occur in the near subsurface above and adjacent to the subsurface lithozone equivalent to SCFa. The SCFb subsurface equivalent lithozone consists of blue and dark grey fossiliferous claystones and marlstones, which alternate with 5 to 10 m-thick sandy bedsets occasionally forming fining-upward sequences (Fig. 6C; Table 3A).

Facies interpretation. F4 facies assemblage suggests a low-energy marine environment, dominated by clastic suspension settling punctuated by very fine sandy layers. F5 facies points to short-time, higher-energy siliciclastic input, recurrently mixed with displaced biota. The abundance of *Cardium* accompanied by an oligotypic benthic foraminifera association (Table 3A) suggests a brackish, coastal lagoon environment, probably associated with freshwater river discharge. This agrees with previous interpretations (Anfossi et al., 1971; Anfossi and Brambilla, 1980). Mixing of infralittoral and circalittoral foraminifera with the lagoonal taxa and with siliciclasts suggests recurrent input from high-energy events like storms and river surges from the mainland.

Lithozone SCFc covers and juxtaposes to the SCFb beds in outcrops (Fig. 6A). It consists of thick, crudely bedded to massive, fossiliferous blue clays and marly clays with cm-thick sand interbeds (facies F6) (Fig. 5; Table 3A). The mudstones contain abundant planktonic foraminifera in association with cold-water benthic foraminifera and bivalves (the well-known "northern guests" *Hyalinea balthica* and *Artica islandica*;, Table 3A). Cm- to dm-thick layers of cross-stratified, fine-grained sands passing upwards to plane stratified silty sands with fossil fragments get abundant and thicken upwards (facies F3) (Figs. 5, 6A; Table 3A). The F6-F3 facies association of lithozone SCFc correlates with dam-thick, grey fossiliferous clays in the subsurface, with 5-10 m-thick sandy layers at the top (SCFc-subsurface equivalent lithozone) (Fig. 6C).

Facies interpretation. The F6 mudstones with abundant planktonic foraminifera were likely deposited by settling and low-energy currents in an offshore setting, passing upwards to a lower shoreface environment with low flow-laminated fine-grained sands (F3). The common occurrence of cold-water taxa reflects the onset of environmental cooling.

4.2. Intra-Calabrian Unconformity (U1) – Calabrian High-Rank Stratigraphic Unit 1 (HRS1)

4.2.1. Facies associations

The High-Rank Stratigraphic Unit 1 encompasses three litho-textural subsurface associations, namely F4, F7, F8 (Figs. 4, 5; Table 3A), forming three Intermediate-Rank Stratigraphic Units. The lowermost **Intermediate-Rank Stratigraphic Unit 1.1** starts with coarse sands, locally gravelly sands, passing upwards to clay-silt associations organised into fining-upwards or stationary stacking patterns reaching a maximum thickness of about 30 m (F8 litho-textural association) (Fig. 5, 7, Table 3A). Atop, a 30 m-thick unit of dark grey-blue clays to silty clays, occasionally gravelly clays, can be traced with continuity over distances of several km (Fig. 7A). These sediments commonly contain dark organic-rich clay levels with plant fragments (F7 litho-textural association) (Table 3A); only in the southern study area, an oligotypic shallow marine fossil assemblage and reworked fragments of microfossils of Miocene age could be described from the only available borehole samples of these clays (Bini et al., 2016) (F4 litho-textural subsurface association) (Figs. 5, 7B, C; Table 3A). The petrographic composition of the rare gravel beds is dominated by metamorphic plus intrusive (*sensu lato*) and serpentinite rock fragments (Fig. 4, 'A1'in Fig. 7B) with subordinate limestones, suggesting provenance from the basement and cover of the Western-Central Alpine nappes and of the Western Southern Alps.

Facies interpretation. The superposition of F7-F4 over F8 litho-textural associations build the Intermediate-Rank Stratigraphic Unit 1.1, whose basal F8 coarse-grained association and stacking patterns suggest the progradation of mixed-load alluvial systems above the High-Rank Stratigraphic Unit 0, slightly

eroded at U1, in an alluvial plain-delta plain setting (Table 3A). The widespread diffusion of F7-F4 assemblage points to the spreading of a floodplain then to a palustrine and brackish lagoon environment (Fig. 7D), during a transgressive stage. This is supported by the association of benthic foraminifera like *Ammonia tepida*, *Haynesina depressula* and *Cribroelphidium decipiens* with ostracods and rare molluscs, that are typical of restricted and brackish environments with high mud input (Murray, 2006), and fits with the palaeoenvironmental interpretation of Bini et al. (2016) who suggested deepening towards a shallow marine environment for the equivalent sediments in the studied boreholes.

The **Intermediate-Rank Stratigraphic Units 1.2** and **1.3**, above S1.2 and S1.3 respectively, are formed by gravelly sands and coarse sand intervals passing to mud-fine sand layers, building 10 to 30 m-thick fining-upward sequences (F8 subsurface litho-textural association) (Fig. 7C; Table 3A). These units are replaced by laterally continuous, up to 20 m-thick intervals of grey to black clays and silty clays with wood fragments (F7 litho-textural association) but without marine fossils, that are here interpreted as flood-plain/swamp sediments (Table 3A).

Facies interpretation. The superposition of subsurface litho-textural association F7 over F8 supports the interpretation of two intermediate-rank phases of progradation and transgression of sandy, mixed load alluvial systems in a possible delta plain setting.

4.3. Early-Middle Pleistocene Unconformity (U2) – Calabrian (?) – Middle Pleistocene High-Rank Stratigraphic Unit 2 (HRS2)

4.3.1. Facies associations

The **Intermediate-Rank Stratigraphic Unit 2.1** is composed of gravelly sands to medium sand layers and of sand-silt alternations organised into 10 to 15 m-thick fining-upwards sequences of F8 and F7 litho-textural associations (Figs. 4, 5, 6B, 7; Table 3A). Gravels are characterised by dominant intrusive and metamorphic lithoclasts in the western study area (mostly from the central Alpine metamorphic nappes), passing to a mixed igneous, metamorphic and sedimentary composition of clasts to the East (mixed provenance from the same metamorphic nappes and the western Southalpine basement-cover thrusts; borehole 'U') (Figs. 4, 7C). The F7 greyish silts and clays, barren of marine fossils with peat layers, which cover F8, thicken from 0 to more than 15 m away from the uplifted San Colombano and Casalpusterlengo-Zorlesco structures (Figs. 3, 7B). The Intermediate-Rank Stratigraphic Unit 2.1 gets progressively more sand-rich, thins and wedges out onlapping the limbs of the San Colombano and Casalpusterlengo-Zorlesco folds (Figs. 3, 7B).

The overlying **Intermediate-Rank Stratigraphic Unit 2.2** shows a quite comparable external shape, litho-textural association and stacking pattern, onlapping and wedging out at progressively increasing elevation onto the limbs of the mentioned anticlines (Fig. 7B). The relative proportions of porphyrites and sedimentary rock fragments from the western Southern Alps increase abruptly in gravels of the Intermediate-Rank Stratigraphic Unit 2.2 compared to the Unit 2.1. The 10 to 20 m-thick unit of fine-grained litho-textural association F7 on top of the Intermediate-Rank Stratigraphic Unit 2.2 gets progressively eroded by the unconformity S2.3 towards the San Colombano and Casalpusterlengo-Zorlesco uplifting structures (Fig. 7A, B).

The proportion of coarse-grained sediments increases within **Intermediate-Rank Stratigraphic Unit 2.3** (sandy gravels alternating with gravel-sand layers; F10 litho-textural association) (Figs. 4, 5, 7; Table 3A) which starts abruptly above intermediate-rank unconformity S2.3. The F10 bodies are capped by grey to dark grey clays, with rare peat layers which maintain nearly constant thickness of less than 10 m if not eroded below the U3 Middle–Late Pleistocene unconformity (F7 litho-textural association; Figs. 5, 7B; Table 3A), forming two fining-upward sequences, 10 to 30 m-thick each. An abrupt increase in crystalline gravel-sized rock fragments (high-grade metamorphic and intrusive igneous clasts, alpine-sourced; Fig. 4), occurs across S2.3.

Facies interpretation. The F8-F7 assemblage forming the Intermediate-Rank Stratigraphic Units 2.1 and 2.2 is here interpreted as the record of alluvial plain cycles, with mixed-load alluvial systems (sand bodies topped by organic-rich sediments forming fining-upward sequences above low-rank erosional surfaces), replaced by organic-rich silts and clays interpreted as floodplain deposits (Miall, 1996; Bridge, 2003). The change of gravel composition across the boundary between Intermediate-Rank Units 2.1 and 2.2 suggests increasing provenance from the Southalpine Mesozoic sedimentary covers with Permo-Triassic volcanites and low-grade metamorphic basement clasts (Montrasio et al., 1990). More specifically, the volcanic components above intermediate-rank unconformity S2.2 (pink ryolitic porphyrites) are typical of the Verbano-Varese-Lario area, suggesting a contribution from the western Southern Alps of Lombardy (Riva, 1957; Bini, 1997b). The couplets S2.1-Intermediate-Rank Stratigraphic Unit 2.1 and S2.2-Intermediate-Rank Stratigraphic Unit 2.2 suggest at least two stages of progradation and inactivation of Central Alpine- and western Southalpine-sourced alluvial depositional systems, that get meandering reaching the study region (Fig. 7E). In the same area, the features of the uppermost Intermediate-Rank Stratigraphic Unit 2.3 indicate relevant changes in depositional style, from former alluvial plain to bedload-dominated systems with braided alluvial style (Miall, 1996) (Fig. 7F), and provenance of sediments, with a strong fingerprint from the metamorphic basement nappes of Southern and Northern Alps (micaschists and gneisses) (Montrasio et al., 1990). Inactivation and

back-stepping of this coarse-grained dispersion system is suggested by the upward transition to the uppermost, alluvial plain, sandy-silty sequences.

4.4. Middle-Late Pleistocene Unconformity (U3) – High-Rank Stratigraphic Unit 3 (HRS3)

4.4.1. S3.1 - Cascina Parina 1 Synthem (CPS1)

The intermediate-rank erosional boundary S3.1 bounds at the base the lowermost synthem of the High-Rank Stratigraphic Unit 3, namely the Cascina Parina 1 Synthem (Zuffetti et al., 2018a). This sand-gravel unit crops out at the San Colombano and Casalpusterlengo-Zorlesco structures. OSL age determinations attribute the upper part of the synthem to the Late Pleistocene, between ca. 107 and 67 ka (Fig. 8A, B; Table 1). In the most complete successions, the age of the base of Cascina Parina 1 Synthem is constrained only by its superposition above the Middle Pleistocene Intermediate-Rank Stratigraphic unit IRS3 (Fig. 7); as a consequence, a Middle Pleistocene age for the base of the Cascina Parina 1 Synthem cannot be excluded. Its thickness ranges between about 5 and 40 m, with the minimum corresponding to the uplifted and truncated successions on top of the San Colombano hill (Fig. 8A). Where preserved, the top of the Synthem corresponds to a m-thick, rubified hydromorphic palaeosol (Zuffetti et al., 2018b) (soil profile 'a', Fig. 8A, B), otherwise it is truncated by S3.2 (Figs. 3, 8A, B). A m-thick loess unit covers the palaeosol (L1, log F; Fig. 8A). The NW flank of the San Colombano hill exposes the thickest succession of Cascina Parina 1 Synthem, which thins from here to the SE (Fig. 8A). The Synthem is formed by two lithozones characterised by two facies associations, F7-F8 and F9-F7 (CPS1a, b lithozones respectively) (Figs. 4, 5, 8, 9; Table 3B).

The lower **CPS1a lithozone** is composed at the base of a m-thick tabular bedset of fine-grained muddy sands and silts, massive to poorly horizontal-laminated, interbedded with mm- to cm-thick massive sands with wood fragments (facies F7; Figs. 5, 8A). On the crest of the San Colombano structure, where the Cascina Parina 1 Synthem is thin, facies F7 is absent and facies F8 beds unconformably lie over the folded Calabrian San Colombano Formation (logs N-P, Fig. 8A). Above F7, facies F8 forms a 5-8 m-thick layer of planar and trough cross-bedded sands and gravelly sands (Fig. 9A) organised into m-thick fining-upwards sequences. The bed-sets are bounded by inclined surfaces; grain-size and height of the beds decrease upwards within two successive inclined surfaces. Some scoured bed-sets are bounded by concave-up bases hosting cm-thick lags of sub-rounded and sometimes highly weathered pebbles frequently associated with cm-sized, often angular mud clasts (Fig. 9B, C). Palaeocurrents show a unimodal, highly variable azimuthal pattern indicating NE to ENE-directed flows (Fig. 8A).

The overlying **CPS1b lithozone** consists of 3 to 5 m-thick co-sets of trough cross-stratified sands with recurrently preserved sigmoidal dunes (facies F9; Fig. 5, 8A; Table 3B). Gravel and mud layers are rare and thin. Palaeocurrent indications from trough-cross-sets are widely dispersed, indicating a SE-ward average trend. These sandy, amalgamated layers contain recurrent post-depositional deformation structures at multiple levels which can be laterally traced with continuity (Fig. 8A). They mainly consist of water escape structures including dish, pillars, and convolute laminae and beds (Pettijohn and Potter, 1964; Lowe and Lopiccolo, 1974). Dishes appear as thin, flat to concave-up laminations. The finer grains, such as mica and clays, are filtered out and trapped in low permeability zones above, often displaying flame structures. The deformation structures occur between specific stratigraphic intervals, separated by undeformed sediments (Fig. 9D). The vertical stacking of lithozones CPS1b over CPS1a in the San Colombano exposures registers increasing amalgamation of the sandy bed-sets and decreasing abundance of gravel-sized clasts. The Cascina Parina 1 Synthem cropping out at the Casalpusterlengo-Zorlesco structure lies above the marine Calabrian equivalent of the San Colombano Formation at the high-rank U3 erosional surface, as observed at very shallow depth on the former quarry floor (Anfossi et al., 1971) and it is constrained by shallow borehole logs (Fig. 8B, D). It consists of coarse- to medium-grained, stationary to normally graded grey (gravelly) sand with large-scale trough-cross-stratification, planar-cross beds and sigmoidal dunes, trough-scoured units and recurrent water-escape structures (F9 facies association). The basal high-rank unconformity U3 was traced-down from the quarry floor to the subsurface borehole logs. Here, U3 underlies stacked gravelly sand units, which form at least two fining-upward, 20 m-thick sequences (litho-textural assemblage comparable to F8 facies association; Figs. 5, 8D; Table 3B) separated by dark clayey silt and peat layers (litho-textures comparable to F7 facies association). These sequences represent a subsurface equivalent to lithozone 1a of Cascina Parina 1 Synthem. The lithozone gets thicker N of the San Colombano hill (cross-sections 2N and 3N, Fig. 8D, E) and corresponds to decametric-thick, stationary sandy sequences, approaching the San Colombano and Casalpusterlengo-Zorlesco fold crests (Fig. 3). A comparable trend is observed up-section where a sandy, amalgamated litho-textural association with a mud layer atop compares to the F9-F7 surface association of the formerly described lithozone CPS1b (Figs. 5, 8D, F; Table 3B). This unit laterally replaces the subsurface equivalent of the lithozone CPS1a where the latter wedges out (Fig. 8D). The composition of Cascina Parina Synthem 1 gravels and sands is characterised by mostly metamorphic (high grade above all) and igneous intrusive rock fragments, with a low percentage of volcanic and sedimentary clasts, usually minor than 20% of the bulk gravel composition (Figs. 4, 9E; Table 3B). A slight increase in volcanic fragments occurs in CPS1b exposed on the San Colombano hill, accompanying a palaeocurrent change (Fig. 8A).

Facies interpretation. The F7 facies association of lithozone CPS1a is interpreted as deriving from floodplain deposition of overbank fines, locally interbedded with crevasse splay deposits (O'Brien and Wells, 1986; Miall, 1996; Bridge, 2003; Amorosi et al., 2008; Milli et al., 2016). It is replaced up-section by the F8 facies association that documents development of channel-bar systems, with sandy bedforms, lateral accretion macroforms, large and minor channel fills (Cant, 1982; Miall, 1985; Blum, 1993; Bridge, 1993; Best et al., 2003; Ashworth et al., 2011; Horn et al., 2012) (Table 3B). Petrographic composition and palaeocurrent trends suggest that these mixed-load, meandering alluvial systems were fed from a western alpine source and by recycling of gravel- and sand- from the underlying units, considering the high-percentage of weathered clasts mixed with the un-weathered ones (Fig. 9B) (Zuffetti, 2019). The transition to lithozone CPS1b suggests the change from a meandering river alluvial setting to a sandy, bedload-dominated river distribution system, fed from the NW. Change in river style and palaeocurrents (Fig. 8A), abundance of water escape structures at specific stratigraphic positions within lithozone CPS1b observed approaching the San Colombano Structure (Fig. 9D) suggest syndepositional seismicity, following the criteria proposed by Obermeier (1996) and McCalpin (2009). Also the lateral replacement between lithozones CPS1a and CPS1b in the subsurface, and the recurrent amalgamation of sand bed-sets towards the Casalpusterlengo–Zorlesco structure (Fig. 8B), suggest syn-tectonic deposition of the Cascina Parina 1 Synthem (Schumm et al., 2002; Hickson et al., 2005), plausibly due to an uplift stage of the tectonic reliefs (Fig. 8F). Syndepositional uplift is suggested also by the slight deformation of the High-Rank Unconformity U3 at the base of the Cascina Parina 1 Synthem. Onlap trends of the sandy lithosomes of the lower Cascina Parina 1 Synthem (Fig. 8D), stationary stacking and thickening of sand deposits approaching to the San Colombano and Casalpusterlengo-Zorlesco structures (Fig. 8F) and the thickening of the interposed mud horizons towards the North, suggest that a relative depocentre formed to the North of, and in between the uplifting structures during deposition of Cascina Parina 1 Synthem.

4.4.2. S3.2 – Cascina Parina 2 Synthem (CPS2)

Three lithozones have been recognised within Cascina Parina 2 Synthem, by the composition of the F7, F9, F10 and F11 facies and litho-textural associations (Fig. 5; Table 3B). In outcrops, the **CPS2a lithozone** is a lenticular unit, with an erosional concave-up base (S3.2 intermediate-rank unconformity) deeply nested within the Cascina Parina 1 Synthem (log H, Fig. 8A). It comprises a cm-thick lag of coarse pebbles, covered by a single, 1.5 m thick fining-upward sequence of trough cross-bedded sand and gravelly sand with sparse granules and pebbles. Massive gravelly sands and silty sands with sparse pebbles and recurrent fragments eroded from a palaeosol follow upwards (F11 facies, Fig. 5; log H, Fig. 8A; Table 3B). Palaeocurrent indicators suggest ESE-

directed palaeoflows (Fig. 8G). CPS2a lithozone occurs only on the San Colombano hill and results from valley incision and filling within the alluvial sediments of Cascina Parina 1 Synthem. Differently, on the Casalpusterlengo hill the F9-F7 facies association characterises the sandy/gravelly **CPS2b lithozone** (Table 3B). At this site, CPS2b lithozone covers S3.2 intermediate-rank unconformity with a 2 m-thick sequence of fine- to coarse-grained, crudely stratified and amalgamated sand/gravel beds with erosive bases (F9 facies, Figs. 5, 8B; Table 3B). These beds are separated by cm-thick interbeds of massive sandy silt (F7 facies, Fig. 5) and cover the topsoil of Cascina Parina 1 Synthem (soil profile "a" in log W, Fig. 8B). Comparable litho-textural associations have been traced in the subsurface of the whole eastern study area and represent the buried equivalent of lithozone CPS2b. The F9-F7 facies intervals are associated with decametric-thick alternations of gravelly sand and gravel (F10 facies, Fig. 5; Table 3B) forming 10 to 20 m-thick, stationary to fining-upward sequences of sands, locally gravelly sands, separated by m-thick, discontinuous mud layers (sections 9N and 4N, Fig. 8D; eastern section 5W, Fig. 8E). In the subsurface of the western study area, the described coarse-grained succession interfingers with three decametric-thick fining upward sequences of gravelly sands and sands, capped by grey to green clays and silty clays up to 20 m-thick (F8-F7 litho-textural associations, Fig.5; cross-sections 2N and 3N, Fig. 8D, E; Table 3B). Since any surface exposure is missing, the stacking of these sand-mud layers was distinguished from the others and named **lithozone CPS2c**, provided the subsurface correlation with the buried interval correlative to CPS2b lithozone (Table 3B). Gravel composition of Cascina Parina 2 Synthem is dominated by high-grade and low-grade metamorphic and intrusive igneous clasts with subordinate sedimentary and volcanic rock fragments (Fig. 4).

Facies interpretation. The lithotextural and facies associations of CPS2b and CPS2c lithozones testify for heteropic alluvial depositional systems (Table 3B) (Miall, 1985), mostly fed from the Alpine basements and routed by glacio-fluvial systems. Their development predated the LGM loess L2, hence plausibly encompassing part of the Late Pleistocene-MIS4. In the subsurface of the western study area, the occurrence of thick mud intervals separating the sandy/gravelly fining upward sequences of CPS2c lithozone documents the establishment of an alluvial plain setting with floodplains and river channel/bar systems (Bridge, 2003; Fig. 8G). Unbundling of gravel/sand bed-sets within thick flood plain mud horizons indicates that aggradation of flood plain fine-grained sediments could overcome sand/gravel deposition, suggesting a subsiding setting. These western systems prograded SE-wards, eroding their alluvial terraces into the slightly deformed Cascina Parina 1 Synthem, along S3.2 intermediate-rank unconformity (Fig. 8D). To the East, the amalgamated sand-gravel units, poor of mud caps (CPS2b lithozone) (Fig. 8D), resulted from bedload deposition in braided river systems. At the same time, on the uplifting San Colombano hill, a wide erosion surface (S3.2) was cut and a

palaeo-valley was incised and filled (CPS2a) then disactivated and abandoned before the deposition of the LGM L2 loess (Fig. 8G) in agreement with pedostratigraphic and morphological interpretations of Zuffetti et al. (2018b), Zuffetti and Bersezio (2020).

4.4.3. S3.3 - Invernino Synthem (INS)

The Invernino Synthem comprises both sand-gravel and very fine-grained facies associations (F7, F8, F10, F12, F13, Fig. 5; Table 3B), forming four lithozones. In the western study area, **lithozone INSa** is formed by fine- to medium-grained sands with rare gravels, in dm- to m-thick beds, with large scale planar and trough-cross stratification and low-angle laminations and small scale sets of oblique laminated fine sand (F8 facies association). Inclined sandy bed-sets form m-thick fining-upward sequences capped by massive silt with very fine sand, ripple-laminated interbeddings (F7-F8 facies association, Fig. 10A). The rare pebbles are dominantly sedimentary and volcanic rock fragments, among which the typical pink rhyolites from the western Southern Alps are abundant, with subordinate metamorphic and intrusive rock fragments (western study area in Fig. 4); sand composition varies from lithic arkose to subarkose with recurrent felsitic volcanites (Fig. 9F). Palaeocurrents indicate SE-ward flows. By tracing the intermediate-rank unconformity S3.3 at its base, lithozone INSa correlates to the comparable F7-F8 litho-textural associations of its subsurface equivalent lithozone (sections 3N, 4N, Fig. 8D, E; Table 3B). In the western study area this lithozone includes sand (gravel) bodies organised into at least two dam-thick fining-upward sequences separated by 5-10 m thick grey-green clay and silt layers. The mud horizons get thicker and more continuous N- and NW-wards. Yellowish to reddish colours of sands just below the topographic surface point to hydromorphic soil development comparable to the exposed profiles (soil profile ‘c’ in Fig. 8C; section 2N, Fig. 8D).

NW of the San Colombano structure, lithozone INSa is covered by a 10 m-thick, mostly fine-grained unit that represents **lithozone INSb** (formerly Villanterio Unit in Zuffetti et al., 2018b) (Fig. 2A), VIL in Fig. 8D. It encompasses trough and planar cross-laminated sands with rare granules and pebbles, showing S- and SW-wards palaeocurrents. Bed-sets are organizsd in thick to medium graded beds (F13 facies, Figs. 5, 10B; Table 3B), passing upwards to thin-medium beds of laminated to massive, burrowed fine-grained sands interbedded with grey to olive clays and silty clays, with parallel lamination (F7 facies, Fig. 5). Continental molluscs (Table 3B) typical of freshwater pond to lacustrine and floodplain environments (Lozek, 1964), are common in both facies. On top, intense burrowing and common mm- to cm-sized calcareous nodules and cemented layers occur. Sedimentary rock pebbles are more abundant than igneous and metamorphic gravel clasts (Fig. 4; Table 3B).

The **lithozone INSc** develops in the plain North of the San Colombano hill and in the eastern study area. It consists of planar and trough cross-bedded gravelly sands and medium sands forming dm- to m-thick fining-upward or stationary sequences (F10 facies, Figs. 5, 8C, H; Table 3B) with rare and thin mud interbeddings (F7 facies). Volcanic clasts are less abundant than in the INSa lithozone (Fig. 4) and palaeocurrent measurements indicate S- and SE-directed palaeoflows. Lithozone INSc is preserved as remnants of perched terraces on the San Colombano hillslopes, that were isolated by extensional faulting during collapse of the San Colombano structure (Fig. 2A) according to Zuffetti and Bersezio (2020). Multiple-levels of soft sediment deformation structures correlate across the hangingwall and footwall of the faults (Figs. 8C, 9G) and include convolute laminae and beds, dm-thick sedimentary dikes and mud injections. The F10-F7 facies association of the "eastern" INSc lithozone compare with the litho-textural subsurface association of the eastern study area (Fig. 8E): one stationary or fining-upward sequence, about 30 m-thick, formed by gravel-sand litho-textural associations, that erodes the Casalpusterlengo–Zorlesco structure (S3.3 intermediate-rank unconformity). Gravels of this lithozone contain a dominant proportion of sedimentary rock fragments over igneous and metamorphic clasts, in keeping with the gravel composition of the other lithozones of the Invernino Synthem. On the San Colombano hillslopes, planar layers of massive fine sand interbedded with silt, with crude planar lamination, subangular intraclasts and pedorelicts, are interposed between the sandy sequences of lithozone INSc and L2 loess deposits. ThisF12 facies association (Fig. 5; Table 3B) characterises a localized **lithozone INSd** (Figs. 8C, H).

Facies interpretation. The sedimentary features of lithozones INSa, b, c, account for alluvial deposition sourced from the Southern Alps, as it is documented by the dominance of sedimentary and volcanic rock fragments over the metamorphic basement-derived clasts. Channel-point bar, levee and floodplain facies associations of lithozone INSa suggest mixed-load, meandering fluvial style (Leopold and Wolman, 1957; Schumm, 1981; Cant, 1982; Galloway and Hobday, 1996; Bridge, 2003). Lithozone INSb is typical of floodplain environment with oxbow lakes and shallow and semi-permanent lacustrine ponds (Lozek, 1964; Einsele, 1992; Freytet and Verrecchia, 2002). The "eastern" lithozone INSc records bedload deposition in unstable water courses with braided channels (Rust and Gibling, 1990; Miall, 1996; Moreton et al., 2002; Bridge, 2003; Bersezio et al., 2004; Smith and Rogers, 2009; Gardner and Ashmore, 2011). In the western study area, lithozone INSa records the progradation of sand-dominated rivers, mainly spreading from the western Southern Alps and the Verbano glacial amphitheratre (Fig. 1B), as it is documented by the relatively high proportions of the typical pink rhyolites. Age determinations that correlate the Invernino Synthem with the LGM time-span, and regional correlations (Bersezio et al., 2004; Bini et al., 2004a) suggest to consider these

systems as the distal reaches of the glacio-fluvial outwash of the Verbano glacier, lateral equivalent of the synthems forming the Laghi Supersynthem (Bini et al., 2014; Francani et al., 2016). The general fining-upward trend that culminates with the deposition of the floodplain facies association of lithozone INSb, might suggest backstepping of the depositional systems during one retreat phase of the LGM Verbano glacier (Bini, 1987; Bini et al., 2004b). The features of the heteropic "eastern" INSc lithozone suggests progradation of braided glacio-fluvial systems, from a closer and eastern source, like the Lario Amphitheatre (Fig. 1B), as it is suggested by the absence of the typical pink volcanic clasts. At the LGM times the San Colombano hill was already raising above the adjacent plain and might have acted as a divide between the western and eastern glacio-fluvial systems. Perching of Invernino Synthem terraces (Fig. 8H), location of colluvial wedges (lithozone INSd), and sediment deformation structures within INSb lithozone beds at the San Colombano structure (Figs. 8C, 9G), testify that faulting occurred during and after deposition of the Invernino Synthem (Zuffetti and Bersezio, 2020).

4.4.4. S3.4 - Paleo Sillaro Synthem (PSS)

The Paleo Sillaro Synthem comprises brownish-grey, medium- to coarse-grained sands and gravelly sands, forming fining-upward sequences of graded to massive beds, inclined bed-sets with large-scale, trough-cross- and planar-cross-stratification (Fig. 10A) and fine-grained rippled sand and silt (F8 facies, lateral accretion bar association) (Fig. 10C; Table 3B). Thin layers of mudstone with peat and fine, ripple cross-laminated sand (F7 facies; Table 3B) occur either as thin bed-sets at the top of the fining-upwards sequences (levee facies association; Table 3B) or as m-thick fining-upward units, in association with cross-stratified sands (channel fill facies association). North of the San Colombano hill (Fig. 2A) these abandoned river traces, that are revealed by field and remote geomorphological mapping, are elongated NNW-SSE, and palaeocurrent consistently indicate SSW to SE-directed flows (Table 3B). S of the same hill, the abandoned river traces are comparable in width and average direction to the Holocene Po-river meanders, whose terrace scarps crosscut the Paleo Sillaro Synthem abandoned traces. The gravels of the northern traces contain mostly sedimentary and volcanic clasts and subordinate metamorphic and intrusive rock fragments, with more abundant pink rhyolites in the western side of study area than to the E (Fig. 4; Table 3B).

Facies interpretation. The geometry and distribution of the Paleo Sillaro Synthem sedimentary bodies and their preserved surface morphologies suggest deposition by different meandering palaeo-rivers, with the development of point bar-channel-abandonment sequences (Fig. 8I). Gravel composition of the northern river bodies of Paleo Sillaro Synthem testifies to provenance from the Southern Alps foothills; the westward enrichment in volcanic clasts is consistent with the recycling of the exposed porphyrite-rich Invernino Synthem

of the western study area (Fig. 4), as well as with the course of a NW-sourced palaeo-river from the Verbano amphitheatre area (Fig. 1B), in keeping with the petrography of the stratigraphic units that correlate with Paleo Sillaro and Invernino synthems North of the study area (Bersezio et al. 2004, 2010). No river diversions or river-style changes occur throughout the development of these river traces that are mildly encased within the average surface of the Pleistocene plain (Bersezio, 1986; Castiglioni and Pellegrini, 2001). These features suggest that Paleo Sillaro Synthem developed in a period of tectonic stability and low uplift rate during retreat of the LGM Verbano and Lario glaciers.

4.5. Latest Pleistocene-Holocene Unconformity (U4) – High-Rank Stratigraphic Unit 4 (HRS4)

The Po Synthem is up to 10 m-thick in the main river valleys. It comprises sandy and gravel-sandy bedforms with planar and trough cross-stratification and planar horizontal stratification (F8 facies; Table 3B), organised into m-thick fining-upward sequences. These are frequently capped by yellow-grey, laminated to massive silt and fine sand, sometimes enriched in organic matter (F7 facies). Anthropic artefacts and reworked Plio-Pleistocene marine and continental fossils and mud clasts occur in the uppermost beds. Gravels of the Po river tributaries from the NW and N contain mixed magmatic, metamorphic and sedimentary rock fragments, suggesting erosion and reworking of the former successions. Apennine-derived gravel clasts mixed with sand fragments from the Western, Central and Southern Alps characterise the Po river sediments.

References

See the References list of the paper.